Chemoenzymatic Glycoengineering to Study and Remodel the *N*-glycocalyx

Rosanne van Beek

Chemoenzymatic Glycoengineering to Study and Remodel the *N*-glycocalyx

Rosanne van Beek

DOI: https://doi.org/10.33540/1627

Printed by: Ridderprint | www.ridderprint.nl

Cover design: Herma Starreveld

Chemoenzymatic Glycoengineering to Study and Remodel the *N*-glycocalyx

Chemo-enzymatische Glycaan Modificatie voor de Studie en Herstructurering van de *N*-glycocalyx

(met een samenvatting in het Nederlands)

Proefschrift

ter verkrijging van de graad van doctor aan de
Universiteit Utrecht
op gezag van de
rector magnificus, prof.dr. H.R.B.M. Kummeling,
ingevolge het besluit van het college voor promoties
in het openbaar te verdedigen op

woensdag 1 februari 2023 des middags te 12.15 uur

door

Rosa Joanna van Beek

geboren op 15 maart 1992

te Alkmaar

Promotor:
Prof. dr. R.J. Pieters

Copromotor:
Dr. K.R. Reiding

Table of Contents

Chapter 1

Introduction

1

N-Glycosylation in health and disease

One thing all living organisms have in common is a dense layer of glycans that covers the surface of every cell[1]. Glycans are complex assemblies of carbohydrate molecules[2] with remarkably diverse structures, which are displayed on the surface of human cells where they are attached to proteins or lipids (Figure 1)[3,4]. The most well-known glycoprotein classes consist of glycan chains attached to the nitrogen atom of an asparagine residue or the oxygen atom of a serine or threonine residue, and are therefore named *N*-linked and *O*-linked glycans. Additionally, proteoglycans form a class of glycoproteins that are defined by the attachment of long glycosaminoglycan (GAG) chains to the hydroxyl group on a serine residue. GAGs can also exist in a free form, not attached to a protein. Glycosylphosphatidylinositol (GPI)-anchored glycoproteins are attached to a phosphatidylinositol embedded in the membrane through a phosphodiester linkage to phosphoethanolamine linked to a trimannosyl-nonacetylated glucosamine core. Last, glycosphingolipids are a class of glycoconjugates where the glycans are directly attached to cellular membrane lipids.

Glycosylation is one of the most common posttranslational modifications on proteins, with *N*-glycosylation being the best studied form of protein glycosylation. *N*-Glycosylation refers to the attachment of a glycan moiety to the asparagine on a protein. This attachment actually already starts co-translationally[5], giving *N*-glycans an essential role in protein folding, quality control and sorting events in the secretory pathway[6–9]. However, the role of *N*-glycans is not limited to structural influences, they also modulate or mediate a wide variety of functions in physiological and pathophysiological states. Glycans produced in the secretory pathway participate in a multitude of cellular regulation mechanisms, such as cell-cell adhesion, receptor activation, signal transduction, and endocytosis[10]. It is therefore no big surprise that aberrant glycosylation has been linked to many disease states, like cancer, Alzheimer's, autoimmune diseases, and even schizophrenia[11–14].

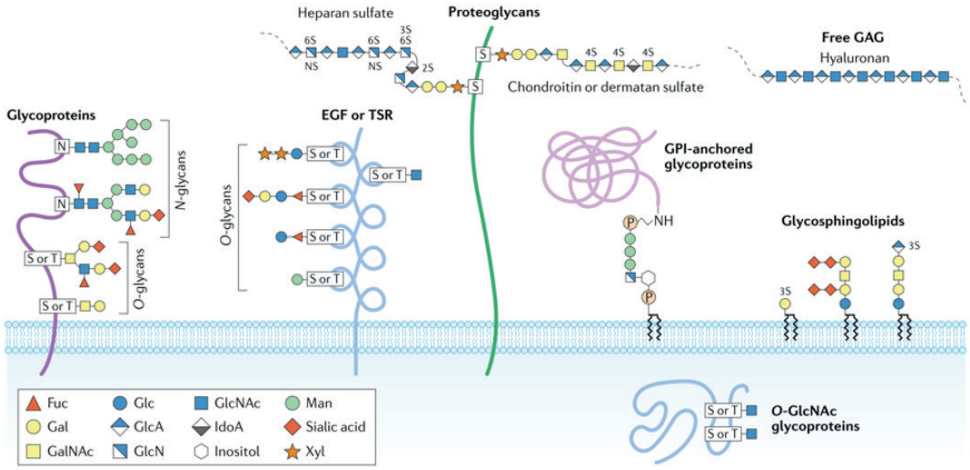

Figure 1. Major types of glycosylation in humans. Image from Reily et al. (2019), Nature reviews Nephrology[3].

Congenital disorders of glycosylation

Congenital disorders of glycosylation (CDGs), first reported in 1980, represent a group of genetic disorders with impairments in the biosynthetic pathway of protein or lipid glycosylation. CDG patients present highly heterogeneous clinical phenotypes, ranging from mild to very severe and mostly involve multiple organs[15,16]. Since the first report the number of known CDG subtypes has never stopped growing, with currently over 150 known subtypes[17]. Nowadays, CDGs are divided into four groups, namely defects in *N*-glycosylation, defects in *O*-glycosylation, defects in lipid and GPI-anchor glycosylation and defects that affect multiple glycosylation pathways[18]. Despite the growing number of subtypes, congenital disorders of *N*-glycosylation is still the most common subtype and giving the scope of this dissertation, this will be the only class of CDGs discussed here.

In *N*-glycosylation biosynthesis, the glycan precursor is first assembled on a dolichol phosphate scaffold on the cytoplasmic side of the endoplasmic reticulum (ER), after which it is transferred to the asparagine in a glycosylation consensus sequence (Asn-Xxx-Ser/Thr) on the growing peptide chain in the lumen of the ER. Remodeling of the glycan precursor then takes place in the ER and Golgi apparatus giving rise to a mature glycan (Figure 2)[19]. Congenital disorders of *N*-glycosylation can roughly be classified as being a type I or a type II[20]. A type I CDG contains a defect in the assembly or transfer of the dolichol-linked glycan in the cytoplasmic ER, resulting in protein hypoglycosylation[21]. In a type II CDG the defect lies in the glycan processing in the ER and Golgi apparatus, resulting in qualitative differences of the protein glycosylation[22]. Most clinical screening for *N*-glycosylation disorders is based on isoelectric focusing of serum transferrin and α1-antitrypsin. When transferrin profiling cannot be used, *N*-glycan profiling by mass spectrometry (MS) can also be used for diagnosis[23]. Due to the highly heterogenic presentation of CDGs, there is no general therapeutic strategy that can be used on all subtypes. It is therefore fundamental to gain knowledge on the pathophysiological aspects of different CDG subtypes to achieve better diagnostics and treatments.

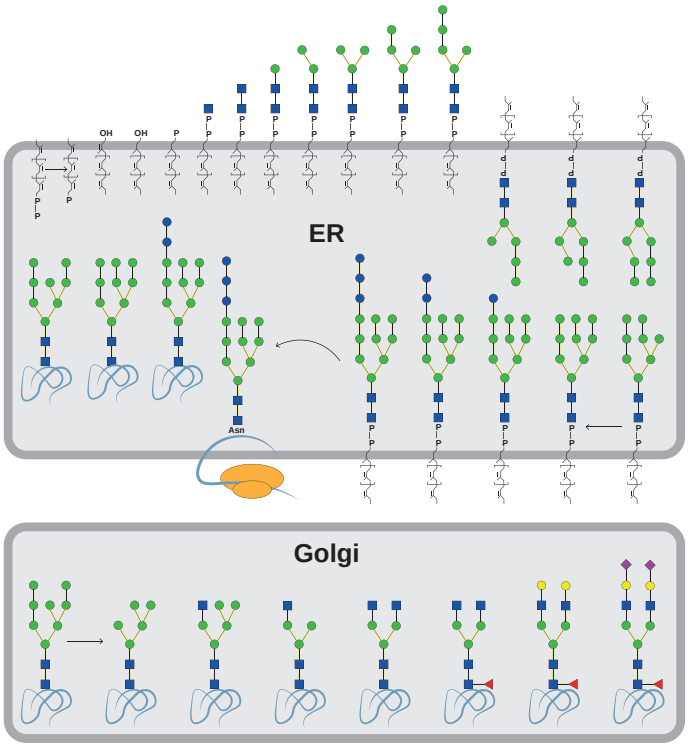

Figure 2. Schematic overview of the N-glycan biosynthesis in the ER and Golgi apparatus. Image adapted from Lefeber et al., Essentials of glycobiology, Chapter 45.

CHO-K1 cells as model system to study CDGs

To investigate the underlying molecular mechanisms and categorize newly discovered mutations in CDGs, the use of in vitro models has proven to be very useful. The group of Pamela Stanley has used resistance against cytotoxic plant lectins to create a large selection of glycosylation mutant CHO cell lines (Lec^r), each of which shows a unique phenotypical resistant pattern[24–28]. Linking the phenotypical glycan characteristics of the individual Lec^r mutants to the underlying genetic defects has greatly helped in the identification of novel CDG subtypes and the discovery of potential biomarkers to facilitate diagnosis[29–32]. Insights into the genetic alterations that lead to certain glycosylation abnormalities obtained by these CHO glycosylation mutants also contributed to our general understanding of the biological roles of glycans.

Glycosylation as Receptor for Influenza A Viruses

Due to the prevalence of glycoconjugates on the cell surface, glycans also play an important role in many host-pathogen interactions[33]. Influenza viruses for example, use the viral surface protein hemagglutinin (HA) as a receptor-binding protein to attach to the cell surface of the host via glycoconjugates. The characteristics of the surface glycosylation therefore largely determines whether a cell, or species, can be infected by a specific virus. Sialic acids act as the primary glycan receptors for HA proteins and are most typically found on the outermost ends of *N*-glycans, *O*-glycans, and glycosphingolipids. The linkage of sialic acids to the penultimate galactose residue of the cell-surface glycan receptors is commonly accepted as the most

important basis for host cell tropism[34]. Sialic acids can be linked to the penultimate galactose in an α2,3- or an α2,6- fashion, where α2,3-linked sialic acids are marked as the avian receptor and α2,6-linked sialic acids as the human-type receptor (Figure 3)[34,35]. However, the sialic acid linkages only partially contribute to the understanding of the complex interactions between influenza viruses and their glycan receptors. Even though a lot remains to uncover, it is now known that besides sialic acids also other glycan moieties or substituents such as sulfates, fucoses, and internal sialic acids can contribute to binding of human influenza viruses[36].

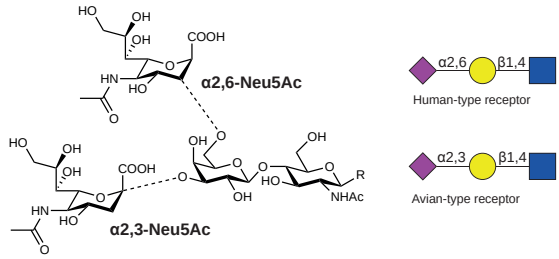

Figure 3. Prototypic glycan receptors for human and avian influenza A viruses.

Additionally, also the glycan moieties preceding the terminal sialic acid can be involved in influenza binding. The penultimate galactose residue is typically linked to an *N*-acetylglucosamine (GlcNAc) moiety, which together are referred to as *N*-acetyllactosamine (LacNAc). The most prevalent LacNAc structure in humans is the type-2 LacNAc, where the galactose and GlcNAc are linked in a β-1,4-fashion. The presence of extended LacNAc structures in human respiratory tissues awoke an interest in the potential role of these moieties in influenza A binding[38–40]. Microarray analyses of the binding specificity of human influenza viruses toward these extended LacNAc structures indeed revealed a varying specificity for shorter or longer LacNAc repeats[41]. A special focus on human A/H3N2 influenza viruses arose due to the shift in binding specificity these viruses underwent. In fact, microarray analyses showed an increasing selectivity of A/H3N2 viruses for extended glycan structures, containing at least two or three consecutive LacNAc moieties[42–44]. This preference for extended glycan branches was proposed to result from an increased avidity attained by simultaneous bidentate binding to two binding sites in an HA trimer[44]. These finding underline a clear involvement of other glycan structures than the terminal sialic acid in influenza binding. Understanding the molecular events involved in influenza binding and the evolution in binding specificity is important for the surveillance and prevention of potential influenza outbreaks.

Methods to study the *N*-glycome and *N*-glycoproteome

The involvement of *N*-glycans and *N*-glycoconjugates in such a wide variety of physiological and pathophysiological conditions makes them highly interesting biomolecules to study. However, the non-template driven nature of glycans makes them also significantly more challenging to study. Nevertheless, with the advent of new technologies such as glycomics, glycoproteomics, glycan arrays, and glycoengineering, the glycobiology field has revolutionized as a promising and fast-growing research area to solve the many mysteries toward the biological functions of cellular glycosylation.

Bio-orthogonal reporter strategies in living systems

Bio-orthogonal click chemistry

In chemical biology, bio-orthogonal click chemistry is a widely used method for the labeling of biomolecules within living systems. It allows for the monitoring of molecules like glycans and proteins in a physiologically relevant environment. Bio-orthogonal click chemistry consists of reactions between a reactive molecular pair that is exquisitely specific, fast, high yielding and occurs under physiological conditions[45–48]. Key is that the reactive groups neither occur in nor react with any functional group in biology and that the reagents are non-toxic. Due to this unique combination of requirements, there is only a small selection of molecules that meet all the criteria, of which azides constitute the most important handle. In fact, the introduction of azides as a bio-orthogonal handle in the Staudinger ligation was a game changer in the field[49]. Azides are special as they don't exist as a functional group in living systems, and they do not cross-react with any functional groups found in biology. On top of this, the small size of azides means the structural integrity of the target molecule is not significantly affected upon introduction. Together, these unique qualities have led to the exploitation of azides in several bio-orthogonal click reactions, which have since been used in many biological applications.

In the Staudinger ligation, an azide reacts with a phosphine to form an aza-ylide. The presence of an electrophilic trap, typically an ester, on the phosphine structure produces a stable amide bond in the presence of water, making the reaction stable under aqueous condition (Figure 4)[49]. Later, a so-called "traceless" Staudinger ligation was introduced, which yields a simple amide bond without an unnatural triarylphosphine oxide group[50]. After the introduction of the Staudinger ligation, development of other bio-orthogonal reactions followed.

Copper(I)-catalyzed azide-alkyne cycloaddition (CuAAC) was introduced as an alternative for the Staudinger ligation. In this reaction azides are also used as chemical reporter, only in this case the reactivity of the azide is exploited to facilitate an azide-alkyne cycloaddition, generating a stable triazole linkage[51]. By using Copper(I) (Cu(I)) as a catalyst the reaction kinetics drastically increases, and the reaction becomes selective for the 1,4 isomer of the product triazole thus not creating the alternative 1,5 isomer[52]. However, the cellular toxicity of Cu makes this reaction incompatible with living cells and tissues[53]. Therefore, approaches were sought to catalyze the cycloaddition in a Cu-free reaction. Important examples in the development of Cu-free click reactions are two generations of strain-promoted azide-alkyne cycloadditions. In the first generation, the alkyne is incorporated into a strained cyclo-octyne system to avoid the need of Cu(I) as a catalyst[54]. This reaction showed improved compatibility with the use in living systems, but reaction kinetics were relatively slow and in fact similar to those of the Staudinger ligation. To improve reaction kinetics a new generation was developed where electron withdrawing fluorine atoms were incorporated into the cylooctynes, termed DIFO[55]. Reaction kinetics of this reagent with benzyl azide were comparable with CuAAC. Several additional modulations of the reactivity of the cyclooctyne were also published[56–58].

Another break-through in the field was caused by the inverse-electron-demand Diels Alder (IEDDA) reactions, a catalyst-free strain-promoted (4+2) cycloaddition between 1,2,4,5-tetrazine (diene) and strained alkenes (dienophile)[59], followed by expulsion of nitrogen gas. After this discovery the toolbox of dienophiles has expanded, and depending on the choice of dienophile, reaction rates can get impressively fast (up till 10^{-6} $M^{-1}S^{-1}$)[60]. With its fast reaction times and catalyst-free nature, the IEDDA has outperformed most other bio-orthogonal reactions.

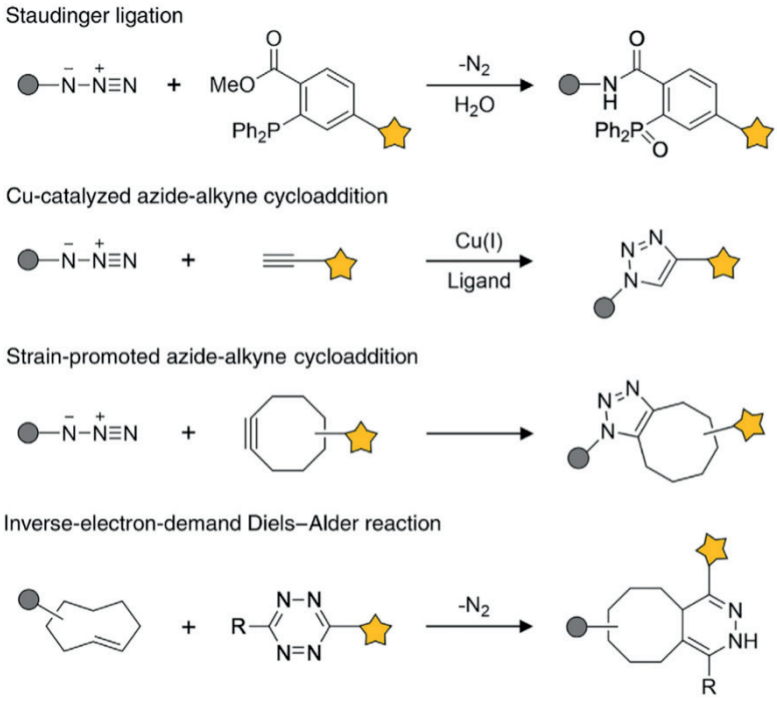

Figure 4. Common bio-orthogonal click reactions for the use in biological labeling and imaging. Image from Kenry and Liu (2019), Trends in chemistry.[48]

Metabolic oligosaccharide engineering

Probably the best-known application of bio-orthogonal click chemistry in glycobiology is metabolic oligosaccharide engineering (MOE). After the early discovery that modifications to sialic acid precursors can be accepted by sialyltransferases in the metabolic pathway[61,62], the group of Bertozzi introduced the combination of MOE with bio-orthogonal click reactions[63]. The discovery that azides are tolerated as a modification on nucleotide sugars in the metabolic pathway of glycosylation, opened the whole bio-orthogonal toolbox for the use of MOE[64]. As mentioned above, MOE is based on the principle that glycosyltransferases in the oligosaccharide biosynthetic pathway show a certain substrate promiscuity, accepting chemical alterations on the monosaccharide precursors. Sialic acids are biosynthesized from the six-carbon precursor N-acetylmannosamine (ManNAc). The modified N-azidoacetylmannosamine (ManNAz) will also be processed by the metabolic pathway in the cell, which will result in the presentation of N-azidoacetylneuraminic acid (SiaNAz) on the cell surface (Figure 5). Acetylation of the ManNAz to Ac4ManNAz improves the membrane permeability of the compound[64]. The same principle can be used to label glycoconjugates by feeding cells with the precursors N-azidoacetylgalactosamine (GalNAz), N-azidoacetylglucosamine (GlcNAz) and 6-azidofucose (6-AzFuc) (Figure 5)[65–67].

MOE has revolutionized research in the field of glycobiology and has found many applications, ranging from (in vivo) imaging of glycans and glycan enrichment for MS analysis to targeted immunomodulation[69–71].

Metabolic labeling has proven to be highly useful in the study of the cellular glycome and has caused a revolution in the way the cellular glycome can be studied. Furthermore, it greatly contributed to our current knowledge on protein glycosylation. However, the technique also knows limitations, for example in its inability to label specific glycan classes. Since all glycoconjugates – *N*- and *O*-linked glycosylation, proteoglycans, and glycolipids – utilize the same pool of monosaccharides for their biosynthesis, metabolic labeling offers little selectivity for the labeling of specific classes of glycoconjugates.

Chemo-enzymatic glycan labeling

Part of the limitations of MOE can be overcome by another approach, called chemo-enzymatic glycan labeling. Chemo-enzymatic glycan labeling makes use of exogenous recombinant glycosyltransferase enzymes to transfer monosaccharide analogues to a specific glycan acceptor (Figure 6)[72]. Thereby, it offers the opportunity to label specific glycan classes and to label glycans in specific linkages, forming a complementary method to MOE. In the early

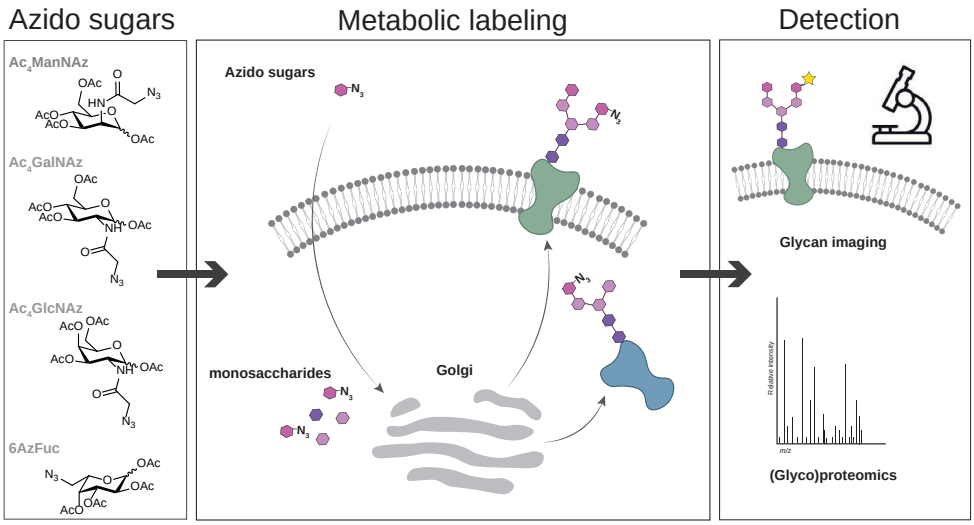

Figure 5. Metabolic labeling in biological systems. Image inspired by Zhang & Zhang (2013), Molecules.[68]

work of the group of Paulson, recombinant bacterial sialyltransferases were already used to install α2,3-linked or α2,6-linked sialic acids on the cell surface of erythrocytes to determine binding specificities of several paramyxoviruses[73]. However, now with the combination of chemo-enzymatic glycan labeling and bio-orthogonal click chemistry, a renewed interest in this labeling technique has emerged.

After the discovery that sialyltransferases tolerate modifications on the C-5 and the C-9 position of CMP-sialic acid[74], selective exo-enzymatic labeling (SEEL) was first introduced using the human sialyltransferase ST6Gal1 to install azide-modified sialic acids on cellular glycans[75]. ST6Gal1 showed specificity for the labeling of *N*-linked glycans and interestingly only labeled glycans present on the cell surface due to its inability to cross the cell membrane. After the initial labeling step, similar to MOE, the azido-labeled glycans can be functionalized for downstream applications such as imaging or a pull down for MS analysis.

A key element for this labeling strategy and a huge factor determining the possibilities of the method is the availability of suitable recombinant glycosyltransferase enzymes. Both bacterial and mammalian glycosyltransferases can be used for the technique[76], however especially for labeling of living systems many bacterial glycosyltransferases show limited activity on the cell surface. Therefore, several years ago an expression vector library for all known human glycosyltransferases was developed[77]. Even though some glycosyltransferases are significantly more difficult to express than others, the availability of this expression vector library has enabled the expression of a wide variety of human glycosyltransferases and thereby expanded the possibilities for chemo-enzymatic labeling. Among the glycosyltransferase enzymes that are reported for the use in chemo-enzymatic labeling to date are ST6Gal1, ST3Gal1, St3Gal4, α1,3-FT, and ST6GalNAc4[78–80].

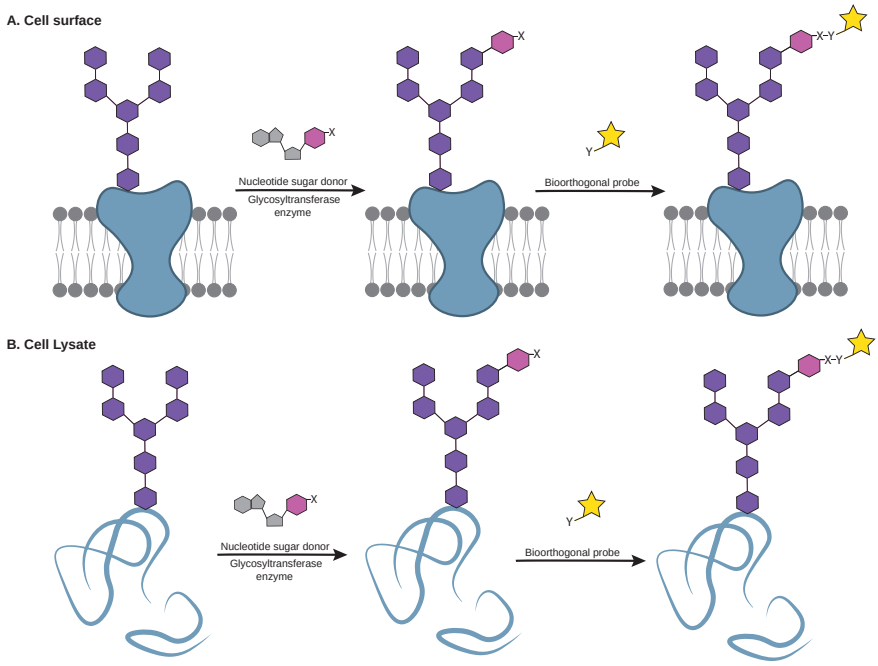

Figure 6. Chemo-enzymatic labeling of glycoproteins on the cell surface or in a cell lysate.

Another important development was the discovery that several sialyltransferases tolerated far larger modifications to the C-5 and C-9 position of CMP-Neu5Ac derivatives than an azide. This introduced one-step chemo-enzymatic labeling, where both the sugar and a functional group could be incorporated in a single step which greatly improved the overall efficiency[81,82]. Substrate tolerance of ST6Gal1 proved to be so large that even a complete heparan sulfate oligosaccharide linked to a CMP-sialic acid could be transferred on to the cell surface[83]. Also, the *Helicobacter pylori* fucosyltransferase α1,3-FT enabled the transfer of a full-length immunoglobulin G (IgG) antibody conjugated to a GDP-fucose donor onto the cell surface of living cells[84]. These discoveries open many possibilities for the enzymatic modification of cell surfaces in living cells using glycan remodeling.

Glycan analysis by mass spectrometry

With the growing knowledge about the intricate roles of glycans in biological processes and the large structural heterogeneity glycans can present, the field of glycobiology is moving toward unraveling the structure-function relationship of these biomolecules. However, the structural analysis of glycans is challenging for multiple reasons. Glycans are assembled by a set of competing glycosyltransferase enzymes, often creating branched structures, unlike other biomolecules like proteins or nucleic acids. The addition of monosaccharides can often occur in multiple linkages, creating isomeric structures. Furthermore, these branched structures do not always reach their "end product," meaning a protein can present a range of structures that vary by linkages, length, number of branches and composition. Possibly the most powerful method for the structural analysis of glycans is nuclear magnetic resonance (NMR). However, in biological samples, especially when analyzing protein *N*- or *O*-glycosylation, there is seldom enough material available for this technique. Therefore, the preferred method for analyzing protein glycosylation is often MS. Mass spectrometric analysis of glycans can range from the analysis of released glycans (glycomics) to the analysis of glycopeptides or intact glycoproteins (glycoproteomics)[85]. Even though both glycomics and glycoproteomics methods have been available for a longer period, in the recent years key advances in enrichment strategies, MS methods and informatics have allowed for a more complete implementation and integration of glycomics and especially glycoproteomics in the life sciences. Given the scope of this dissertation, the focus of the following will be on *N*-glycomics and peptide-centric *N*-glycoproteomics.

N-Glycomics

Typically, an *N*-glycomic analysis starts with the enzymatic detachment of *N*-glycans from the glycoproteins in the sample. This is mostly done by enzymatic or chemical release strategies. The most widely used enzyme for *N*-glycan release is peptide-*N*-glycosidase F (PNGase F) because of its wide range of recognition, but in some cases other endoglycosidase enzymes have advantages because of their specificity for certain glycan structures[86]. Efforts have been made to improve enzymatic release methods in their efficiency and incubation times, such as by the addition of detergents for increased protein solubility, the development of microware-assisted enzymatic hydrolysis or the use of immobilized PNGase F microcolumns[87–89].

After release, further enrichment of the free *N*-glycans from the biological sample is required. *N*-glycoproteins are typically present in low levels in biological samples, and free *N*-glycans in even lower levels. In addition, the hydrophilic nature of the glycans makes it harder to ionize them, resulting in a suppression of the glycan signals compared to the peptide signals in the sample. Enrichment is often performed using lectin affinity enrichment or by solid phase extraction (SPE) cartridges based on porous graphitic carbon (PGC) or C18 solid phases[90,91]. PGC is a popular stationary phase for the efficient separation of isomers with high retention time repeatability[92,93]. Hydrophilic interaction liquid chromatography (HILIC) is another popular enrichment strategy, which can separate *N*-glycans based on the polar groups they bear, creating predictable retention times[94].

Before they are subjected to MS analysis, glycans are often derivatized and labeled, mostly to increase their ionization efficiency by introducing hydrophobic groups[90,95]. Finally, the enriched *N*-glycans are subjected to MS analysis. The most widely used ionization techniques for the analysis of *N*-glycans are matrix-assisted laser desorption ionization (MALDI) and electrospray ionization (ESI)[96]. MALDI samples are co-crystallized in a matrix substance, and ionization and

evaporation occurs upon irradiation by a laser beam. In ESI, the analyte is sprayed in solution through a needle with an electrical potential forming charged aerosols that ionize the sample upon evaporation toward the MS. MALDI predominantly generates singly charged glycans, which results in a cleaner spectrum for released *N*-glycans from complex samples. Additionally, MALDI is better compatible with high-throughput MS[97]. Advantages of ESI on the other hand, are the ability to perform online fragmentation and purification of samples by the coupling to liquid chromatography (LC), improving structural information of the glycans detected, and allowing detection of low abundant glycan species by separation prior to MS analysis.

N-Glycoproteomics

Peptide-centric (or bottom-up) *N*-glycoproteomics focuses on the analysis of intact glycopeptides. Like glycomics, the field glycoproteomics faces several challenges. Glycoproteins often display variation in the occupancy of glycosylation sites (macroheterogeneity) and in the type of glycan presented on each specific glycosylation site (microheterogeneity), resulting in an enormously heterogeneous pool of glycopeptides, with each variant present at very low quantities. Also, just as with glycomics, the glycopeptides show a reduced ionization efficiency compared to non-modified peptides, resulting in a signal suppression of the glycopeptides in the MS[98]. To overcome these barriers, many innovative methods have been developed on the enrichment, detection, and analysis of glycopeptides, which together have significantly improved the analysis of the glycoproteome.

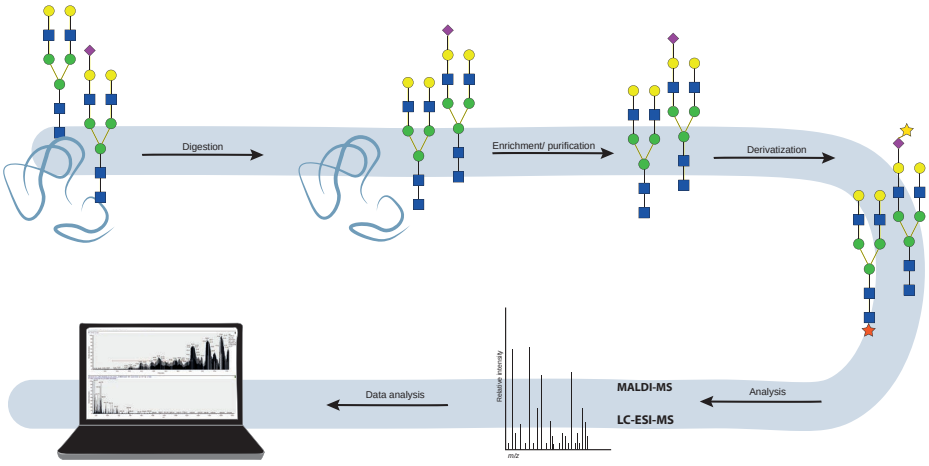

Figure 7. Schematic overview of N-glycomic workflow.

A variety of techniques has been developed for the enrichment of glycopeptides. Important to note is that every technique has its advantages and its drawbacks, therefore it depends on the application which enrichment method is best suitable and there is not one universal enrichment technique. Similar to glycomics, enrichment tools like lectin affinity chromatography, chemical coupling, HILIC and PGC can be used for the enrichment of glycopeptides[99]. Additionally, chemical biology tools like MOE and chemo-enzymatic labeling can be used to facilitate the enrichment of glycoconjugates from living cells or tissues. Advantages of using these techniques is that they are highly selective in the labeling of glycoconjugates and the use of a bio-orthogonal handle allows for enrichment under very stringent conditions, minimizing nonspecific interactions. However, these enrichment strategies also have their

drawbacks. Metabolic incorporation efficiency of unnatural sugars is usually low, leading to limited quantitative capacities of the technique. Chemo-enzymatic labeling is more efficient in its labeling capacity but depends on the number of glycans presenting the correct substrate. Labeling capacity can be increased by trimming of natural monosaccharides to increase the number of available substrates, with a loss of structural information of the natural glycan as a consequence. Despite these drawbacks, chemical biology tools for glycoproteomics is a rapidly moving field, and MOE and chemo-enzymatic labeling have enabled several recent glycoproteomic studies[100–103].

Another contribution to the advancements in the field of glycoproteomics was made by the development of various (hybrid) fragmentation methods for the structural elucidation of both glycans and peptide sequences on intact glycopeptides. Contemporary peptide-compatible fragmentation methods are collision-induced dissociation (CID), higher-energy collision dissociation (HCD) and electron-based dissociation techniques (electron-transfer dissociation, ETD, or electron-capture dissociation, ECD). CID/HCD involves the collisions of selected precursor ions with neutral gas molecules to produce fragment ions. In ECD/ETD the dissociation is prompted by the electron movement from anions to the precursor ions. For glycopeptides, CID and HCD preferentially fragment the glycosidic linkages, whereas ETD preferentially cleaves the peptide linkages. With this knowledge in mind, interest has grown for the development of hybrid fragmentation methods, combining the fragmentation methods to increase the generated ion types that can be used for structural elucidation of the analytes from complex glycopeptide mixtures[104,105]. In recent years multiple studies have published proteome-wide *N*-glycoproteomic analyses[106–108].

Last, a big obstacle in the field of glycoproteomics has been the complex analysis of the extensive data obtained from the complex MS measurements described above. Luckily, in the recent decade more and more automated software has been developed that makes the analysis of the complex MS data available for a wider group of researchers. Software like Byonic, P-Glyco 2.0, and MS-Fragger Glyco aid in the annotation of glycopeptides from the raw MS data[109–112]. A development that is essential for glycoproteomics to become a standard tool in the life sciences.

Scope and Outline

The research discussed in this dissertation describes the use and development of chemoenzymatic glycan labeling tools to both analyze and modify protein glycosylation on the cell surface.

In **Chapter 2**, the effects of dolichol deficiency on membrane protein *N*-glycosylation were analyzed. Dolichol deficiency is caused by a genetic defect in the polyprenol reductase enzyme that converts polyprenol to dolichol, leading to the congenital disorder of *N*-glycosylation SRD5A3-CDG. Dolichol is the most important lipid scaffold for oligosaccharides in the biosynthesis of glycoproteins with *N*-glycosylation, and thus a deficiency likely leads to protein hypoglycosylation. Previous studies found an underrepresentation of membrane proteins in dolichol-deficient CDG patient cells and in Lec9 cells. Lec9 cells are a CHO glycosylation mutant cell line that mimics the dolichol deficiency found in CDG patients. In this study we aimed to deepen our understanding of the effect of the dolichol deficiency on the glycosylation patterns and membrane abundance of membrane proteins. To accomplish this, we used a newly developed derivative for SEEL, containing an acid-cleavable linker that releases the biotin tag after enrichment. By using this next-generation SEEL for membrane glycoprotein enrichment coupled to hybrid MS fragmentation we were able to perform a proteome-wide glycoproteomics analysis of membrane proteins in Lec9 cells.

In **Chapter 3**, we investigated the evolution of receptor specificity of human influenza A/H3N2 viruses over the last decades. In the last decades, A/H3N2 viruses with altered receptor specificity have emerged. These viruses lost their ability to agglutinate fowl erythrocytes, thereby hampering the antigenic characterization of these viruses. Alterations in receptor specificity of representative A/H3N2 viruses over several evolutionary time points were studied using glycan microarray analysis. We tested the presence of these required receptors on fowl erythrocytes by glycomic analysis and developed glycan-remodeled erythrocytes presenting the required receptors of recent A/H3N2 viruses. Hemagglutination assays analyzed the agglutinating ability of recent A/H3N2 viruses toward our glycan-remodeled erythrocytes, and in collaboration with the department of Viroscience at Erasmus MC the cells were tested for their use in antigenic characterization of A/H3N2 viruses by hemagglutination inhibition (HI) assays.

The potential to extend the stability and thereby the shelf life of our glycan-remodeled erythrocytes is explored in **Chapter 4**. Glycan-remodeled erythrocytes were fixated with glutaraldehyde and the stability was tested in a series of weekly hemagglutination assays over the course of 20 weeks. The applicability of the fixated erythrocytes in HI assays was assessed using a subset of contemporary A/H3N2 viruses that show impaired agglutination of regular fowl erythrocytes and of which the antigenic properties are known. We visualized the data in an antigenic map using antigenic cartography.

Another important aspect in the influenza surveillance is the propagation of viruses from clinical samples. This propagation is essential to obtain the virus concentrations that are needed to perform antigenic characterization. Madin-Darby canine kidney (MDCK) cells are the most used cell line for the propagation of influenza viruses and are also used for the generation of cell-based influenza vaccines. Over the years, A/H3N2 viruses showed impaired propagation in MDCK cells, which recently led to the development of a genetically engineered MDCK cell line, called hCK. In hCK cells the prototypic human-

type glycan receptor, α2,6-linked sialic acid, is upregulated and the prototypic avian-type receptor, α2,3-linked sialic acid, is downregulated. As a result, recent A/H3N2 viruses propagate efficiently in hCK cells. However, besides the sialic acid patterns, information about the glycosylation in these cell lines is scarce. Therefore, in **Chapter 5**, we analyzed the *N*-glycosylation in both MDCK and hCK cells by glycomic analysis to assess potential differences in glycosylation other than the sialic acid linkages that can contribute to the increased infectivity of hCK cells toward A/H3N2 viruses.

References

1. Pascal Gagneux, Markus Aebi, A. V. Chapter 20 - Evolution of glycan diversity. in Essentials of Glycobiology, 3rd edition (2017). doi:10.1101/glycobiology.3e.020
2. James H. Prestegard, Jian Liu, G. W. Chapter 3- Oligosaccharides and Polysaccharides. in Essentials of Glycobiology, 3rd edition (2017). doi:10.1101/glycobiology.3e.003
3. Reily, C., Stewart, T. J., Renfrow, M. B. & Novak, J. Glycosylation in health and disease. Nat. Rev. Nephrol. 15, 346–366 (2019).
4. Moremen, K. W., Tiemeyer, M. & Nairn, A. V. Vertebrate protein glycosylation: Diversity, synthesis and function. Nat. Rev. Mol. Cell Biol. 13, 448–462 (2012).
5. Girirajan, S., Campbell, C. & Eichler, E. Cotranslational and posttranslocational N-glycosylation of proteins in the endoplasmic reticulum. Physiol. Behav. 176, 139–148 (2011).
6. Helenius, A. & Aebi, M. Roles of N-linked glycans in the endoplasmic reticulum. Annu. Rev. Biochem. 73, 1019–1049 (2004).
7. Haga, Y., Ishii, K. & Suzuki, T. N-glycosylation is critical for the stability and intracellular trafficking of glucose transporter GLUT4. J. Biol. Chem. 286, 31320–31327 (2011).
8. Xu, C. & Ng, D. T. W. Glycosylation-directed quality control of protein folding. Nat. Rev. Mol. Cell Biol. 16, 742–752 (2015).
9. Shental-Bechor, D. & Levy, Y. Effect of glycosylation on protein folding: A close look at thermodynamic stabilization. Proc. Natl. Acad. Sci. U. S. A. 105, 8256–8261 (2008).
10. Ohtsubo, K. & Marth, J. D. Glycosylation in Cellular Mechanisms of Health and Disease. Cell 126, 855–867 (2006).
11. Pinho, S. S. & Reis, C. A. Glycosylation in cancer: Mechanisms and clinical implications. Nat. Rev. Cancer 15, 540–555 (2015).
12. Van de Geijn, F. E. et al. Immunoglobulin G galactosylation and sialylation are associated with pregnancy-induced improvement of rheumatoid arthritis and the postpartum flare: Results from a large prospective cohort study. Arthritis Res. Ther. 11, 1–10 (2009).
13. Wang, X. et al. MK-8719, a novel and selective O-GlcNAcase inhibitor that reduces the formation of pathological tau and ameliorates neurodegeneration in a mouse model of tauopathy. J. Pharmacol. Exp. Ther. 374, 252–263 (2020).
14. Williams, S. E., Mealer, R. G., Scolnick, E. M., Smoller, J. W. & Cummings, R. D. Aberrant glycosylation in schizophrenia: a review of 25 years of post-mortem brain studies. Mol. Psychiatry 25, 3198–3207 (2020).
15. Péanne, R. et al. Congenital disorders of glycosylation (CDG): Quo vadis? Eur. J. Med. Genet. 61,

643–663 (2018).

16. Pérez-Cerdá, C. et al. A Population-Based Study on Congenital Disorders of Protein N- and Combined with O-Glycosylation Experience in Clinical and Genetic Diagnosis. J. Pediatr. 183, 170-177. e1 (2017).

17. Verheijen, J., Tahata, S., Kozicz, T., Witters, P. & Morava, E. Therapeutic approaches in Congenital Disorders of Glycosylation (CDG) involving N-linked glycosylation: an update. Genet. Med. 22, 268–279 (2020).

18. Ondruskova, N., Cechova, A., Hansikova, H., Honzik, T. & Jaeken, J. Congenital disorders of glycosylation: Still "hot" in 2020. Biochim. Biophys. Acta- Gen. Subj. 1865 (2021).

19. Dirk J. Lefeber, Hudson H. Freeze, Richard Steet, and T. K. Essentials of Glycobiology, Chapter 45- Congenital disorders of glycosylation.

20. Pamela Stanley, Naoyuki Taniguchi, M. A. Chapter 9- N-glycans. in Essentials of Glycobiology, 3rd edition (2017). doi:10.1101/glycobiology.3e.009

21. Lefeber, D. J., Morava, E. & Jaeken, J. How to find and diagnose a CDG due to defective N-glycosylation. J. Inherit. Metab. Dis. 34, 849–852 (2011).

22. Morava, É. et al. Congenital disorder of glycosylation type Ix: Review of clinical spectrum and diagnostic steps. J. Inherit. Metab. Dis. 31, 450–456 (2008).

23. Mohamed, M. et al. Clinical and diagnostic approach in unsolved CDG patients with a type 2 transferrin pattern. Biochim. Biophys. Acta- Mol. Basis Dis. 1812, 691–698 (2011).

24. Abu Bakar, N., Lefeber, D. J. & van Scherpenzeel, M. Clinical glycomics for the diagnosis of congenital disorders of glycosylation. J. Inherit. Metab. Dis. 41, 499–513 (2018).

25. Stanley, P. Selection of specific wheat germ agglutinin-resistant (WgaR) phenotypes from Chinese hamster ovary cell populations containing numerous lecR genotypes. Mol. Cell. Biol. 1, 687–696 (1981).

26. Stanley, P. & Siminovitch, L. Complementation between mutants of CHO cells resistant to a variety of plant lectins. Somatic Cell Genet. 3, 391–405 (1977).

27. Stanley, P., Caillibot, V. & Siminovitch, L. Selection and characterization of eight phenotypically distinct lines of lectin-resistant chinese hamster ovary cells. Cell 6, 121–128 (1975).

28. Stanley, P. Lectin-Resistant CHO Cells : Selection of New Mutant Phenotypes. 9 (1983).

29. Patnaik, S. K. & Stanley, P. Lectin-Resistant CHO Glycosylation Mutants. Methods Enzymol. 416, 159–182 (2006).

30. Lu, H., Sathe, A. A., Xing, C. & Lehrman, M. A. The Lec5 glycosylation mutant links homeobox genes with cholesterol and lipid-linked oligosaccharides. Glycobiology 29, 106–109 (2018).

31. Lefeber, D. J. et al. Deficiency of Dol-P-Man Synthase Subunit DPM3 Bridges the Congenital Disorders of Glycosylation with the Dystroglycanopathies. Am. J. Hum. Genet. 85, 76–86 (2009).

32. Schenk, B. et al. Erratum: MPDU1 mutations underlie a novel human congenital disorder of glycosylation, designated type if (Journal of Clinical Investigation (2001) 108 (1687-1695)). J. Clin. Invest. 111, 925 (2003).

33. He, P., Ng, B. G., Losfeld, M. E., Zhu, W. & Freeze, H. H. Identification of intercellular cell adhesion molecule 1 (ICAM-1) as a hypoglycosylation marker in congenital disorders of glycosylation cells. J. Biol. Chem. 287, 18210–18217 (2012).

34. Lin, B., Qing, X., Liao, J. & Zhuo, K. Role of Protein Glycosylation in Host-Pathogen Interaction. Cells 9, 1–24 (2020).

35. Rogers, G. N. & Paulson, J. C. Receptor determinants of human and animal influenza virus isolates: Differences in receptor specificity of the H3 hemagglutinin based on species of origin. Virology 127, 361–373 (1983).

36. Connor, R. J., Kawaoka, Y., Webster, R. G. & Paulson, J. C. Receptor Specificity in Human, Avian, and Equine H2 and H3 Influenza Virus Isolates. Virology 205, 17–23 (1994).

37. Stevens, J. et al. Glycan microarray analysis of the hemagglutinins from modern and pandemic influenza viruses reveals different receptor specificities. J. Mol. Biol. 355, 1143–1155 (2006).

38. Bateman, A. C. et al. Glycan analysis and influenza A virus infection of primary swine respiratory epithelial cells: The importance of NeuAcα2-6 glycans. J. Biol. Chem. 285, 34016–34026 (2010).

39. Chandrasekaran, A. et al. Glycan topology determines human adaptation of avian H5N1 virus hemagglutinin. Nat. Biotechnol. 26, 107–113 (2008).

40. Walther, T. et al. Glycomic Analysis of Human Respiratory Tract Tissues and Correlation with Influenza Virus Infection. PLoS Pathog. 9 (2013).

41. Nycholat, C. M. et al. Recognition of sialylated poly-N-acetyllactosamine chains on N- and O-linked glycans by human and avian influenza A virus hemagglutinins. Angew. Chemie- Int. Ed. 51, 4860–4863 (2012).

42. Gulati, S. et al. Human H3N2 Influenza Viruses Isolated from 1968 To 2012 Show Varying Preference for Receptor Substructures with No Apparent Consequences for Disease or Spread. PLoS One 8 (2013).

43. Yang, H. et al. Structure and receptor binding preferences of recombinant human A(H3N2) virus hemagglutinins. Virology 477, 18–31 (2015).

44. Peng, W. et al. Recent H3N2 Viruses Have Evolved Specificity for Extended, Branched Human-type Receptors, Conferring Potential for Increased Avidity. Cell Host Microbe 21, 23–34 (2017).

45. Baskin, J. M. & Bertozzi, C. R. Bioorthogonal click chemistry: Covalent labeling in living systems. QSAR Comb. Sci. 26, 1211–1219 (2007).

46. Sletten, E. M. & Bertozzi, C. R. Bioorthogonal chemistry: Fishing for selectivity in a sea of functionality. Angew. Chemie- Int. Ed. 48, 6974–6998 (2009).

47. McKay, C. S. & Finn, M. G. Click chemistry in complex mixtures: Bioorthogonal bioconjugation. Chem. Biol. 21, 1075–1101 (2014).

48. Kenry & Liu, B. Bio-orthogonal Click Chemistry for In Vivo Bioimaging. Trends Chem. 1, 763–778 (2019).

49. Saxon, E. & Bertozzi, C. R. Cell surface engineering by a modified Staudinger reaction. Science (80-.). 287, 2007–2010 (2000).

50. Saxon, E., Armstrong, J. I. & Bertozzi, C. R. A "traceless" Staudinger ligation for the chemoselective synthesis of amide bonds. Org. Lett. 2, 2141–2143 (2000).

51. Rostovtsev, V. V., Green, L. G., Fokin, V. V. & Sharpless, K. B. A stepwise huisgen cycloaddition process: Copper(I)-catalyzed regioselective "ligation" of azides and terminal alkynes. Angew. Chemie- Int. Ed. 41, 2596–2599 (2002).

52. Himo, F. et al. Copper(I)-catalyzed synthesis of azoles. DFT study predicts unprecedented reactiv-

ity and intermediates. J. Am. Chem. Soc. 127, 210–216 (2005).

53. Chen, Z. et al. Acute toxicological effects of copper nanoparticles in vivo. Toxicol. Lett. 163, 109–120 (2006).

54. Agard, N. J., Prescher, J. A. & Bertozzi, C. R. A strain-promoted [3 + 2] azide-alkyne cycloaddition for covalent modification of biomolecules in living systems. J. Am. Chem. Soc. 126, 15046–15047 (2004).

55. Baskin, J. M. et al. Copper-free click chemistry for dynamic in vivo imaging. Proc. Natl. Acad. Sci. U. S. A. 104, 16793–16797 (2007).

56. Ning, X., Guo, J., Wolfert, M. A. & Boons, G.-J. Visualizing Metabolically Labeled Glycoconjugates of Living Cells by Copper-Free and Fast Huisgen Cycloadditions. Angew. Chemie 120, 2285–2287 (2008).

57. Debets, M. F. et al. Aza-dibenzocyclooctynes for fast and efficient enzyme PEGylation via copper-free (3+2) cycloaddition. Chem. Commun. 46, 97–99 (2010).

58. Jewett, J. C., Sletten, E. M. & Bertozzi, C. R. Rapid Cu-free click chemistry with readily synthesized biarylazacyclooctynones. J. Am. Chem. Soc. 132, 3688–3690 (2010).

59. Devaraj, N. K., Weissleder, R. & Hilderbrand, S. A. Tetrazine-based cycloadditions: Application to pretargeted live cell imaging. Bioconjug. Chem. 19, 2297–2299 (2008).

60. Darko, A. et al. Conformationally strained trans-cyclooctene with improved stability and excellent reactivity in tetrazine ligation. Chem. Sci. 5, 3770–3776 (2014).

61. Kayser, H. et al. Biosynthesis of a nonphysiological sialic acid in different rat organs, using N-propanoyl-D-hexosamines as precursors. J. Biol. Chem. 267, 16934–16938 (1992).

62. Wieser, J. R., Heisner, A., Stehling, P., Oesch, F. & Reutter, W. In vivo modulated N-acyl side chain of N-acetylneuraminic acid modulates the cell contact-dependent inhibition of growth. FEBS Lett. 395, 170–173 (1996).

63. Lara K. Mahal, Kevin J. Yarema, Carolyn R. Bertozzi. Engineering chemical reactivity on cell surfaces through oligosaccharide biosynthesis. Science (80-.). 276, 1125–1128 (1997).

64. Saxon, E. et al. Investigating cellular metabolism of synthetic azidosugars with the Staudinger ligation. J. Am. Chem. Soc. 124, 14893–14902 (2002).

65. Rabuka, D., Hubbard, S. C., Laughlin, S. T., Argade, S. P. & Bertozzi, C. R. A chemical reporter strategy to probe glycoprotein fucosylation. J. Am. Chem. Soc. 128, 12078–12079 (2006).

66. Boyce, M. et al. Metabolic cross-talk allows labeling of O-linked β-N- acetylglucosamine-modified proteins via the N-acetylgalactosamine salvage pathway. Proc. Natl. Acad. Sci. U. S. A. 108, 3141–3146 (2011).

67. Vocadlo, D. J., Hang, H. C., Kim, E. J., Hanover, J. A. & Bertozzi, C. R. A chemical approach for identifying O-GlcNAc-modified proteins in cells. Proc. Natl. Acad. Sci. U. S. A. 100, 9116–9121 (2003).

68. Zhang, X. & Zhang, Y. Applications of azide-based bioorthogonal click chemistry in glycobiology. Molecules 18, 7145–7159 (2013).

69. Laughlin, S. T. et al. Metabolic Labeling of Glycans with Azido Sugars for Visualization and Glycoproteomics. Methods Enzymol. 415, 230–250 (2006).

70. Yoon, H. I. et al. Bioorthogonal Copper Free Click Chemistry for Labeling and Tracking of Chondro-

cytes In Vivo. Bioconjug. Chem. 27, 927–936 (2016).

71. Wang, H. et al. Metabolic labeling and targeted modulation of dendritic cells. Nat. Mater. 19, 1244–1252 (2020).

72. Lopez Aguilar, A. et al. Tools for Studying Glycans: Recent Advances in Chemoenzymatic Glycan Labeling. ACS Chem. Biol. 12, 611–621 (2017).

73. Paulson, J. C., Sadler, J. E. & Hill, R. L. Restoration of specific myxovirus receptors to asialoerythrocytes by incorporation of sialic acid with pure sialyltransferases. J. Biol. Chem. 254, 2120–2124 (1979).

74. Kajihara, Y. et al. Synthesis of CMP-9″-modified-sialic acids as donor substrate analogues for mammalian and bacterial sialyltransferases. Carbohydr. Res. 342, 1680–1688 (2007).

75. Ng Chee Ping. Selective exo-enzymatic labeling (SEEL) of N-glycans of living cells by recombinant ST6Gal1. Bone 23, 1–7 (2013).

76. Hong, S. et al. Bacterial glycosyltransferase-mediated cell-surface chemoenzymatic glycan modification. Nat. Commun. 10 (2019).

77. Moremen, K. W. et al. Expression system for structural and functional studies of human glycosylation enzymes. Nat. Chem. Biol. 14, 156–162 (2018).

78. Jiang, H. et al. Modulating Cell-Surface Receptor Signaling and Ion Channel Functions by In Situ Glycan Editing. Angew. Chemie- Int. Ed. 57, 967–971 (2018).

79. Briard, J. G., Jiang, H., Moremen, K. W., MacAuley, M. S. & Wu, P. Cell-based glycan arrays for probing glycan-glycan binding protein interactions. Nat. Commun. 9, 1–11 (2018).

80. Yu, S. H. et al. Selective exo-enzymatic labeling detects increased cell surface sialoglycoprotein expression upon megakaryocytic differentiation. J. Biol. Chem. 291, 3982–3989 (2016).

81. Wen, L. et al. A One-Step Chemoenzymatic Labeling Strategy for Probing Sialylated Thomsen-Friedenreich Antigen. ACS Cent. Sci. 4, 451–457 (2018).

82. Sun, T. et al. One-Step Selective Exoenzymatic Labeling (SEEL) Strategy for the Biotinylation and Identification of Glycoproteins of Living Cells. J. Am. Chem. Soc. 138, 11575–11582 (2016).

83. Capicciotti, C. J. et al. Cell-Surface Glyco-Engineering by Exogenous Enzymatic Transfer using a Bi-Functional CMP-Neu5Ac Derivative. J. Am. Chem. Soc. jacs.7b05358 (2017). doi:10.1021/jacs.7b05358

84. Li, J. et al. A Single-Step Chemoenzymatic Reaction for the Construction of Antibody-Cell Conjugates. ACS Cent. Sci. 4, 1633–1641 (2018).

85. Yang, Y., Franc, V. & Heck, A. J. R. Glycoproteomics : A Balance between High-Throughput and In-Depth Analysis. 35, 598–609 (2017).

86. Maley, F., Trimble, R. B., Tarentino, A. L. & Plummer, T. H. Characterization of glycoproteins and their associated oligosaccharides through the use of endoglycosidases. Anal. Biochem. 180, 195–204 (1989).

87. Szigeti, M. et al. Rapid N-glycan release from glycoproteins using immobilized PNGase F microcolumns. J. Chromatogr. B Anal. Technol. Biomed. Life Sci. 1032, 139–143 (2016).

88. Zhu, R. et al. Enhanced Quantitative LC-MS/MS Analysis of N-linked Glycans Derived from Glycoproteins Using Sodium Deoxycholate Detergent. J. Proteome Res. 17, 2668–2678 (2018).

89. Zhang, L. et al. Microwave irradiation-assisted high-efficiency N-glycan release using oriented

immobilization of PNGase F on magnetic particles. J. Chromatogr. A 1619 (2020).

90. Zhang, Y., Peng, Y., Yang, L. & Lu, H. Advances in sample preparation strategies for MS-based qualitative and quantitative N-glycomics. TrAC- Trends Anal. Chem. 99, 34–46 (2018).

91. Cao, W. Q. et al. Novel methods in glycomics: a 2019 update. Expert Rev. Proteomics 17, 11–25 (2020).

92. Davies, M., Smith, K. D., Harbin, A. M. & Hounsell, E. F. High-performance liquid chromatography of oligosaccharide alditols and glycopeptides on a graphitized carbon column. J. Chromatogr. A 609, 125–131 (1992).

93. Song, T., Aldredge, D. & Lebrilla, C. B. A Method for In-Depth Structural Annotation of Human Serum Glycans That Yields Biological Variations. Anal. Chem. 87, 7754–7762 (2015).

94. Buszewski, B. & Noga, S. Hydrophilic interaction liquid chromatography (HILIC)-a powerful separation technique. Anal. Bioanal. Chem. 402, 231–247 (2012).

95. Harvey, D. J. Derivatization of carbohydrates for analysis by chromatography; electrophoresis and mass spectrometry. J. Chromatogr. B Anal. Technol. Biomed. Life Sci. 879, 1196–1225 (2011).

96. Han, L. & Costello, C. E. Mass spectrometry of glycans. Biochem. 78, 710–720 (2013).

97. Huffman, J. E. et al. Comparative performance of four methods for high-throughput glycosylation analysis of immunoglobulin G in genetic and epidemiological research. Mol. Cell. Proteomics 13, 1598–1610 (2014).

98. Stavenhagen, K. et al. Quantitative mapping of glycoprotein micro-heterogeneity and macro-heterogeneity: An evaluation of mass spectrometry signal strengths using synthetic peptides and glycopeptides. J. Mass Spectrom. 48, 627–639 (2013).

99. Riley, N. M., Bertozzi, C. R. & Pitteri, S. J. A pragmatic guide to enrichment strategies for mass spectrometry-based glycoproteomics. Mol. Cell. Proteomics 20, 100029 (2021).

100. Li, H. et al. Chemoenzymatic Method for Glycoproteomic N-Glycan Type Quantitation. Anal. Chem. 92, 1618–1627 (2020).

101. Smeekens, J. M., Chen, W. & Wu, R. Mass spectrometric analysis of the cell surface n-glycoproteome by combining metabolic labeling and click chemistry. J. Am. Soc. Mass Spectrom. 26, 604–614 (2015).

102. Woo, C. M. et al. Mapping and quantification of over 2000 O-linked glycopeptides in activated human T cells with isotope-targeted glycoproteomics (Isotag). Mol. Cell. Proteomics 17, 764–775 (2018).

103. Woo, C. M., Iavarone, A. T., Spiciarich, D. R., Palaniappan, K. K. & Bertozzi, C. R. Isotope-targeted glycoproteomics (IsoTaG): A mass-independent platform for intact N- and O-glycopeptide discovery and analysis. Nat. Methods 12, 561–567 (2015).

104. Reiding, K. R., Bondt, A., Franc, V. & Heck, A. J. R. The benefits of hybrid fragmentation methods for glycoproteomics. TrAC- Trends Anal. Chem. 108, 260–268 (2018).

105. Riley, N. M., Malaker, S. A., Driessen, M. D. & Bertozzi, C. R. Optimal Dissociation Methods Differ for N- A nd O-Glycopeptides. J. Proteome Res. 19, 3286–3301 (2020).

106. Reiding, K. R. et al. Neutrophil myeloperoxidase harbors distinct site-specific peculiarities in its glycosylation. 294, 20233–20245 (2019).

107. Yu, Q. et al. Electron-Transfer/Higher-Energy Collision Dissociation (EThcD)-Enabled Intact Glyco-

peptide/Glycoproteome Characterization. J. Am. Soc. Mass Spectrom. 28, 1751–1764 (2017).

108. Riley, N. M., Hebert, A. S., Westphall, M. S. & Coon, J. J. Capturing site-specific heterogeneity with large-scale N-glycoproteome analysis. Nat. Commun. 10, 1–13 (2019).

109. Liu, M. Q. et al. PGlyco 2.0 enables precision N-glycoproteomics with comprehensive quality control and one-step mass spectrometry for intact glycopeptide identification. Nat. Commun. 8, 1–14 (2017).

110. Polasky, D. A., Yu, F., Teo, G. C. & Nesvizhskii, A. I. Fast and comprehensive N- and O-glycoproteomics analysis with MSFragger-Glyco. Nat. Methods 17, 1125–1132 (2020).

111. Bern, M., Kil, Y. J. & Becker, C. Byonic: Advanced peptide and protein identification software. Curr. Protoc. Bioinforma. 1–17 (2012). doi:10.1002/0471250953.bi1320s40

112. Cao, W. et al. Recent advances in software tools for more generic and precise intact glycopeptide analysis. Mol. Cell. Proteomics 20, 100060 (2021).

Chapter 2

SEEL-Enriched Membrane Glycoproteomics Reveals Hypoglycosylation to Be Site-Specific in Dolichol-Deficient Cells

Rosanne J. van Beek[1], Maria J. Moure[2], Mirjam J.A. Damen[3], Gerlof P. Bosman[1], Albert J.R. Heck[3,4], Karli R. Reiding[3,4], Geert-Jan Boons[1,4,5,6*]*

[1]Department of Chemical Biology & Drug Discovery, Utrecht Institute for Pharmaceutical Sciences, Utrecht University, 3584 CG Utrecht, The Netherlands;

[2]Chemical biology lab, CIC bioGUNE, Basque Research & Technology Alliance (BRTA), Bizkaia Technology Park, Building 800, 4816 Derio, Spain;

[3]Biomolecular Mass Spectrometry and Proteomics, Bijvoet Center for Biomolecular Research and Utrecht Institute for Pharmaceutical Sciences, University of Utrecht, 3584 CH Utrecht, The Netherlands;

[4]Netherlands Proteomics Center, The Netherlands;

[5]Complex Carbohydrate Research Center, University of Georgia, 315 Riverbend Rd, Athens, GA 30602, USA;

[6]Department of Chemistry, University of Georgia, Athens, GA 30602, USA.

2

Abstract

Protein glycosylation is essential to many biological functions, including protein folding, stability, protein translocation and cell-to-cell communication. For instance, while dolichol is an essential lipid scaffold for initiating protein *N*-glycosylation, genetic defects in its production may lead to hypoglycosylation and disrupt protein maturation pathway- a type I CDG. Studies have accordingly reported an underrepresentation of membrane proteins in dolichol-deficient CDG patient cells and Lec9 cells (a CHO mutant mimicking the CDG), although the actual state and effect of the *N*-glycosylation are still poorly understood. To investigate the glycosylation characteristics of the membrane proteins in a dolichol-deficient setting, we here synthesized and employed a next-generation functionalized CMP-sialic acid with cleavable linker that enables cleaving of the biotin tag after enrichment, effectively labeling and enriching cell-surface proteins by means of sialylation. We combined the enrichment with state-of-the-art LC-MS/MS to assess the heterogeneity of protein glycosylation. By this, we uncovered that hypoglycosylation within dolichol-deficient cells unexpectedly appears to be site-specific – an apparent new level of biological regulation that exists for protein glycosylation.

Introduction

Glycosylation is one of the most common and complex co- and posttranslational protein modifications. Typically, oligosaccharides are attached to proteins via serines or threonines (*O*-glycosylation) or via asparagines (*N*-glycosylation). Protein glycosylation is essential to many biological functions, including protein folding, stability, protein translocation and cell-to-cell communication[1–5], and changes in protein glycosylation can have dramatic biological effects[6–9]. This is exemplified by congenital disorders of glycosylation (CDGs), a rapidly growing family of genetic diseases[10]. CDGs are caused by deficiencies in genes involved in the glycan biosynthesis. Currently, a little over 150 CDG subtypes are known[11,12], of which *N*-glycosylation disorders are the most diagnosed. CDGs are typically classified as type 1 or type 2[13]. In type 1, genetic defects lead to protein hypoglycosylation (macroheterogeneity), while in type 2 the defects lead to altered processing of protein-linked glycan chains (microheterogeneity).

Glycosylation-deficient CHO cells form an important genetic model system to identify novel CDGs and aid to define the biological processes affected by the defective genes[14,15]. One such mutant CHO cell line, Lec9, is deficient in the synthesis of dolichol[16], the most important lipid carrier for the glycan precursor in the early stages of *N*-glycosylation[17], making it a good model to study type 1 CDGs. Previously, research using this cell line, as well as patient cell lines, identified a significant underrepresentation of several membrane proteins and specifically revealed intercellular adhesion molecule 1 (ICAM1) as a hypoglycosylation marker for the diagnosis of several type 1 CDGs[18]. While the above study was performed on a proteomics level, gaining insight into the glycosylation of the involved protein could greatly aid the etiological understanding of type 1 CDGs and may lead to novel insights toward diagnostic biomarkers and treatment.

MS is an attractive analytical method to analyze the glycoproteome. It offers a fast and sensitive readout and requires very low sample amounts. In the last decade, developments in fragmentation methods and improvements in software for automated glycopeptide identification have greatly increased the detection capacities in glycoproteomics[19–27]. Yet, despite the progress, MS analysis of complex glycoprotein samples is still challenging; high microheterogeneity of protein glycosylation significantly decreases detection compared to unmodified peptides, the hydrophilic nature of glycan moieties decreases ionization efficiency, and glycans can interfere with peptide fragmentation which hampers the identification of the underlying peptide. As a result, glycopeptide enrichment prior to measurements is the standard in glycoproteomic studies. On top of the challenges in glycopeptide detection, there is a unique challenge in the analysis of membrane glycoproteins. Their low abundance in comparison with the rest of the proteome, their low solubility due to their hydrophobic properties, and their lack of trypsin cleavage sites cause a bias against membrane proteins in many standard proteomic workflows[28].

SEEL is a technique that was developed for the specific labeling and enrichment of membrane glycoproteins[29,30]. SEEL uses the sialyltransferase ST6Gal1 to sialylate *N*-glycoproteins with a CMP-sialic acid functionalized at the C5 position by a biotin tag. It allows for very selective capturing of membrane *N*-glycoproteins, making it a valuable enrichment technique to gain further insights in, e.g., the effect of dolichol deficiency in Lec9 cells. However, the downside of a one-step SEEL approach for glycoproteomics is the large functional group that is attached to the glycan moiety upon labeling. Large functional groups can interfere with glycan fragmentation and hamper the identification of the labeled glycopeptides. In 2010, a cleavable biotin

linker containing a silane scaffold was developed for specific cleavage under mild condition to preserve glycosidic linkages in the biomolecules[31], and was shown to be compatible for glycoproteomics analysis using MS[32,33].

In the current study, we synthesized and employed a next-generation functionalized CMP-sialic acid with the cleavable linker that enables cleaving of the biotin tag after enrichment and combined this with state-of-the-art MS-based glycoproteomics. By this, we uncovered that hypoglycosylation within dolichol-deficient cells is remarkably site-specific – an apparent new level of biological regulation that exists for protein glycosylation.

Results

Synthesis of sialic acid derivative

To allow the enrichment of membrane glycoproteins from CHO-K1 and Lec9 cells and subsequent study by MS, we synthesized and tested an MS-compatible *N*-acetylneuraminic acid derivative with cleavable biotin affinity tag. Previously, it was shown that cytidine-5'-monophosphate (CMP)-Neu5Ac derivatives modified with a biotin at C-5 can be easily transferred to an *N*-acetyllactosamine (LacNAc) acceptor by sialyltransferases[30]. To make use of this characteristic, we synthesized CMP-sialic acid **derivative 2** to contain a biotin at the C-5 position, connected by a linker with an acid-cleavable dialkoxydiphenylsilane motif (Figure 1)[31]. Condensation of C-5 azido-modified mannosamine (**3**) was carried out with pyruvate and cytidine 5'-triphosphate (CTP) in the presence of the aldolase from Pasteurella multocida and recombinant CMP-sialic acid synthetase from *Neisseria meningitis*, yielding CMP-Neu5Ac **derivative 4**[34]. Then, a copper (I)-catalyzed alkyne-azide cycloaddition (CuAAC) was used to attach linker 5 to **derivative 4**[35]. Target **derivative 2** was ultimately formed by a copper (I)-catalyzed alkyne-azide in the presence of copper sulfate ($CuSO_4$), sodium ascorbate, and tris(benzyltriazolylmethyl)amine (TBTA), and was purified by size exclusion column chromatography over Biogel P2. To assess the labeling efficiency of **derivative 2**, we also synthesized the established SEEL *N*-acetylneuraminic acid derivative with non-cleavable biotin tag following previously published protocol[30], named **derivative 1**.

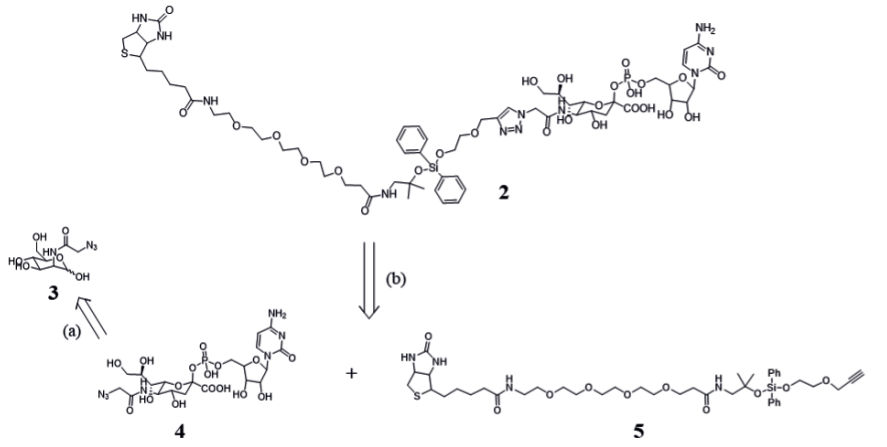

◄ Figure 1. Retrosynthesis scheme of derivative 2. Reagents and conditions: (**A**) Na pyruvate, CTP, 100 mM Tris-HCl buffer (20 mM MgCl2, pH 8.9), aldolase, CMP-sialic acid synthetase; (**B**) CuSO4, Na ascorbate, DMF/100 mM Tris-HCl buffer pH 7.5, TBTA.

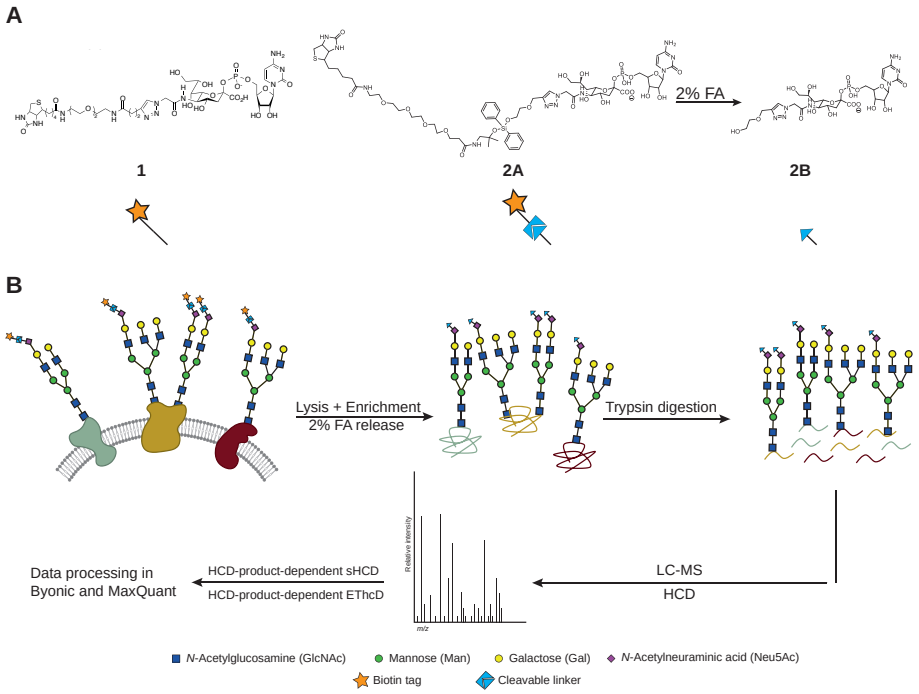

Figure 2. SEEL labeling derivatives, enrichment, and mass spectrometry workflow. (**A**) CMP-Neu5Ac derivative 1 with noncleavable biotin linker, and derivative 2 with cleavable silane linker, resulting in 2B upon incubation with 2% FA. (**B**) SEEL labeled cells are enriched using streptavidin Sepharose and released using 2% FA. Captured proteins labeled with derivative 2B are in-gel digested and analyzed on an Orbitrap Fusion MS.

MS/MS fragmentation of the cleavable linker on serotransferrin

We assessed the behavior of the linker during MS/MS fragmentation on labeled serotransferrin, a glycoprotein carrying two complex-type *N*-glycans on Asn432 and Asn630. Serotransferrin was labeled with the original non-cleavable SEEL derivative (**derivative 1**, Figure 2A), as well as with the cleavable SEEL derivative (**derivative 2**, Figure 2A), using ST6GAL1 in the presence of an *Arthrobacter ureafaciens* (AU) sialidase for 2 h at 37 °C. Afterward, the linker was cleaved by incubation in 2% formic acid (FA) to release the biotin. Finally, the labeled serotransferrin was proteolytically digested with trypsin before LC-MS(/MS) measurements.

For MS/MS, we applied a set of hybrid fragmentation methods for identification of both peptides and glycans[36,37]: 1) HCD, 2) HCD-product-dependent stepping-energy HCD (HCD-pd-sHCD) and 3) HCD-product-dependent electron-transfer/higher-energy collisional dissociation (HCD-pd-EThcD) (Figure 2B). Fragmentation spectra identified on both *N*-glycosylation sites on the labeled serotransferrins (Asn432 and Asn630) were compared with spectra identified in unlabeled serotransferrin and serotransferrin labeled with **derivative 1** (Figure 3). In general, compared to **derivative 1**, **derivative 2** yielded higher intensity oxonium ions and lower

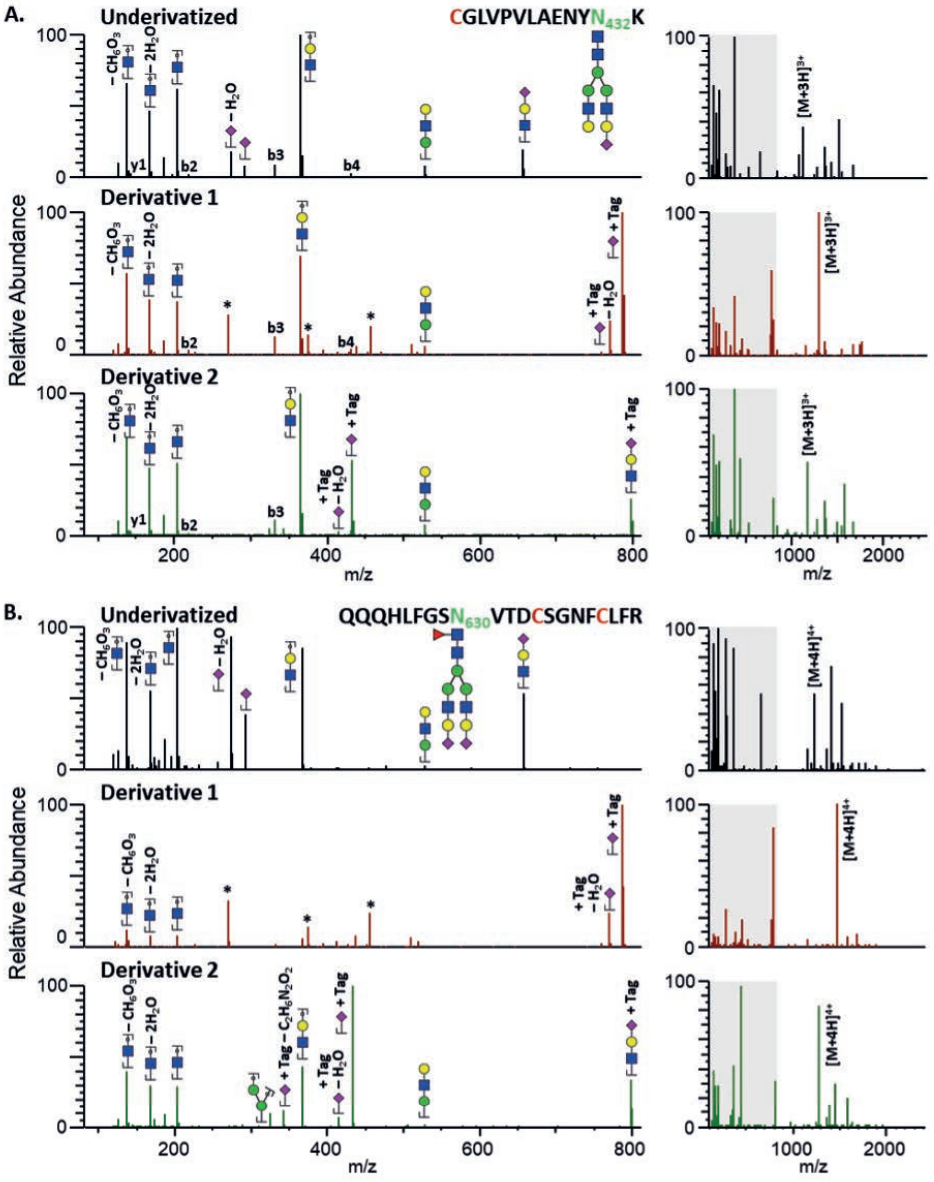

Figure 3. Fragment spectra of two common serotransferrin glycopeptides, covering (**A**) Asn432 and (**B**) Asn630, after stepping-HCD at NCEs of 10, 25 and 40%. The zoom-ins of the oxonium ion range (left; m/z 120-820) correspond with the grey areas of the full spectra (right; m/z 120-2400). Listed from top to bottom are the same glycopeptides with underivatized sialic acids (residue mass 291.0954 Da), as well as their derivatives 1 (786.3218 Da) and 2 (432.1492 Da). Asterisks indicate additional fragmentation products which co-appear with sialylated glycopeptides of derivative 1, but which have not been further characterized.

intensity unfragmented precursor – both beneficial for glycopeptide sequencing. The short linker 2B gave an increment mass of 141.054 Da over the unmodified sialic acid and could be identified in fragmentation spectra with an oxonium ion at m/z 433.157. As this m/z value was ubiquitously present in sialylated glycopeptides, it was included in further experiments for the targeted triggering of labeled glycopeptides (Supplementary Table 1).

Labeling efficiency of the cleavable linker derivative

We then determined whether there are any effects of the silane linker on labeling efficiency on cell lines, relative to the previously reported biotin derivative for 1-step SEEL[38]. To achieve this, CHO-K1 and Jurkat cells were labeled with the original non-cleavable SEEL derivative (**derivative 1**, Figure 2A) and the cleavable SEEL derivative (**derivative 2**, Figure 2A) as described previously. The labeling efficiency of both derivatives was then compared by an SDS-PAGE of the labeled cell lysates with subsequent Western blotting using an anti-biotin HRP antibody (Supplementary Figure 1). The experiment showed no significant differences in both signal intensity and pattern between both derivatives. We therefore concluded that the silane linker on **derivative 2** did not interfere with the labeling efficiency.

Workflow for glycoproteomic analysis of CHO-K1 and Lec9 cells

With the knowledge that **derivative 2** is cell-line- and MS-compatible, and facilitates triggering events for MS/MS fragmentation, we moved on to compare the protein expression levels and glycosylation patterns of membrane proteins in CHO-K1 cells and the glycosylation mutant cell line Lec9 (Figure 2B). Cells from both cell lines were labeled with **derivative 2** using the procedure as described above – in biological triplicates across different cell passages (Supplementary Figure 2). Labeled glycoproteins were captured from 1 mg cell lysate by streptavidin Sepharose affinity chromatography and released via the cleavable linker by incubation with 2% FA. Released glycoproteins were in-gel digested with trypsin (Supplementary Figure 3) and no further glycopeptide enrichment was performed to ensure the identification of both occupied and unoccupied *N*-glycan sites on the captured proteins. The digested peptides were separated by reversed-phase LC and analyzed on an Orbitrap Fusion mass spectrometer using the same hybrid fragmentation strategy as mentioned before. Triggering of the different methods occurred upon the detection of glycan-derived oxonium ions or detection of the oxonium ion of the modified sialic acid (Supplementary Table 1).

Quantitative proteomic analysis of CHO-K1 and Lec9 cells

Label-free protein quantification was performed using MaxQuant. Since only 241 proteins of the Chinese Hamster proteome (Cricetulus griseus) are reviewed on Uniprot, we used the unreviewed proteome for our searches (56,342 proteins). Identified peptides were curated on the minimal detection of two unique peptides and presence in two or more samples, which led to the identification of 3857 proteins (Figure 4A, Table S2). Despite the limited available information about the proteome of Chinese hamster cells in UniProt, we could assign a subcellular location to 1628 proteins by making use of the retrieve/ID mapping tool. As such, 30% of all assigned proteins could be assigned as membrane proteins (Figure 4B), other abundant classifications being the cytoplasm and nucleus.

Comparing CHO-K1 and Lec9 cells, 68 proteins showed a significant alteration in abundance of at least twofold between the cell lines ($p \leq 0.05$) (Figure 4A). 22 of the 68 proteins were overexpressed in CHO-K1, of which 13 could be assigned as membrane proteins. In Lec9 cells

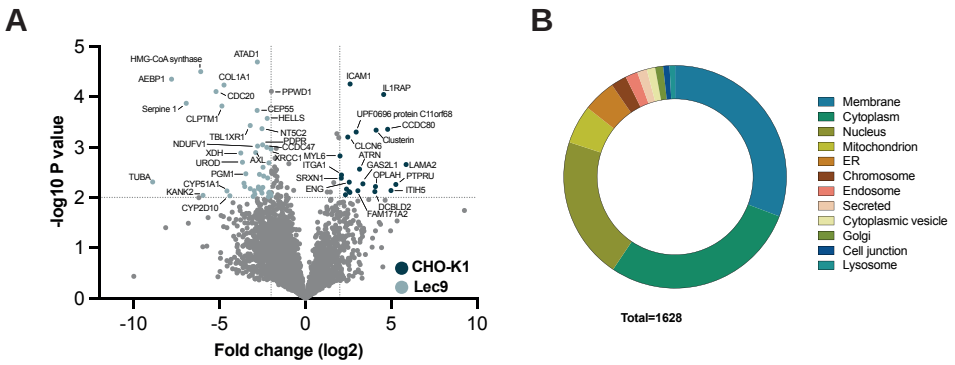

Figure 4. Proteomic statistics. (**A**) Volcano plot of enriched proteins quantified between CHO-K1 and Lec9 cells in triplicate. Light blue dots represent significantly enriched proteins in Lec9 cells compared to CHO-K1 cells (-log10 p-value > 2, fold change > 2), dark blue dots represent significantly enriched proteins in CHO-K1 cells compared to Lec9 cells (-log10 p-value > 2, fold change > 2). (**B**) Distribution of subcellular compartments assigned by UniProt. 1628 proteins from the total of 3857 detected proteins could be assigned to a subcellular location.

46 proteins were significantly overexpressed, of which nine were membrane proteins (see Supplementary Table 3 for a full list of protein detections). The most significant overexpressed protein in CHO-K1 cells was ICAM1 ($p = 5.6 \cdot 10^{-5}$, log2 fold change = 2.59), the same protein that was previously assigned as hypoglycosylation marker due to underexpression in Lec9 cells. To further investigate the changes in glycosylation patterns, and the potential correlation with the protein abundances in both cell lines, we continued with a glycopeptide analysis using Byonic.

Site-specific hypoglycosylation of *N*-glycan sites in Lec9 cells

For the analysis of protein glycosylation patterns and site occupancy, the raw MS data were analyzed with Byonic. 246 *N*-glycan compositions following the biosynthetic pathway were included (see Supplementary Table 4 for the full list)[39]. Then, for each composition, a modification of up to four branches by the silane linker were included, resulting in a total of 556 glycan inclusions for the search. Since several CHO glycosylation mutant cell lines are known to show a rich fucosylation pattern[40], we included up to five fucose moieties on the *N*-glycan structures. In addition, to cover possibly truncated and lysosomal compositions, we included pauci- and phosphomannosylated structures as well. After the search, the Byonic output was curated as previously established (score ≥ 150, |log prob| ≥ 1 and delta mod ≥ 10)[41], and triplicates were combined per cell line. In CHO-K1 cells, we identified a total of 1050 unique glycopeptides belonging to 189 glycoproteins (Supplementary Table 5). In Lec9 cells, we identified a total of 734 unique glycopeptides belonging to 97 glycoproteins (Supplementary Table 6).

First, we analyzed the occupancy of *N*-glycan sites in the cell lines by comparing the number of detected Asn-Xxx-Thr/Ser sequences with the glycosylated variants thereof (Figure 5A). In doing so, we detected in CHO-K1 cells across samples an average of 8893 putative *N*-glycopeptides, of which 1422 were occupied (15.8 %). In the Lec9 cells, on the other hand, a total of 11,376 putative *N*-glycopeptides only displayed occupancy of 936 sites (8.1 %). As such,

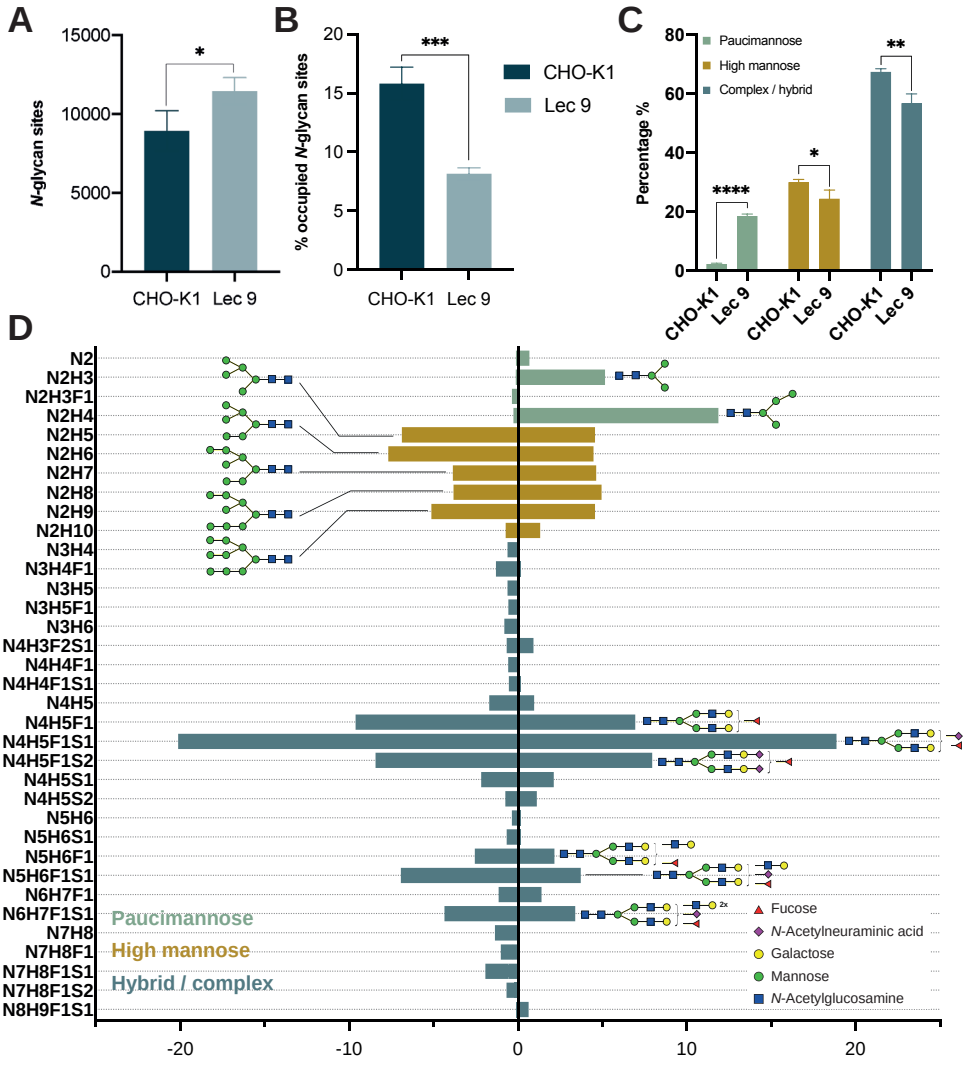

Figure 5. Quantitative overview of N-glycopeptide detections. (**A**) Average detected *N*-glycan sites and (**B**) percentage of occupied *N*-glycan sites in CHO-K1 and Lec9 cells. Data was analyzed with an unpaired t-test (n=3); total *N*-glycan sites ($p = 0.04$), percentage unoccupied *N*-glycan sites ($p = 0.0009$). (**C**) Comparison of quantitative glycan type distribution between CHO-K1 and Lec9 cells. The data was analyzed with an unpaired t-test (n = 3); high-mannose ($p = 0.03$), hybrid/complex ($p = 0.005$), paucimannose ($p < 0.0001$). (**D**) Relative distribution of glycoforms detected in CHO-K1 cells (left) and Lec9 cells (right). Shown are all detected glycoforms with 1% abundance or higher. H = hexose, N = N-acetylhexosamine, F = deoxyhexose (fucose), S = N-acetylneuraminic acid.

we detected a 1.9-fold lower *N*-glycosylation site occupancy in Lec9 cells compared to their CHO-K1 counterparts ($p < 0.001$, Figure 5B), indicating that the expected CDG type I effect of dolichol deficiency could be readily determined from our MS analyses.

We then made an overview of the different glycan types detected in both cell lines. Our SEEL labeling strategy biases our capture toward glycoproteins containing at least one complex-type *N*-glycan containing a terminal galactose as a substrate for the sialyltransferase ST6GAL1. All additional glycosylation sites on the same proteins will however be co-captured, allowing us to not only analyze complex-type *N*-glycans but also look at the distribution of other glycosylation types within the cell lines. In general, both CHO-K1 and Lec9 cells were mostly decorated with diantennary complex and high-mannose *N*-glycans (Figure 5C and 5D). Next to this, we unexpectedly identified a 7.7-fold increase in the presence of paucimannose structures in Lec9 cells ($p < 0.0001$) (Figure 5C). For both high-mannose structures and complex glycans, detections were increased 1.2-fold in CHO-K1 cells ($p = 0.03$ and $p = 0.005$).

To see whether the underoccupancy of *N*-glycosylation sites correlated with protein abundance, we selected 16 proteins with rich glycopeptide information in both cell lines and plotted the underoccupancy per protein: galectin-3-binding protein (Gal-3BP), prolow-density lipoprotein receptor-related protein 1 (LRP1), urikonase plasminogen activator surface receptor, basigin

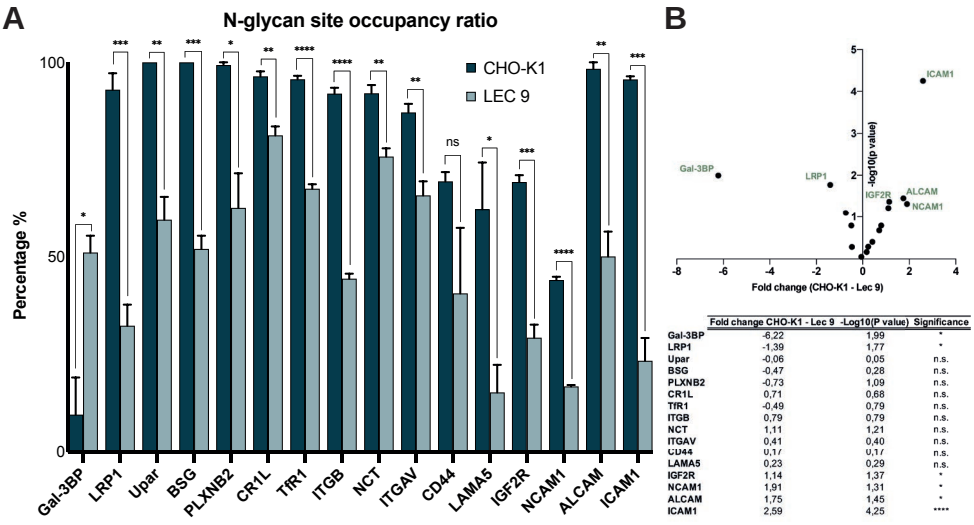

Figure 6. Relative N-glycan site occupancy of 16 membrane proteins. (**A**) Average *N*-glycan site occupancy detected in CHO-K1 and Lec9 cells (n = 3) in enriched membrane proteins. Differences are analyzed using an unpaired t-test (* = p <0.05, ** = p <0.01, *** = p <0.001, **** = p <0.0001) (**B**) relative abundance of the proteins in CHO-K1 and Lec9 cells. Plotted are the fold-change differences in abundance based on the MaxQuant iBAQ values.

(BSG), plexin-B2 (PLXNB2), complement component receptor 1-like protein (CR1L), transferrin receptor protein 1 (TfR1), integrin beta (ITGB), nicastrin (NCT), integrin alpha-V (ITGAV), CD44, laminin subunit alpha-5 (LAMA5), cation-independent mannose-6-phosphate receptor (IGF2R), neural cell adhesion molecule 1 (NCAM1), activated leucocyte cell adhesion molecule (ALCAM), as well as intercellular adhesion molecule 1 (ICAM1) (Figure 6A). Out of 16 proteins, 14 showed a significant decrease in site occupancy in Lec9 cells, ranging from 1.2-fold in CR1L to 4.1-fold in LAMA5 and ICAM1. The same trend was visible in CD44, albeit not significant. Interestingly, one protein, Gal-3BP, showed a 5.4-fold increase in occupancy in Lec9 cells.

We plotted the relative abundance of all 16 proteins in both cell lines to identify a potential correlation between the altered occupancy and membrane abundance (Figure 6B). Galectin-3-binding protein and LRP1 were significantly enriched in Lec9 cells, whereas IGF2R, NCAM1, ALCAM and ICAM1 were significantly enriched in CHO-K1. Even though Gal-3BP and ICAM1 showed a clear correlation between *N*-glycosylation site occupancy and protein abundance, this direct correlation could not be found when looking at all 16 proteins ($r = 0.1559$).

To further study the underoccupancy in Lec9 cells, we mapped the site-specific *N*-glycan distribution of ICAM1 and LRP1, which showed a similar pattern in underoccupancy but an opposite pattern in membrane abundance (Figure 7). In our measurements, we detected six out of 10 theoretical *N*-glycan sites on ICAM1 and 10 out of 49 theoretical *N*-glycan sites on LRP1. For the sites detected, ICAM1 showed almost full site occupancy in CHO-K1 cells, with a low percentage of underoccupancy at Asn355 specifically (Figure 7A). In Lec9 cells on the other hand, ICAM1 showed a complete unoccupancy of *N*-glycans at sites Asn204 and Asn355 (Figure 7A), and 88% unoccupancy at Asn185. Two *N*-glycan sites (Asn149 and Asn449) were fully occupied in Lec9 cells, showing a clear site-specificity in hypoglycosylation. The other example protein, LRP1, showed a clear site-specific distinction in occupancy as well (Figure 7B). However, for LRP1 the underoccupancy was more distributed across the different *N*-glycan sites and Asn3769 and Asn3883 showed significant underoccupancy in CHO-K1 cells as well. Interestingly, in both proteins the sites carrying high-mannose glycosylation appeared spared from dolichol-induced macroheterogeneity, instead showing a switch toward paucimannose structures.

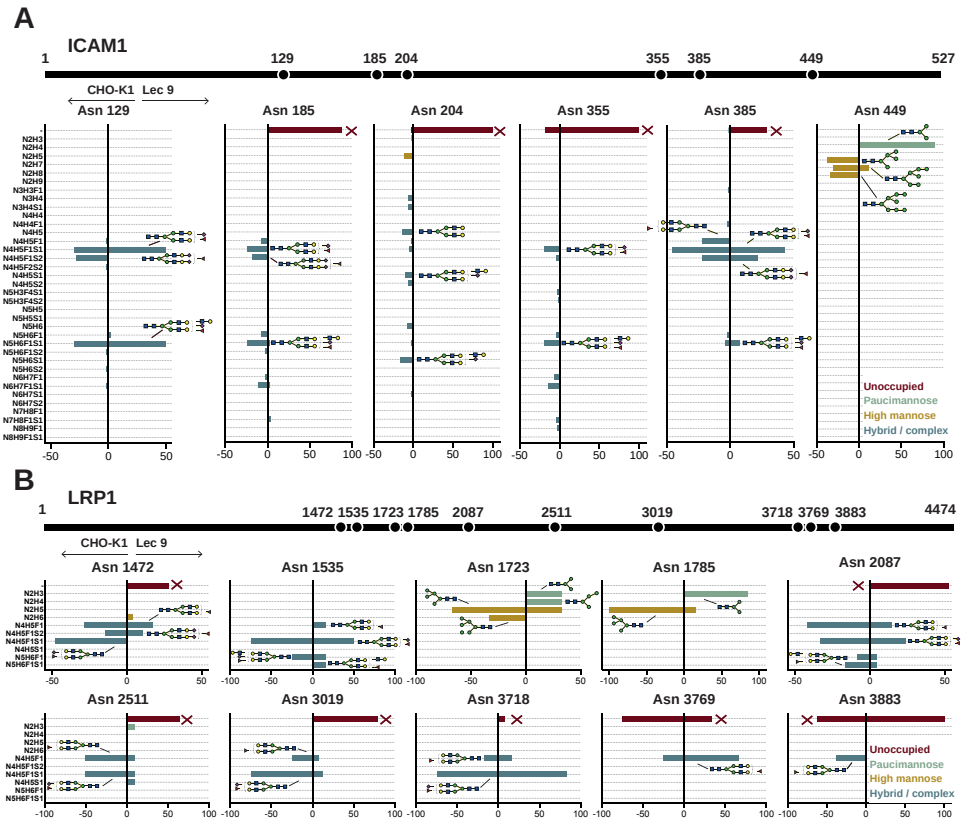

Figure 7. Site-specific distribution of N-linked glycosylation on ICAM1 and LRP1 proteins. (**A**) Site-specific distribution of all detected *N*-glycan sites on ICAM1 in CHO-K1 (left) and Lec9 (right). (**B**) Site-specific distribution of all detected *N*-glycan sites on LRP1 in CHO-K1 (left) and Lec9 (right) cells. Non-occupancy mainly occurs in the impaired Lec9 cell line, but not for all *N*-glycosylation sites.

Discussion

To improve the compatibility of SEEL with glycoproteomic analysis, and to add to the toolbox for glycosylation analysis, we here present a glycoproteomics workflow that allows for a proteome-wide analysis of the *N*-glycosylation after membrane-protein enrichment. Using the workflow, we could identify that dolichol deficiency in CHO cell lines (via Lec9), leads to an overall underoccupancy of *N*-glycan sites. Importantly, we could also identify that changes in *N*-glycan site occupancy differed wildly on a protein-specific level, and that even within a given protein not all glycosylation sites were affected equally.

The cleavable linker in **derivative 2** led to an increased fragmentation efficiency and generated a stable linker fragment that could be used as a fragmentation trigger to further increase the sensitivity of the glycopeptide detections. Thereby, the use of **derivative 2** made SEEL better compatible with a proteome-wide analysis of *N*-glycosylation by MS-based glycoproteomics. Even though the co-capturing of intracellular proteins could not be avoided in its entirety, the SEEL labeling provided an enrichment of membrane proteins, and a rich glycopeptide detec-

tion that would otherwise have been challenging for a complex sample like a cell lysate.

Type I CDGs lead to unoccupied glycan sites[13]. It has been rationalized that this underoccupancy leads to an underrepresentation of membrane proteins, which was shown by He et al. in a quantitative proteomic analysis of the Lec9 CHO mutants and patient cell lines, in which ICAM1 was identified as a hypoglycosylation marker for type 1 CDGs[18]. Interestingly, while we replicated this underrepresentation of ICAM1 in Lec9 cells from the previous study, now with site-specific glycoprofiling, we generally did not observe a correlation between protein hypoglycosylation and membrane abundances. The lack of correlation can have multiple reasons. For instance, genetic defects leading to the misfolding of proteins in the ER can activate the unfolded-protein response (UPR), which increases the expression of target proteins and thereby can restore cellular homeostasis upon cellular stress[42,43]. Many genes involved in protein glycosylation and lipid synthesis are able to activate the UPR upon gene depletion, so it can be reasoned that the UPR is able to (partly) compensate the expression levels of proteins that are affected by the hypoglycosylation[44,45]. One other explanation would be that the effect of individual *N*-glycosylation on protein folding or stability is variable. Where one site might be critical to define protein folding and function, other sites might have no effect on the stability of the protein[2]. Additional research into individual proteins appears to be a necessity to understand the interplay between site occupancy and membrane localization.

The lack of correlation between the hypoglycosylation and the membrane localization of proteins in this study suggests that not only membrane occupancy, but also the quality of the proteins present on the membrane are affected by the dolichol deficiency. The significant increase in paucimannose structures in Lec9 cells underlines this change in glycosylation quality. Paucimannose glycans have been associated with cell aging, inflammation and tumorogenesis[46–48], therefore the presence of the glycosylation characteristic implies a decreased protein quality. Recently, paucimannose structures have also been linked to a presence of proteins in the lysosome[37], suggesting that a part of the detected proteins in Lec9 cells might have been shuttled to the lysosome for degradation.

Even though CHO-K1 and Lec9 cells form a solid model system to study genetic defects, caution is always needed when interpreting intricate cellular effects in non-human immortalized cell lines. Therefore, further study in a biologically more relevant system, like patient cells, is a valuable way to confirm the results obtained here. Nevertheless, the information gained in this study about the effect of glycosylation defects on protein behavior aids in a better understanding of type 1 CDGs, and will help us to deepen our knowledge about the functions of *N*-glycosylation on protein behavior.

To conclude, we here presented an in-depth site-specific *N*-glycosylation characterization of membrane glycoproteins between two cell lines - representative of type 1 CDG - facilitated by improvements in SEEL labeling for membrane glycoprotein enrichment. With this platform, we identified site-specific *N*-glycosylation alterations in dolichol-deficient Lec9 cells, thereby showing that dolichol deficiency-induced glycan macroheterogeneity is unexpectedly site-specific.

Acknowledgments

This project is supported by the Netherlands Organization for Scientific Research (NWO TOPPUNT 718.015.003) to G.-J.B.. K.R.R. acknowledges support from NWO project number VI.Veni.192.058. We thank Prof. Dr. Pamela Stanley (Albert Einstein College of Medicine, New York) for kindly providing Lec9 cells.

Author Contributions

G.-J.B., K.R.R., and R.J.vB. designed the project; M.J.M. synthesized the derivatives; G.P.B. labeled the serotransferrin; R.J.vB., K.R.R., and M.J.A.D. performed the remaining experiments; R.J.vB. performed data analysis; G.-J.B. and K.R.R. provided scientific guidance on experimental setup and data interpretation; R.J.vB., K.R.R., and M.J.M. wrote the manuscript; all authors provided comments and suggestions on the manuscript.

References

1. Haga, Y., Ishii, K. & Suzuki, T. N-glycosylation is critical for the stability and intracellular trafficking of glucose transporter GLUT4. J. Biol. Chem. 286, 31320–31327 (2011).
2. Shental-Bechor, D. & Levy, Y. Effect of glycosylation on protein folding: A close look at thermodynamic stabilization. Proc. Natl. Acad. Sci. U. S. A. 105, 8256–8261 (2008).
3. Gu, J. et al. Potential roles of N-glycosylation in cell adhesion. Glycoconj. J. 29, 599–607 (2012).
4. Rudd, P. M., Wormald, M. R. & Dwek, R. A. Glycosylation and the immune system. J. Protein Chem. 17, 519 (1998).
5. Esmail, S. & Manolson, M. F. Advances in understanding N-glycosylation structure, function, and regulation in health and disease. Eur. J. Cell Biol. 100, 151186 (2021).
6. Reily, C., Stewart, T. J., Renfrow, M. B. & Novak, J. Glycosylation in health and disease. Nat. Rev. Nephrol. 15, 346–366 (2019).
7. Yuzwa, S. A. et al. Increasing O-GlcNAc slows neurodegeneration and stabilizes tau against aggregation. Nat. Chem. Biol. 8, 393–399 (2012).
8. Pinho, S. S. & Reis, C. A. Glycosylation in cancer: Mechanisms and clinical implications. Nat. Rev. Cancer 15, 540–555 (2015).
9. Tucholski, J. et al. Abnormal N-linked glycosylation of cortical AMPA receptor subunits in schizophrenia. Schizophr. Res. 146, 177–183 (2013).
10. Ng, B. G. & Freeze, H. H. Perspectives on Glycosylation and Its Congenital Disorders. Trends Genet. 34, 466–476 (2018).
11. Ondruskova, N., Cechova, A., Hansikova, H., Honzik, T. & Jaeken, J. Congenital disorders of glycosylation: Still “hot” in 2020. Biochim. Biophys. Acta- Gen. Subj. 1865 (2021).
12. Verheijen, J., Tahata, S., Kozicz, T., Witters, P. & Morava, E. Therapeutic approaches in Congenital Disorders of Glycosylation (CDG) involving N-linked glycosylation: an update. Genet. Med. 22, 268–279 (2020).
13. Péanne, R. et al. Congenital disorders of glycosylation (CDG): Quo vadis? Eur. J. Med. Genet. 61, 643–663 (2018).

14. Aebi, M. & Hennet, T. Congenital disorders of glycosylation: Genetic model systems lead the way. Trends Cell Biol. 11, 136–141 (2001).

15. Patnaik, S. K. & Stanley, P. Lectin-Resistant CHO Glycosylation Mutants. Methods Enzymol. 416, 159–182 (2006).

16. Rosenwald, A. G. & Krag, S. S. Lec9 CHO glycosylation mutants are defective in the synthesis of dolichol. J. Lipid Res. 31, 523–533 (1990).

17. Burda, P. & Aebi, M. The dolichol pathway of N-linked glycosylation. Biochim. Biophys. Acta- Gen. Subj. 1426, 239–257 (1999).

18. He, P., Ng, B. G., Losfeld, M. E., Zhu, W. & Freeze, H. H. Identification of intercellular cell adhesion molecule 1 (ICAM-1) as a hypoglycosylation marker in congenital disorders of glycosylation cells. J. Biol. Chem. 287, 18210–18217 (2012).

19. Khatri, K. et al. Comparison of Collisional and Electron-Based Dissociation Modes for Middle-Down Analysis of Multiply Glycosylated Peptides. J. Am. Soc. Mass Spectrom. 29, 1075–1085 (2018).

20. Riley, N. M., Malaker, S. A., Driessen, M. D. & Bertozzi, C. R. Optimal Dissociation Methods Differ for N- A nd O-Glycopeptides. J. Proteome Res. 19, 3286–3301 (2020).

21. Reiding, K. R., Bondt, A., Franc, V. & Heck, A. J. R. The benefits of hybrid fragmentation methods for glycoproteomics. TrAC- Trends Anal. Chem. 108, 260–268 (2018).

22. Reiding, K. R. et al. Neutrophil myeloperoxidase harbors distinct site-specific peculiarities in its glycosylation. J. Biol. Chem. 294, 20233–20245 (2019).

23. Riley, N. M., Hebert, A. S., Westphall, M. S. & Coon, J. J. Capturing site-specific heterogeneity with large-scale N-glycoproteome analysis. Nat. Commun. 10, 1–13 (2019).

24. Polasky, D. A., Yu, F., Teo, G. C. & Nesvizhskii, A. I. Fast and comprehensive N- and O-glycoproteomics analysis with MSFragger-Glyco. Nat. Methods 17, 1125–1132 (2020).

25. Cao, W. et al. Recent advances in software tools for more generic and precise intact glycopeptide analysis. Mol. Cell. Proteomics 20, 100060 (2021).

26. Liu, M. Q. et al. PGlyco 2.0 enables precision N-glycoproteomics with comprehensive quality control and one-step mass spectrometry for intact glycopeptide identification. Nat. Commun. 8, 1–14 (2017).

27. Bern, M., Kil, Y. J. & Becker, C. Byonic: Advanced peptide and protein identification software. Curr. Protoc. Bioinforma. 1–17 (2012). doi:10.1002/0471250953.bi1320s40

28. Waas, M. et al. Combine and conquer: Surfactants, solvents, and chaotropes for robust mass spectrometry based analyses of membrane proteins. Anal. Chem. 86, 1551–1559 (2014).

29. Capicciotti, C. J. et al. Cell-Surface Glyco-Engineering by Exogenous Enzymatic Transfer using a Bi-Functional CMP-Neu5Ac Derivative. J. Am. Chem. Soc. jacs.7b05358 (2017). doi:10.1021/jacs.7b05358

30. Sun, T. et al. One-Step Selective Exoenzymatic Labeling (SEEL) Strategy for the Biotinylation and Identification of Glycoproteins of Living Cells. J. Am. Chem. Soc. 138, 11575–11582 (2016).

31. Szychowski, J. et al. Cleavable biotin probes for labeling of biomolecules via azide-alkyne cycloaddition. J. Am. Chem. Soc. 132, 18351–18360 (2010).

32. Woo, C. M., Iavarone, A. T., Spiciarich, D. R., Palaniappan, K. K. & Bertozzi, C. R. Isotope-targeted

glycoproteomics (IsoTaG): A mass-independent platform for intact N- and O-glycopeptide discovery and analysis. Nat. Methods 12, 561–567 (2015).

33. Woo, C. M. et al. Mapping and quantification of over 2000 O-linked glycopeptides in activated human T cells with isotope-targeted glycoproteomics (Isotag). Mol. Cell. Proteomics 17, 764–775 (2018).

34. Yu, H., Yu, H., Karpel, R. & Chen, X. Chemoenzymatic synthesis of CMP-sialic acid derivatives by a one-pot two-enzyme system: Comparison of substrate flexibility of three microbial CMP-sialic acid synthetases. Bioorganic Med. Chem. 12, 6427–6435 (2004).

35. Woo, C. M. et al. Development of IsoTaG, a Chemical Glycoproteomics Technique for Profiling Intact N- and O-Glycopeptides from Whole Cell Proteomes. J. Proteome Res. 16, 1706–1718 (2017).

36. Reiding, K. R., Bondt, A., Franc, V. & Heck, A. J. R. Trends in Analytical Chemistry The benefits of hybrid fragmentation methods for glycoproteomics. 108, 260–268 (2018).

37. Reiding, K. R. et al. Neutrophil myeloperoxidase harbors distinct site-specific peculiarities in its glycosylation. 294, 20233–20245 (2019).

38. Wen, L. et al. A One-Step Chemoenzymatic Labeling Strategy for Probing Sialylated Thomsen-Friedenreich Antigen. ACS Cent. Sci. 4, 451–457 (2018).

39. Stanley, P., Taniguchi, N., Aebi, M. Chapter 9- N-glycans. in Essentials of Glycobiology, 3rd edition (2017).

40. North, S. J. et al. Glycomics profiling of Chinese hamster ovary cell glycosylation mutants reveals N-glycans of a novel size and complexity. J. Biol. Chem. 285, 5759–5775 (2010).

41. Reiding, K. R., Lin, Y. H., van Alphen, F. P. J., Meijer, A. B. & Heck, A. J. R. Neutrophil azurophilic granule glycoproteins are distinctively decorated by atypical pauci- and phosphomannose glycans. Commun. Biol. 4, 1–13 (2021).

42. Thibault, G., Ismail, N. & Ng, D. T. W. The unfolded protein response supports cellular robustness as a broad-spectrum compensatory pathway. Proc. Natl. Acad. Sci. U. S. A. 108, 20597–20602 (2011).

43. Thibault, G. et al. The Membrane Stress Response Buffers Lethal Effects of Lipid Disequilibrium by Reprogramming the Protein Homeostasis Network. Mol. Cell 48, 16–27 (2012).

44. Samraj, B. comprehensive characterization of genes required for protein folding in the Endoplasmatic Reticulum. Routledge Handb. English Acad. Purp. 403–415 (2016). doi:10.4324/9781315657455-44

45. DeRossi, C. et al. Trappc11 is required for protein glycosylation in zebrafish and humans. Mol. Biol. Cell 27, 1220–1234 (2016).

46. Zipser, B., Bello-DeOcampo, D., Diestel, S., Tai, M. H. & Schmitz, B. Mannitou monoclonal antibody uniquely recognizes paucimannose, a marker for human cancer, stemness, and inflammation. J. Carbohydr. Chem. 31, 504–518 (2012).

47. Thaysen-Andersen, M. et al. Human neutrophils secrete bioactive paucimannosidic proteins from azurophilic granules into pathogen-infected sputum. J. Biol. Chem. 290, 8789–8802 (2015).

48. Simon, F. et al. Increased expression of immature mannose-containing glycoproteins and sialic acid in aged mouse brains. Int. J. Mol. Sci. 20, 1–3 (2019).

49. Qin, K. et al. Quantitative Profiling of Protein O-GlcNAcylation Sites by an Isotope-Tagged Cleav-

able Linker. ACS Chem. Biol. 13, 1983–1989 (2018).

50. Moremen, K. W. et al. Expression system for structural and functional studies of human glycosylation enzymes. Nat. Chem. Biol. 14, 156–162 (2018).

Materials and Methods

Chemicals, reagents, and materials

Lec9 cells were kindly provided by Prof. Dr. Pamela Stanley (Albert Einstein college of medicine, New York). The ST6Gal1 used in this study was expressed according to literature reports[50], and cleaved and purified from GFP prior to use. Human plasma serotransferrin (ref nr. 616397), Tris-HCL, tris(2-carboxyethyl)phosphine (TCEP), chloroacetamide (CAA), sodium deoxycholate (SDC), TFA, PBS (ref. D8537-500ML), RIPA lysis buffer (ref. 20-188), dithiothreitol (DTT) (ref. 43815), and iodoacetamide (IA) (ref. RPN6302V) were purchased at Sigma Aldrich. The Oasis elution HLB 96-well plate were obtained from Waters (Wexford, Ireland). Acetonitrile (ACN) was acquired from Biosolve (Valkenswaard, the Netherlands). FA was purchased at Merck and LysC was obtained from FIJUFILM Wako Chemicals. MEM alpha medium (ref. 11510616), Alkaline phosphatase (ref. EF0651), protease inhibitor cocktail (ref. A32953), BCA assay kit (ref. 23225), and Gelcode blue stain (ref. 24592) were purchased at Thermo Fisher Scientific. Trypsin (ref. V5280) was acquired from Promega. 6-well plates (ref. 3516) were purchased at Costar. Western blot sample buffer (ref. 161-0791), Clarity Western ECL Substrate (ref. 1705062) and gradient 4%-12% Tris-HCl gels (ref. 3450127) were obtained from Biorad. 10% SDS gels were poured in-house. The HRP-conjugated anti-biotin antibody was purchased at Jackson Immuno Research laboratories (ref. 200-032-211). The MilliQ pump was acquired from Milipore. 2-cm trap columns (100 µm inner diameter, packed with 3 µm ReproSil-Pur C18-AQ) were obtained from Dr. Maisch GmbH (Ammerbuch-Entringen, Germany). 50 cm analytical columns (50 µm inner diameter, packed with 2.7 µm Poroshell 120 EC-C18) were purchased at Agilent Technologies (Santa Clara, CA).

NMR spectroscopy and Time-Of-Flight (TOF) MS

1H and 13C NMR spectra were recorded on a Varian INOVA 300 MHz and 500 MHz spectrometers. Chemical shifts are reported in parts per million (ppm) relative to residual solvent signals used as the internal standard. NMR data is presented as follows: chemical shift, multiplicity (s = singlet, d = doublet, t = triplet, dd = doublet of doublet, m = multiplet and/or multiple resonances), integration, coupling constant in Hertz (Hz). All NMR signals were assigned based on 1H NMR and gHSQC experiments. Mass spectra were recorded on a Shimadzu LCMS-IT-TOF mass spectrometer or an Applied Biosystems SCIEX MALDI TOF/TOF 5800 using 2,5-dihydroxybenzoic acid (DHB) as a matrix. TLC-analysis performed on Silica gel 60 F254 (EMD Chemical inc.) with detection by UV-absorption (254 nm) when applicable, and by spraying with a solution of 5% sulphuric acid in ethanol followed by charring.

Derivative synthesis

To a solution of **5**[49] (15 mg, 1.3 eq, 17.5 µmol) and CMP-Neu5Az **4**[30] (9 mg, 14 µmol) in 1 mL 0.1 M NH_4HCO_3 was added 0.1 M sodium L-ascorbate (120 µL), 0.1 M CuSO4 (96 µL), and 2 mg TBTA. The resulting mixture was stirred at room temperature for 2 h. After completion of the reaction as indicated by ESI-MS, the mixture was lyophilized. The residue was purified by P2 column us-

ing 0.1 NH_4HCO_3 as eluent to yield **derivative 2** (13 mg, 70%). 1H NMR (500 MHz, D2O): δ 7.92 (d, J = 7.7 Hz, 1H, $H6^A$), 7.80 (s, 1H, CH-triazole), 7.58-5.52 (m, 4H), 7.39-7.30 (m, 6H), 6.05 (d, J = 7.7 Hz, 1H, $H1^A$), 5.83 (s, 1H), 5.19 (s, 1H), 5.14 (s, 2H, triazole-N-CH_2), 4.48 (dd, J = 9.0, 4.9 Hz, 1H, CHNH, biotin), 4.30 (dd, J = 8.0, 4.5 Hz, 1H, CHNH, biotin), 4.23-3.98 (m, $H3^{ribA}$, $H2^{ribA}$, $H5^{ribA}$, $H6^B$, $H4^B$), 3.90-3.77 (m, $H5^B$, $H8^B$, $H9a^B$), 3.59-3.37 (m, $H9b^B$+ OCH_2CH_2O+$NHCH_2CH_2O$, $H7_B$), 3.22-3.17 (m, CHS, biotin), 3.08-3.02 (m, 2H, triazole-CH_2CH_2C=O), 2.82-2.72 (m, 2H, C*H*HS), 2.58-2.53 (m, 1H, CH*H*S), 2.36 (dd, J = 13.3, 4.8 Hz, 1H, $H3eq^B$), 2.06 (t, J = 7.3 Hz, 2H, $CH_2CH_2CH_2CH_2$C=O, biotin), 1.55-1.32 (m, $H3ax^B$, C*H*$_2$$CH_2$C*H*$_2$$CH_2$C=O, biotin), 1.23-1.09 (m, $(CH_3)_2O$). ^{13}C NMR-HSQC (126 MHz, D_2O): δ 137.4, 137.3, 133.3, 130.6, 98.9, 91.6, 85.6, 76.8, 74.2, 73.5, 72.2, 72.0, 71.9, 71.3, 69.4, 69.2, 67.4, 65.5 (2xC), 65.4 (2xC), 64.9, 64.5, 62.7 (2xC), 57.7, 54.7, 54.6, 52.9 (2xC), 49.4, 45.9, 43.8, 43.5, 42.3, 42.1, 41.5, 38.6, 38.0, 30.7, 30.5, 30.3, 29.7, 29.5, 27.7. The ESI-MS m/z calculated for $C_{62}H_{91}N_{11}O_{26}$ PSSi, [M-1H]- is 1496.5370, which was detected at *m/z* 1496.8625.

SEEL labeling of serotransferrin

50 µg serotransferrin was diluted in a 100 mM Tris buffer for labeling with **derivatives 1** or **2** (10 µg) by the human glycosyltransferase ST6GAL1 (2 µg). After labeling with **derivative 2** the labeled serotransferrin was incubated in 2% FA for 1 h to allow cleaving of the silane linker.

Serotransferrin in-solution digestion and solid phase extraction

The serotransferrin samples were reduced, alkylated, and proteolytically digested with LysC and trypsin as described previously, with minor deviations[22]. Briefly, the samples were brought to 200 mM Tris, 10 mM TCEP, 60 mM CAA, 2% SDC. This mixture was incubated for 4 h at 37 °C with LysC in an enzyme:protein ratio of 1:75 (*w/w*), followed by an overnight incubation at 37 °C with trypsin in an enzyme:protein ratio of 1:100. After overnight incubation the sample was brought to 0.5% TFA to precipitate the SDC and centrifuged at max speed for 10 min. The supernatant was collected for subsequent SPE using an Oasis Elution HLB 96-well plate connected to a vacuum pump. After conditioning of the plate with ACN and equilibration in 0.5% TFA, the supernatant was loaded and washed with 0.5% TFA. The samples were eluted with 50% ACN 0.5% TFA. The eluted sample was dried in a SpeedVac and reconstituted in 2% FA for subsequent LC-MS/MS measurements.

Cell culture

CHO-K1 and Lec9 cells were cultured in MEM alpha medium supplemented with 10% fetal bovine serum (FBS). Cells were maintained at a humid 5% CO_2 atmosphere at 37 °C for CHO-K1 cells and at 34 °C for Lec9 cells. Cells were passaged at 80% confluency using trypsin (1x).

SEEL labeling of cell lines

For one-step SEEL, cells were plated in a 6-well plate at 200,000 cells/well and grown until 90% confluency. Cells were labeled as described previously[30]. Briefly, cells were washed twice in PBS and incubated for 2 h at 37 °C under gentle shaking in cell culture medium without FBS containing derivative 2 (100 µM), ST6Gal1 (42 µg/mL), 6 µL BSA (2 mg/mL) and 6 µL alkaline phosphatase. After labeling the cells were washed 3x in PBS and cells were lysed in RIPA lysis buffer with 1X protease inhibitor cocktail on ice for 30 min. Cell lysates were centrifuged at 14,000 RPM for 10 min and the protein concentration of the supernatant was determined using BCA assay.

Western blotting

For western blotting, 10 µg protein was denatured by heating at 95 °C for 7 min in a reducing sample buffer (50 mM DTT). The denatured protein was resolved in a 10% SDS page gel and transferred on a PVDF membrane using a Bio-Rad Trans-Blot Turbo system (settings: transfer standard 1x mini gel, 30 min). The transferred membrane was blocked in blocking buffer (5% milk in PBS 0.1% Tween) for 1 h and incubated with mouse anti-Biotin HRP (1:20,000) in blocking buffer for 1 h at RT. After washing (3x 10 min) in PBS-tween, the membrane was incubated with ECL substrate and developed.

Immunoprecipitation

For immunoprecipitation, streptavidin Sepharose beads were conditioned in RIPA buffer without protease inhibitors (immunoprecipitation buffer). 1 mg of total protein was incubated overnight with 100 µL streptavidin Sepharose in a total volume of 500 µL immunoprecipitation buffer at 4 °C while rotating. After incubation, beads were washed 3x in immunoprecipitation buffer and the captured biotinylated proteins were eluted by two times 1 h incubation in 100 µL 2% FA at RT while rotating. Both eluates were combined and dried in the SpeedVac overnight.

Sample preparation for LC-MS/MS analysis

Dried samples were reconstituted in 10 µL of MilliQ, 10 µL 200 mM DTT and 10 µL sample buffer and samples were incubated for 7 min at 95°C. After short centrifugation 10 µL 77 mM iodoacetamide was added to the samples and proteins were separated on a gradient 4%-12% Tris-HCl gel. After separation the gels were fixed with 50% ethanol/10% acetic acid, stained with Gelcode Blue Stain and destained with MilliQ. Each lane was excised in 10 bands for in gel digestion using trypsin (3 ng/µL). After extraction with 100% ACN, the samples were dried and stored at-80 till further use.

LC-MS/MS analysis

LC-MS/MS analysis was performed as published previously with minor alterations[22]. For the LC-MS run, dried samples were reconstituted in 80 µL 2% FA and 2 µL sample was analyzed on an Orbitrap Fusion Tribid Mass Spectrometer (Thermo Fischer Scientific). The samples were separated on an Agilent 1290 Infinity LC system on a 2-cm trap column (100 µm inner diameter, packed with 3 µm ReproSil-Pur C18-AQ) coupled to a 50 cm analytical column (50 µm inner diameter, packed with 2,7 µm Poroshell 120 EC-C18). Table S7 gives an overview of the buffers, flow rates, and gradient program. Every sample was measured in triplicate, with the same methods for MS1 acquisition, but different methods for MS2 acquisition. The mass range for the MS^1 acquisitions was set from m/z 350–2000 with a resolution of 60,000 and an AGC target of 400,000 with a maximum injection time of 50 ms. Three different MS^2 methods were used, each of which was initiated with HCD fragmentation (30% normalized collision energy) on the highest charge state, lowest *m/z* signals within a cycle time of 3 s, followed by an exclusion time of 30 s. The first MS^2 method consisted only of HCD fragmentation. HCD was recorded with a resolution of 30,000 from *m/z* 120–4000, with an AGC target of 50,000 and a maximum injection time of 50 ms. For the second method, stepping-HCD was triggered on a precursor signal after the detection of at least three oxonium ions within the HCD spectrum. Stepping-HCD combined the HCD fragments with normalized collision energy of 10, 25 and 40% and was recorded with a resolution of 30,000 from *m/z* 120-4000, with an AGC target of 200,000 and a maximum injection time of 250 ms. An overview of triggering oxonium is listed in Table S1. Finally, method three triggered EThcD (30% supplemental activation) upon

detection of oxonium ions and was recorded with a resolution of 30,000 from *m/z* 120-4000, with an AGC target of 200,000 and a maximum injection time of 250 ms.

Proteomics data analysis using MaxQuant and Byonic

Protein quantification was performed using MaxQuant (V.1.6.17.0) and bottom-up data were interpreted with Byonic v3 10.0. For all data analysis we made use of the Cricetulus griseus proteome as available on UniProt (accessed August 13th 2020). For MaxQuant, raw data was searched with a first search tolerance of 20 ppm and a main search tolerance of 4.5 ppm. We allowed only specific trypsin digestion, but the maximum number of miscleavages was set to five. Carbamidomethylation was set as fixed modification, included variable modifications being Met oxidation, protein N-term acetylation, Ser, Thr or Tyr phosphorylation, Asp deamidation, and Gln or Glu to pyroglutamate conversion. Inclusion of proteins occurred upon detection in at least two out of three samples in both cell lines with a minimum of two unique peptide detections. The iBAQ values were used for the quantification of the proteins in both cell lines. The fold changes were plotted against the-log10 p-value in a volcano plot. The same criteria were used for the Byonic search with a few minor alterations. A maximum of three trypsin miscleavages were allowed, a precursor mass tolerance of 10 ppm and a fragment mass tolerance of 20 ppm. For *N*-glycosylation we included 566 compositions following the biosynthesis pathways of *N*-glycosylation and including up to three modified sialic acids as a variation. The data output of the triplicates was combined per cell line and curated on the score (≥ 150), logprob (≥ 1), and DeltaMod (≥ 10).

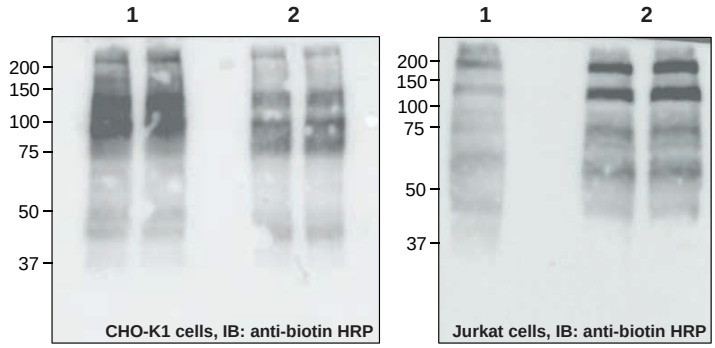

Supplementary Figure 1. SEEL labeling efficiency of derivative 1 (noncleavable linker) and 2 (cleavable linker). Shown are western blot analyses of lysates from SEEL-labeled CHO-K1 cells (A) and human Jurkat cells (B) using derivative 1 and 2. 10 µg protein was loaded per lane and the biotin label was visualized using an HRP-conjugated anti-biotin antibody.

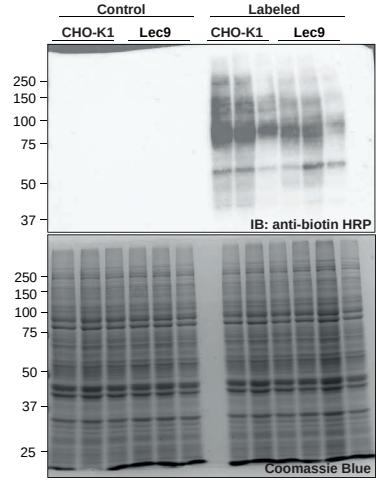

Supplementary Figure 2. SEEL-labeled cell lysates for glycoproteomic analysis. Shown are a Western blot analysis and Coomassie blue stain from the SEEL-labeled cell lysates with derivative 2 in triplicates. Also shown are control lysates, labeled with the labeling mixture minus the sialyltransferase. 10 µg of protein was loaded per lane and the biotin label was visualized using an HRP-conjugated anti-biotin antibody.

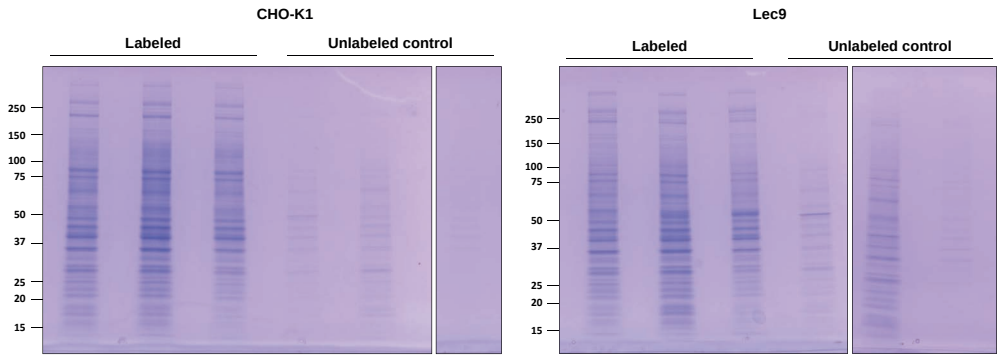

Supplementary Figure S3. Enriched labeled lysates for glycoproteomic analysis. Shown are the Coomassie blue stained gradient (4-12%) SDS-page gels of the labeled lysates after enrichment with Streptavidin Sepharose. As a control the mock-labeled lysates (Figure S2) were also enriched with Streptavidin Sepharose. The complete elute was loaded on the gel for in-gel trypsin digestion prior to LC-MS measurements.

Supplementary Table 1. Oxonium ions for MS/MS triggering. List of oxonium ions allowed after HCD to trigger fragmentation by sHCD or EThCD.

Hex	Phospho-Hex	HexNAc	Neu5Ac	Neu5Ac-Linker	Complex
127.0390	243.0264	138.0550	274.0921	433.1562	366.1395
145.0495	405.0793	168.0655	292.1027		407.1660
163.0601		186.0761			512.1974
		204.0867			657.2349

Supplementary Table 7. LC-MS gradient program.

Buffer A	0.05% TFA
Buffer B	0.1% TFA in 40% water 30% ACN 30% MeOH

Gradient program

Time (min)	Flow rate (ml/min)	A (%)	B (%)
0.0	0.05	100	0
0.1	0.005	100	0
5.0	0.005	100	0
5.1	0.200	87	13
45.0	0.200	56	44
48.0	0.200	0	100
49.0	0.200	0	100
50.0	0.200	100	0
60.0	0.200	100	0

Chapter 3

Glycan-Remodeled Erythrocytes Facilitate Antigenic Characterization of Recent A/H3N2 Influenza Viruses

Frederik Broszeit[1†], Rosanne J. van Beek[1†], Luca Unione[1], Theo M. Bestebroer[2], Digantkumar Chapla[3], Jeong-Yeh Yang[3], Kelley W. Moremen[3], Sander Herfst[2], Ron A.M. Fouchier[2], Robert P. de Vries[1] & Geert-Jan Boons[1,3,4,5]

†These authors contributed equally.

[1]Department of Chemical Biology & Drug Discovery, Utrecht Institute for Pharmaceutical Sciences, Utrecht University, 3584 CG Utrecht, The Netherlands;

[2]Department of Viroscience, Erasmus MC, P.O. Box 2040, 3000 CA, Rotterdam, The Netherlands;

[3]Complex Carbohydrate Research Center, University of Georgia, 315 Riverbend Rd, Athens, GA 30602, USA;

[4]Bijvoet Center for Biomolecular Research, Utrecht University, Utrecht, The Netherlands;

[5]Department of Chemistry, University of Georgia, Athens, GA 30602, USA.

3

Abstract

During circulation in humans and natural selection to escape antibody recognition for decades, A/H3N2 influenza viruses emerged with altered receptor specificities. These viruses lost the ability to agglutinate erythrocytes critical for antigenic characterization and give low yields and acquire adaptive mutations when cultured in eggs and cells, contributing to recent vaccine challenges. Examination of receptor specificities of A/H3N2 viruses reveals that recent viruses compensated for decreased binding of the prototypic human receptor by recognizing α2,6-sialosides on extended LacNAc moieties. Erythrocyte glycomics shows an absence of extended glycans providing a rationale for the lack of agglutination by recent A/H3N2 viruses. A glycan remodeling approach installing functional receptors on erythrocytes allows antigenic characterization of recent A/H3N2 viruses, confirming the co-circulation of antigenically different viruses in humans. Computational analysis of HAs in complex with sialosides having extended LacNAc moieties reveals that mutations distal to the RBD reoriented the Y159 side chain resulting in an extended receptor-binding site.

Introduction

Human influenza A viruses have a remarkable ability to evolve and evade neutralization by antibodies elicited by prior infections or vaccinations[1,2]. This antigenic evolution, or drift, is mainly caused by amino acid substitutions in the globular head of the hemagglutinin (HA) protein where binding occurs with sialic acid receptors of host cells[3,4]. These substitutions in circulating influenza viruses lead to antigenic differences as compared to employed vaccines, resulting in poor vaccine-mediated protection[5]. Therefore, the World Health Organization (WHO) Global Influenza Surveillance and Response System (GISRS) continuously monitors antigenic changes in circulating influenza viruses and recommends updated compositions of influenza vaccines biannually[6].

Antigenic surveillance and vaccine strain selection rely predominantly on the HI assay, in which the ability of serum antibodies to block receptor binding by the influenza virus HA protein is quantified[7]. Such antibodies prevent virus-mediated agglutination of erythrocytes and are measured as a correlate of protection[8]. The HI assay makes it possible to select virus strains that are antigenically representative of circulating viruses for vaccine development[9-11]. It is easy to perform in a high-throughput manner, can be standardized and is highly reproducible across laboratoria[12].

A/H3N2 viruses, which have become the leading cause of seasonal influenza illness and death since their introduction in the human population in 1968[13,14], exhibit a particularly rapid antigenic drift. As a result, the WHO has recommended 28 vaccine strain updates since these viruses started circulating in humans[13]. The rapid antigenic evolution of A/H3N2 viruses coincided with altered receptor usage, which in turn has resulted in an inability to agglutinate erythrocytes commonly employed for HI assays. As a result, antigenic characterization of circulating A/H3N2 viruses using the HI assay is increasingly difficult, complicating the selection of appropriate vaccine strains[1,8-10]. The receptor-binding phenotype of recent A/H3N2 viruses is also hampering virus replication under laboratory conditions for amplification of clinical isolates and leads to adaptive substitutions when grown in embryonated chicken eggs[15,16]. The difficulties to antigenically characterize circulating A/H3N2 viruses, in particular those belonging to the dominant 3C.2a clade, and the inability of large-scale virus production without egg-adaptation has led to serious problems with A/H3N2 influenza vaccine production and effectiveness[1,11].

HAs of human influenza viruses bind to cell-surface glycans carrying terminal α2,6-linked sialic acid moieties (Neu5Ac(α2,6)Gal), which is referred to as the prototypic human receptor[17]. These receptors are usually part of *N*-linked glycans, which are highly complex biomolecules composed of a core pentasaccharide modified by various numbers and patterns of branching *N*-acetylglucosamine (GlcNAc) moieties[18]. These branching points can be extended by several *N*-acetyl-lactosamine (Gal(β1,4)GlcNAc, LacNAc) repeating units, which in turn can be capped by various types of fucosylation and sialylation. Several studies have shown that not only the α2,6-linked sialoside but also the underlying oligosaccharide structure of *N*-linked glycans can contribute to HA binding selectivities[19-23]. Antigenic pressure results mainly in amino acid substitutions near the receptor-binding site of HA, which may result in changes in glycan receptor specificities. Thus, failure of contemporary A/H3N2 viruses to agglutinate erythrocytes, the poor replication in mammalian cells and the emergence of egg adaptive mutations are probably due to an adaptation to glycan receptors that are not expressed by these cell substrates. Understanding of the evolution of receptor usage by A/H3N2 viruses at a molecular level will open avenues to address challenges in surveillance and vaccine production for these viruses.

In this work, we examined receptor specificities of A/H3N2 viruses representing different evolutionary time points and clades using a novel glycan microarray to identify the minimal receptor requirements for recent, non-agglutinating A/H3N2 strains. Glycan analysis of cell surface *N*-glycans on various erythrocytes reveal an absence of such receptors. We developed an exo-enzymatic cell-surface glycan remodeling strategy to install appropriate receptors on fowl erythrocytes to regain binding by contemporary A/H3N2 viruses. Such viruses can agglutinate the glyco-engineered erythrocytes and made it possible to antigenically characterize A/H3N2 viruses by HI assays. We reveal substantial antigenic differences of circulating virus isolates to current vaccine strains providing a rationale for poor vaccine performance.

Results

Glycan microarray analysis to determine A/H3N2 receptor specificity

Although glycan microarray technology has been used to examine receptor requirements of HAs[24], these were not populated with biologically relevant glycans to establish minimal receptor requirements. This information is, however, critical to understand how receptor binding has evolved over time and how a lack of expression of specific glycans by erythrocytes or laboratory hosts may have resulted in a loss of agglutination or a lack of propagation, respectively.

We have constructed a glycan array that is populated with biologically relevant bi-antennary *N*-glycans having different numbers of LacNAc repeating units in various structural configurations. They resemble structures found on human respiratory tissue, which abundantly expresses *N*-glycans having multiple consecutive LacNAc repeating units that can be capped by sialic acid[25,26]. The synthetic glycans are either unmodified (compounds **1-3**), capped by avian α2,3-linked (compounds **4-6**) or human α2,6-linked sialosides (compounds **7-17**). Most naturally occurring *N*-linked glycans have asymmetrical architectures in which the various antennae are modified by oligo-LacNAc moieties of different lengths[27]. To probe the importance of such architectures for HA recognition, we prepared symmetrical as well as asymmetrical glycans (**8**, **9**, **11**, **12**, **13**, **15**, **16** and **17**) that are modified by either one or two sialosides linked to LacNAc chains of different length. The collections of compounds made it possible to probe the importance of mono- vs. bidentate binding interactions, and a possible preference or requirement for a sialoside at specific antenna or at an extended LacNAc chain. All glycans contain an anomeric asparagine moiety and its α-amine facilitated immobilization on amine reactive, NHS-activated glass slides. The quality of the printing was validated by probing the array with the lectins ECA, SNA and, MAL1 as well as an anti-H3 antibody (Figure 1A and Supplementary Figure 1).

The glycan array was probed with various A/H3N2 viruses, representing distinct evolutionary time points and clades and having different abilities to agglutinate erythrocytes derived from species commonly used in HI assays (Supplementary Figure 2). In this respect, chicken and turkey erythrocytes are widely employed in HA assays because they are nucleated, which un-

► **Figure 1. Receptor binding specificities of representative A/H3N2 viruses using glycan microarray analysis and glycomic analysis of N-glycosylation of unmodified fowl erythrocytes.** (**A**) Binding was visualized using a human anti-H3 stalk antibody (CR8020). Bars represent the background-subtracted average relative fluorescence units (RFU) of four replicates ± SD. Values for all individual datapoints are represented in the Supplementary Source Data file. (**B**) The 30 most abundant *N*-glycans on erythrocytes from chicken and turkey organized by the number of LacNAc repeating units and relative intensity. High-mannose type *N*-glycans are not shown and their abundance is presented in Supplementary Figure 5. The structures of all detected glycans are shown in Data S1.

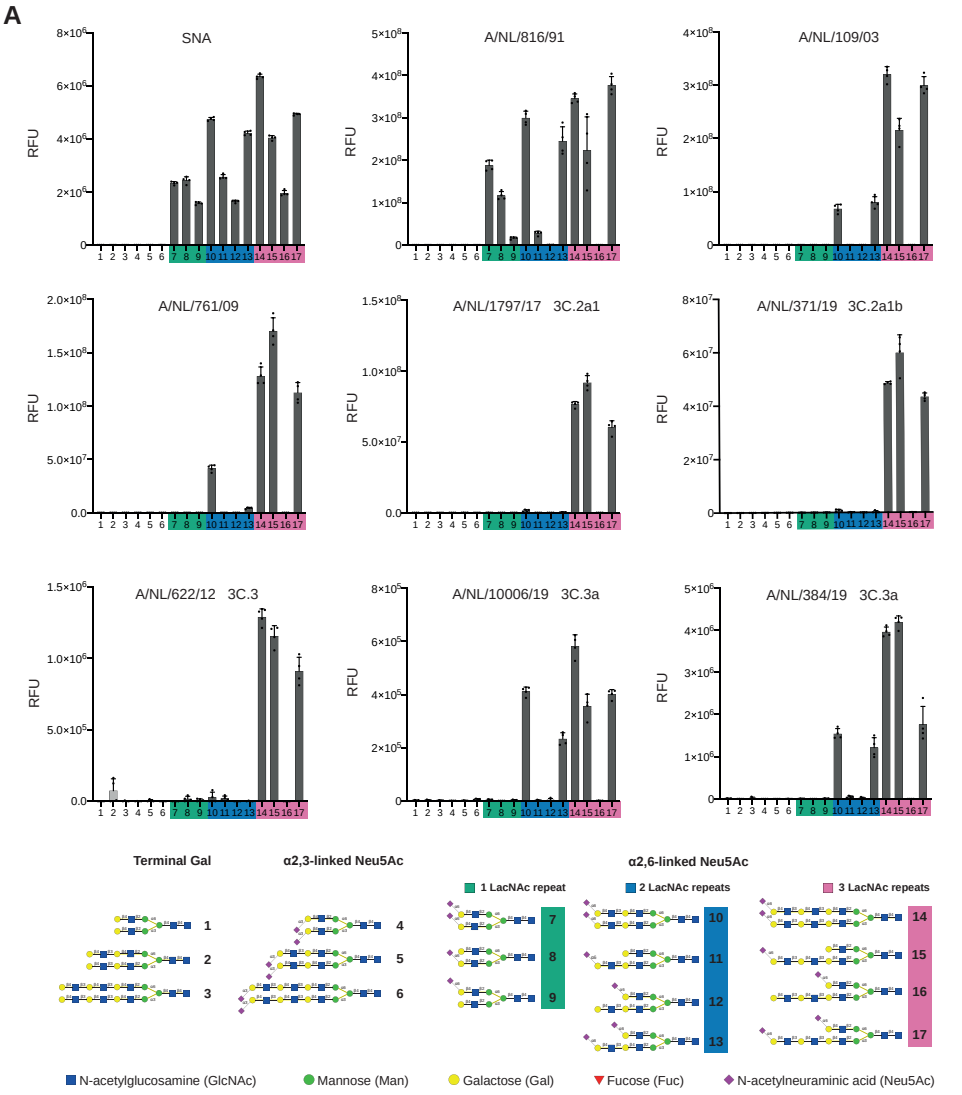
A
SNA
A/NL/816/91
A/NL/109/03
A/NL/761/09
A/NL/1797/17 3C.2a1
A/NL/371/19 3C.2a1b
A/NL/622/12 3C.3
A/NL/10006/19 3C.3a
A/NL/384/19 3C.3a
RFU
Terminal Gal
α2,3-linked Neu5Ac
α2,6-linked Neu5Ac
1 LacNAc repeat
2 LacNAc repeats
3 LacNAc repeats
N-acetylglucosamine (GlcNAc)
Mannose (Man)
Galactose (Gal)
Fucose (Fuc)
N-acetylneuraminic acid (Neu5Ac)

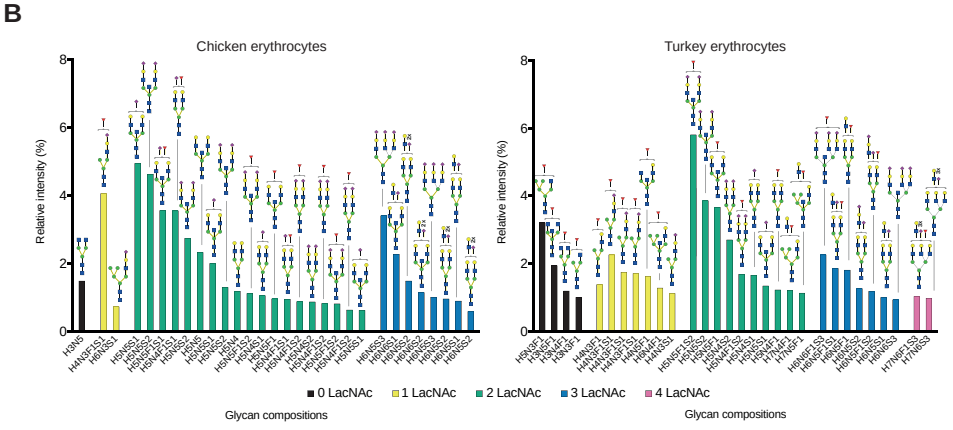
B
Chicken erythrocytes
Turkey erythrocytes
Relative intensity (%)
0 LacNAc
1 LacNAc
2 LacNAc
3 LacNAc
4 LacNAc
Glycan compositions

like mammalian erythrocytes, sediment rapidly thereby greatly facilitating the visual readout of the assay[7]. They express α2,3- and α2,6-linked sialosides and can be agglutinated by avian as well as human influenza viruses. Other types of erythrocytes have been employed for HI assays[28] and in particular those of guinea pig erythrocytes have been proven to be useful because they exhibit a somewhat broader agglutination ability and can for example be employed to antigenically characterize A/H3N2 viruses of the 3C.2 clade which cannot be agglutinated turkey and chicken erythrocytes[29].

In the studies, we included A/NL/816/91 (NL91) which can agglutinate chicken, turkey and guinea pig erythrocytes, A/NL/109/03 (NL03) which only agglutinates turkey and guinea pig erythrocytes[29] and A/NL/761/09 (NL09) which only agglutinates α2,6-resialylated turkey and guinea pig erythrocytes[30-32]. During the past decade, A/H3N2 viruses have evolved into distinct, cocirculating antigenic groups, referred to as clades (Supplementary Figure 2). We examined A/NL/1797/17 (NL17) and A/NL/371/19 (NL19) as recent examples of the 3C.2a clade that insufficiently hemagglutinate all commonly used erythrocytes for HI assays, and poorly infect MDCK cells[33]. The 3C.3a clade is represented by A/NL/10006/19 and A/NL/384/19, and their evolutionary predecessor A/NL/622/12 (3C.3). Although 3C.3 viruses cannot agglutinate any erythrocyte type, 3C.3a viruses are unique as they regained an ability to agglutinate turkey and guinea pig erythrocytes (Supplementary Figure 2).

Whole viruses were applied to the microarray and detection of binding was accomplished by a human anti-H3 stalk antibody (CR8020) (Supplementary Figure 1). NL91 recognized most of the human-type receptors, including compounds that have an α2,6-sialoside on a mono-LacNAc residue (glycans **7-9**, Figure 1A and Supplementary Figure 3). Compound **8** exhibited a substantial greater responsiveness compared to **9** indicating that this virus has a preference for a sialoside at the α1,3-arm. Interestingly, the sialyltransferase, ST6Gal1, which is solely responsible for installing human-type receptors, preferentially modifies the α1,3-arm of *N*-linked glycans[34]. Compounds **7** and **8** did bind similarly demonstrating that an additional sialic acid at the α1,6-arm does not substantially contribute to binding. Another unanticipated observation was that compounds **12** and **16** did not exhibit binding whereas **9** showed responsiveness highlighting that an extended and unmodified LacNAc moiety at the α1,3-arm can block recognition of the other arm. Collectively, the results show that the minimal receptor for NL91 is a biantennary *N*-glycan having two LacNAc moieties modified by a single sialoside (glycan **8**).

NL03 and NL09 recognized far fewer glycans and did not bind to structures having their α2,6-sialosides at a mono-LacNAc moiety (**7-9**, **12** and **16**). This observation indicates that the minimal receptor for these viruses is a bis-sialylated *N*-glycan having at least one di-LacNAc moiety (glycan **13**). NL17 and NL19 (3C.2a) showed only strong responsiveness to **14**, **15** and **17**. These glycans have in common that at least one of the arms is extended by three consecutive LacNAc units that is further modified by an α2,6-sialoside. Thus, a glycan having four LacNAc units arranged in an asymmetrical manner (**15**) represents the minimal receptor for these viruses. Mono-sialylated derivative **15** gave a similar responsiveness compared to the bis-sialosides **14** and **17** indicating that a bidentate binding event does not substantially contribute to recognition as previously suggested[22]. Instead, it appears that reduction in binding of an α2,6-sialyl-Gal moiety, which is widely regarded as the prototypic human receptor, has been compensated by recognition of sialosides at extended LacNAc chains. 3C.3a viruses (A/NL/10006/19 and A/NL/384/19) exhibited a similar binding profile as NL03 and 09 and bound to bis-sialosides **10** and **13** having the Neu5Ac residue at a di-LacNAc chain. Interestingly, their ancestor (A/NL/622/12, 3C.3) required the Neu5Ac residue to be presented on a

tri-LacNAc structure similar to the requirement of 3C.2a viruses. Thus, recent 3C.3a viruses have regained an ability to recognize shorter structures.

Glycomic analysis of chicken and turkey erythrocytes

Next, we examined structures of *N*-linked glycans expressed by chicken and turkey erythrocytes and compared the data with the receptor requirements of the various A/H3N2 viruses. Membrane fractions of the cells were treated with PNGase F to release the *N*-glycans which were isolated by SPE using C18 and PGC cartridges, and then analyzed by liquid chromatography mass spectrometry (LC-MS)[35]. The 30 most abundant complex-type *N*-glycan compositions for the two cell types are presented in Figure 1B. The compounds are organized according to an increasing number of LacNAc moieties (indicated by different color coding) and include hybrid-type and core structures having none (black bars) or one LacNAc moiety (yellow bars) and complex *N*-glycans having variable numbers of LacNAc repeating units (2-4 LacNAc, green, blue and purple bars, respectively). High-mannose type *N*-glycans were also detected and their structures and abundance are shown in Supplementary Figure 5. Strikingly, chicken erythrocytes do not substantially express *N*-glycans having 4 LacNAc units which is the minimal epitope requirement for contemporary non-agglutinating A/H3N2 viruses. Turkey erythrocytes do express some glycans with this number of LacNAc units (purple bars in Figure 1B), but the majority was assigned as tri- and tetra-antennary glycans because of substitution with three or four sialic acids. The latter was supported by selective release of biantennary *N*-glycans by Endo F2, and in this case LC-MS analysis did not detect glycans having four LacNAc moieties (Supplementary Figure 4). Thus, turkey erythrocytes also do not substantially display sialylated epitopes having three consecutive LacNAc moieties. The majority of the glycans released by Endo F2 lacked fucose indicating that the fucosides observed in some of the structures depicted in Figure 1 can be assigned to core modification. Chicken erythrocytes express substantial quantities of high-mannose glycans (Supplementary Figure 5) whereas turkey cells display almost none of these structures. The greater abundance of complex-type glycans on turkey erythrocytes offers a possible rationale for the ability of the NL03 and NL09 A/H3N2 viruses to agglutinate unmodified or α2,6-resialylated turkey erythrocytes, respectively.

Erythrocyte glycoengineering to install functional receptors

We embarked on a strategy to enzymatically remodel glycans of fowl erythrocytes to install receptors for A/H3N2 viruses of the 3C.2 clade to make them suitable for HI assays (Figure 2A). Treatment of erythrocytes with a neuraminidase was expected to remove sialic acids and reveal terminal galactosides which are appropriate acceptors for installing additional LacNAc moieties. The latter residues can be introduced by the concerted action of the enzymes B4GalT1 and B3GnT2, which sequentially install α1,4-linked galactoside and α1,3-linked *N*-acetyl-glucosamines, respectively. The terminal galactosides of the resulting extended LacNAc moieties can then be modified by the sialyltransferase ST6Gal1 to install terminal α2,6-linked sialosides[36]. The enzymatic remodeling was conveniently performed by incubating the erythrocytes with the neuraminidase from *Arthrobacter ureafaciens* (AU) for 6 h after which B4GalT1, B3GnT2[37], UDP-Gal and UDP-GlcNAc were added followed by incubation overnight. Next, the cells were pelleted by centrifugation, washed to remove the enzymes and sugar nucleotides and then incubated with ST6Gal1 in the presence of CMP-Neu5Ac for 4 h. Glycomic analysis of the resulting cells, which were denoted as 2,6-Sia Poly-LN cells, confirmed that the antennae of the *N*-linked glycans had been extended by additional LacNAc moieties, and both

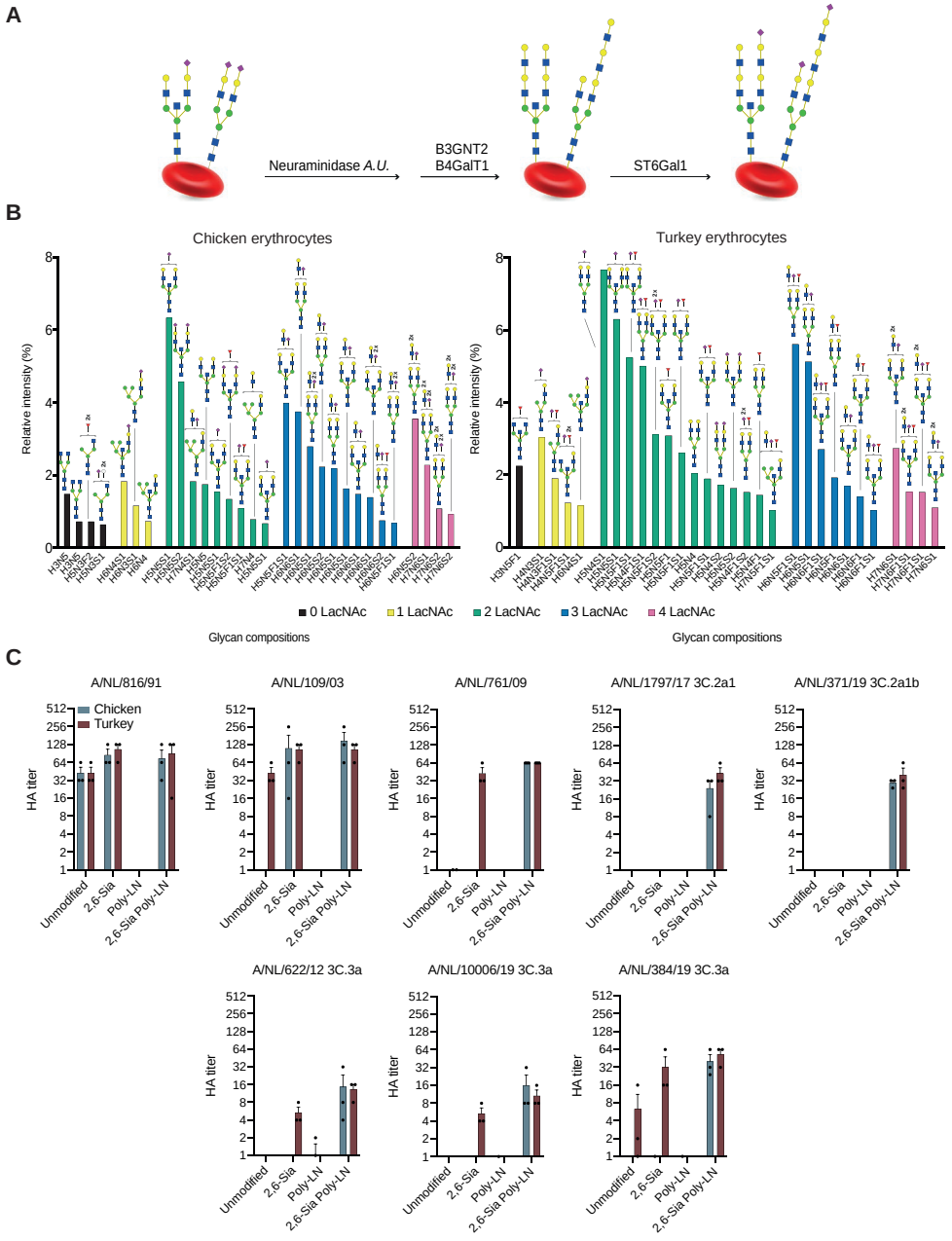
A
Neuraminidase A.U.
B3GNT2
B4GalT1
ST6Gal1
B
Chicken erythrocytes
Turkey erythrocytes
Relative intensity (%)
0 LacNAc
1 LacNAc
2 LacNAc
3 LacNAc
4 LacNAc
Glycan compositions
C
A/NL/816/91
A/NL/109/03
A/NL/761/09
A/NL/1797/17 3C.2a1
A/NL/371/19 3C.2a1b
A/NL/622/12 3C.3a
A/NL/10006/19 3C.3a
A/NL/384/19 3C.3a
Chicken
Turkey
HA titer
Unmodified
2,6-Sia
Poly-LN
2,6-Sia Poly-LN

◄ **Figure 2. Schematic overview of enzymatic modification of erythrocytes followed by glycomic analysis of N-glycosylation and their use in hemagglutination assays.** (**A**) Neuraminidase A.U.: Neuraminidase from *Arthrobacter ureafaciens*; B3GnT2: β-1,3-*N*-acetylglucosaminyltransferase 2; B4GalT1: β-1,4-galactosyltransferase 1; ST6Gal1: α-2,6-sialyltransferase 1. (**B**) The 30 most abundant *N*-glycans on the enzymatically modified erythrocytes from chicken and turkey (based on relative intensity, excluding high-mannose type *N*-glycans, for all structures refer to Data S2) sorted by abundance and number of LacNAc units. Proposed structures are assigned to detected glycan compositions. (**C**) A/NL/816/91, A/NL/109/03, A/NL/761/09, A/NL/1797/17, A/NL/371/19, A/NL/622/12, A/NL/10006/19 and A/NL/384/19 tested with modified erythrocytes (2,6-Sia Poly-LN) from chicken (blue) and turkey (red). Unmodified, 2,6 resialylated (2,6-Sia) and extended desialylated (Poly-LN) erythrocytes were added as controls. Assays were performed in biological triplicates in the presence of oseltamivir and the means ± SEM were plotted.

cell types expressed sialylated structures having four LacNAc units (Figure 2B, 4 LacNAc units are indicated in purple bars). Analysis of glycans on turkey erythrocytes released by Endo F2 treatment confirmed the presence of biantennary glycans that have 4 LacNAc moieties and are potentially suitable receptors for contemporary A/H3N2 viruses (Supplementary Figure 4, glycans having 4 LacNAc units are indicated by purple bars). Chicken and turkey erythrocytes express a mixture of α2,3- and α2,6-linked sialosides. To examine whether an increase in the abundance of α2,6-sialosides would improve agglutination, control cells were prepared by treatment with neuraminidase and resialylation with ST6Gal1 (denoted as 2,6-Sia cells). As negative control, we employed cells that have extended LacNAc moieties but lack sialic acids (denoted as Poly-LN cells).

Phenotypic properties of the glyco-engineered erythrocytes were examined using the hemagglutination (HA) assay (Figure 2C). As expected, NL91 agglutinated unmodified, 2,6-Sia and 2,6-Sia poly-LN erythrocytes, which was in agreement with the finding that these viruses can employ *N*-glycans that have simple and extended α2,6-sialylated structures. NL03 agglutinated unmodified turkey erythrocytes, but interestingly also α2,6-resialylated chicken erythrocytes. The latter may be due to an increase in the abundance of α2,6-linked sialosides having two consecutive LacNAc repeating units, which are present on chicken erythrocytes. α2,6-Resialylation of turkey erythrocytes was sufficient to recover agglutination of NL09, and in this case the greater abundance of α2,6-sialylation on extended structures already present on these cells is probably responsible for the improved agglutination. Importantly, NL17 and NL19 (3C.2a) agglutinated only erythrocytes that were enzymatically remodeled to have extended sialylated LacNAc moieties (2,6-Sia Poly-LN cells). Similar results were obtained for A/NL/622/12 (3C.3), which is in agreement with receptor requirements similar to viruses of the 3C.2a clade. As anticipated, the 3C.3a viruses (A/NL/10006/19 and A/NL/384/19), which have reverted to recognize shorter structures, could also agglutinate α2,6-resialyated turkey erythrocytes.

Next, HA assays were performed with a wider collection of A/H3N2 viruses (Table 1) to validate the robustness of the glyco-engineering method with a focus on contemporary A/H3N2 viruses that have lost the ability to hemagglutinate unmodified erythrocytes and do not replicate efficiently in wild-type MDCK cells. Several recent vaccine strains heavily adapted to growing in eggs (X-161B, IVR-147, X-223A, NIB-104, NIB-112, X-327), an A/H1N1 (A/Singapore/GP1908/15) and an influenza B (B/Maryland/15/15) strain were included as controls. As expected, pre-2000 A/H3N2 (A/Bilthoven/16190/68, A/Beijing/353/89, A/Netherlands/816/91) strains efficiently agglutinated unmodified chicken and turkey erythrocytes. Importantly, A/H3N2 viruses that emerged after 2010 only agglutinated the 2,6-Sia Poly-LN cells having extended sialylated epitopes. Although some contemporary A/H3N2 viruses can agglutinate turkey erythrocytes when applied undiluted, especially the two 2019 3C3a viruses, extended

sialylated LacNAc moieties increased the efficiency of agglutination by 3 to 10-fold, including the A/H1N1 and influenza B controls. We performed a time course to determine the stability of the glyco-engineered cells, and no loss in titer or autoagglutination for up to three weeks was observed similar to unmodified cells (Supplementary Figure 6).

The 2,6-Sia Poly-LN cells were employed to antigenically characterize typical recent seasonal A/H3N2 viruses of various clades by HI assay using post-infection ferret sera (Table 2). All antisera showed robust inhibition of the homologous viruses and variable inhibition of heterologous viruses. Egg-derived vaccine strains displayed poor correspondence with data generated with cell-passaged viruses of the same clade. Antisera raised against cell-passaged virus isolates showed greater clade specificity compared to antisera raised against egg-derived vaccine strains. Additionally, egg-derived vaccine strains were inhibited stronger by various antisera than cell-passaged viruses. The HI assay also revealed that antisera raised against recent vaccine viruses, including A/Kansas/14/17 that was selected for the 2019/2020 northern hemisphere influenza vaccine[38], exhibited only minimal cross reactivity against circulating viruses from the same clades, indicating that the circulating viruses differ antigenically from the vaccine strains of the same clade.

The results of the HI assay were compared with a focus reduction assay (FRA) using the same sera and viruses (Supplementary Table 1)[39]. In this assay, the ability of antibodies to block virus infection in mammalian cell culture (MDCK-Siat cells, which overexpress Sia(α2,6)Gal moieties) is quantified. The FRA confirmed the trends observed in the HI assay (Supplementary Figure 7), indicating that the modified erythrocytes are reliable for antigenic characterization of A/H3N2 viruses.

Molecular dynamics simulations of HAs in complex with their receptors

α2,6-Sialyl-Gal is widely considered as the prototypic human receptor for IAVs[17]. All viruses we examined, including A/H1N1 viruses (Supplementary Figure 8), recognized with high avidity *N*-glycans having an α2,6-linked sialoside on an extended LacNAc moiety. Human respiratory tissue abundantly expresses such extended structures[25,26], and thus we reasoned that mutational changes in recent A/H3N2 viruses led to a reduced binding avidity of the prototypic human receptor (α2,6-sialyl-Gal), which was compensated by making interactions with an extended LacNAc chain.

X-ray crystal structures[31,40,41] have shown that sialic acid is recognized in a conserved hydrophobic pocket (Y98, H183, Y195 and W153) (Supplementary Table 2). It makes further interactions through a hydrogen bonding network with residues 135-137, E190 and S228. Sequence alignments showed that post-2000 strains acquired single point mutations at one of these residues (Supplementary Table 2), which disrupted the hydrogen bonding network, and likely resulted in a reduced binding affinity of the prototypic human receptor, which is a sialoside α2,6-linked to galactose[31]. Furthermore, HAs of early human A/H3N2 strains have Glu at residue 190, which can form a hydrogen bond with O9 of sialic acid, whereas post-2000 strains, favor Asp190 at this position, which due to its shorter side chain, cannot form such an interaction. The 190E/D mutation was accompanied by a 225G/D mutation, which resulted in a rotation of Gal-2 allowing a hydrogen bond interaction with the site chain of 225D[31,40]. This rotation places the extended LacNAc chain closer to the 190-helix and potentially allows for addition interactions. To examine this mode of binding, we compared molecular dynamics generated structures of α2,6-sialyl poly-LacNAc in complex with NL91, NL03, and NL17 (Figure 3). It recapitulated observations made by X-ray crystallography studies and provided insight in

Table 1. Hemagglutination assay of A/H3N2 virus isolates using unmodified and 2,6-Sia Poly-LacNAc fowl erythrocytes and unmodified guinea pig erythrocytes.

			Hemagglutination titres (HAU per 25ul)						
			Chicken			Turkey			Guinea pig
Virus	Type	Clade	Unmodified	2,6-Sia	2,6-Sia Poly-LN	Unmodified	2,6-Sia	2,6-Sia Poly-LN	Unmodified
A/Bilthoven/16190/68	H3N2	*unknown*	24	32	64	64	48	64	48
A/Beijing/353/89	H3N2	*unknown*	24	64	64	64	64	96	64
A/Netherlands/816/91	H3N2	*unknown*	64	128	128	64	128	128	*n.t.*
A/Netherlands/109/03	H3N2	*unknown*	neg.	256	256	64	128	128	*n.t.*
X-161B (A/Wisconsin/067/05)	H3N2	*unknown*	12	neg.	64	32	32	64	*n.t.*
IVR-147 (A/Brisbane/10/07)	H3N2	*unknown*	4	neg.	8	16	neg.	8	*n.t.*
A/Netherlands/761/09	H3N2	*unknown*	neg.	neg.	64	neg.	64	64	*n.t.*
X-223A (A/Texas/50/12)	H3N2	3C.1	8	neg.	8	12	neg.	8	*n.t.*
NIB-104 (A/Singapore/INFH-16-0019/16)	H3N2	3C.2a1	8	2	16	24	12	24	32
A/Netherlands/2413/16	H3N2	3C.2a1	neg.	neg.	96	3	24	128	*n.t.*
A/Netherlands/751/17	H3N2	3C.2a1	neg.	neg.	6	neg.	neg.	512	1
A/Netherlands/757/17	H3N2	3C.2a1	neg.	neg.	64	6	16	128	*n.t.*
A/Netherlands/1797/17	H3N2	3C.2a1	neg.	neg.	32	neg.	neg.	32	neg.
A/Netherlands/295/19	H3N2	3C.2a1b	neg.	neg.	192	neg.	neg.	192	*n.t.*
A/Netherlands/314/19	H3N2	3C.2a1b	neg.	neg.	128	neg.	neg.	192	neg.
A/Netherlands/371/19	H3N2	3C.2a1b	neg.	neg.	32	neg.	neg.	32	neg.
A/Netherlands/03466/17	H3N2	3C.2a	neg.	neg.	2048	neg.	6	512	neg.
NIB-112 (A/Switzerland/8060/17)	H3N2	3C.2a2	*n.t.*	*n.t.*	*n.t.*	neg.	neg.	4	neg.
A/Netherlands/10616/18	H3N2	3C.2a2	neg.	neg.	3	neg.	neg.	4	neg.
A/Netherlands/622/12	H3N2	3C.3	neg.	neg.	12	neg.	neg.	12	1
A/Switzerland/9715293/13	H3N2	3C.3a	neg.	neg.	16	2	3	24	2
A/Netherlands/153/16	H3N2	3C.3a	neg.	neg.	96	12	24	128	*n.t.*
X-327 (A/Kansas/014/17)	H3N2	3C.3a	neg.	2	16	6	4	16	8
A/Netherlands/384/19	H3N2	3C.3a	neg.	neg.	2048	12	192	1536	6
A/Netherlands/10002/19	H3N2	3C.3a	neg.	neg.	64	12	16	96	*n.t.*
A/Netherlands/10006/19	H3N2	3C.3a	neg.	2	32	8	12	64	12
IVR-180 (A/Singapore/GP1908/15)	H1N1	6B	32	16	48	24	32	24	32
BX-69A (B/Maryland/15/15)	B	*n.a.*	32	16	64	32	32	32	32

unknown = clade designation was not used at that time
n.t. = not tested
n.a. = not applicable
neg. = no titer obtained

Table 2. Hemagglutination inhibition assay.

			Post-infection ferret sera raised against						
			NIB 104	A/NL/314/19	NIB-112	A/NL/3466/17	A/NL/1802/18	X-327	A/NL/384/19
Virus	Passage	Clade	3C.2a1a	3C.2a1b	3C.2a2	3C.2a2	3C.2a2	3C.3a	3C.3a
A/Singapore/INFH-16-0019/16 (NIB 104)	E7Mdck_Siat2hCK	3C.2a1a	**640**	320	960	160	480	<5	60
A/Netherlands/1797/17	Mdck1Siat2hCK	3C.2a1	15	160	30	40	80	<5	30
A/Netherlands/314/19	MdckSiat2hCK	3C.2a1b	30	**240**	30	60	80	<5	40
A/Netherlands/10009/19	mixhCK2	3C.2a1b	20	160	40	120	120	<5	30
A/Netherlands/371/19	MdckSiatmixhCK	3C.2a1b	<5	160	5	30	40	<5	15
A/Switzerland/8060/17 (NIB-112)	E7E1hCK	3C.2a2	640	120	**1920**	1280	240	<5	<5
A/Netherlands/3466/17	Siat1hCK1 10-2	3C.2a2	15	80	320	**480**	80	<5	30
A/Netherlands/1802/18	Siat1hCK1 10-1	3C.2a2	15	80	40	40	**640**	<5	20
A/Netherlands/10616/19	MdckSiatmixhCK	3C.2a2	15	80	320	640	80	<5	20
A/Kansas/14/17 (X-327)	E17E1Siat1hCK	3C.3a	640	<5	<5	<5	<5	**320**	60
A/Netherlands/384/19	Siat2hCK 10-2	3C.3a	30	30	60	40	80	40	**240**
A/Netherlands/10006/19	MdckSiatmixhCK2	3C.3a	<5	<5	20	20	30	<5	240

how mutational changes allowed for interactions with an extended LacNAc chains. The MD trajectory of NL91 only showed interactions with sialic acid, including the important hydrogen bond between Sia-1 O9 and Glu190 (Figure 3A)[31,40]. In the case of NL03 and NL17, Asp190 is at a distance of 4.5 Å to Sia-1 O9, and thus cannot establish a hydrogen bond (Figure 3D and G). The G225D substitution resulted in a rotation of the bond between the sialic acid and Gal-2 to form an H-bond with its O316 (Figure 3E and 3H). As anticipated, the resulting rotation of Gal-2 placed the extended LacNAc moieties near the 190-helix[41] resulting in a hydrogen bond between Asp190 and Gal-4 O2, while either Ser or Asn193 provided a H-bond with the acetamide moiety of GlcNAc-3 (Figure 3E). In addition, Gal-6 (Figure 3E and 3H) makes a CH-π interaction with the side chain of Y159 (Supplementary Figure 10). Such interactions are often observed in glycan-protein complexes and contribute substantially to binding[42]. Structural analysis of the HAs of NL91 and NL03 showed that mutations distal to the receptor-binding domain (A131T, H155T and E156H), reorient the side chain of Y159 resulting in an extended receptor-binding site allowing interactions with Gal-6 (Supplementary Figure 9). The MD simulations support that A/H3N2 of the 3C.2 clade have undergone mutations to create and extended binding site to compensate for reduced binding of the non-extended human receptor (Figure 3C, F and I). Interestingly, 3C.3a viruses, which can utilize shorter receptors having two LacNAc units (Figure 1A), have a tyrosine to serine mutation at position 159 (Supplementary Table 2). Thus, the dependence on extended receptors is reversible, and these viruses have found a way to bind shorter structures with sufficient affinity for infection. The observation that distant mutations can alter the position of a side chain of an amino acid in the receptor-binding site, which subsequently can become susceptible to antigenic pressure, indicates that such remote mutations need to be considered for the evolution of receptor binding and antigenic distance.

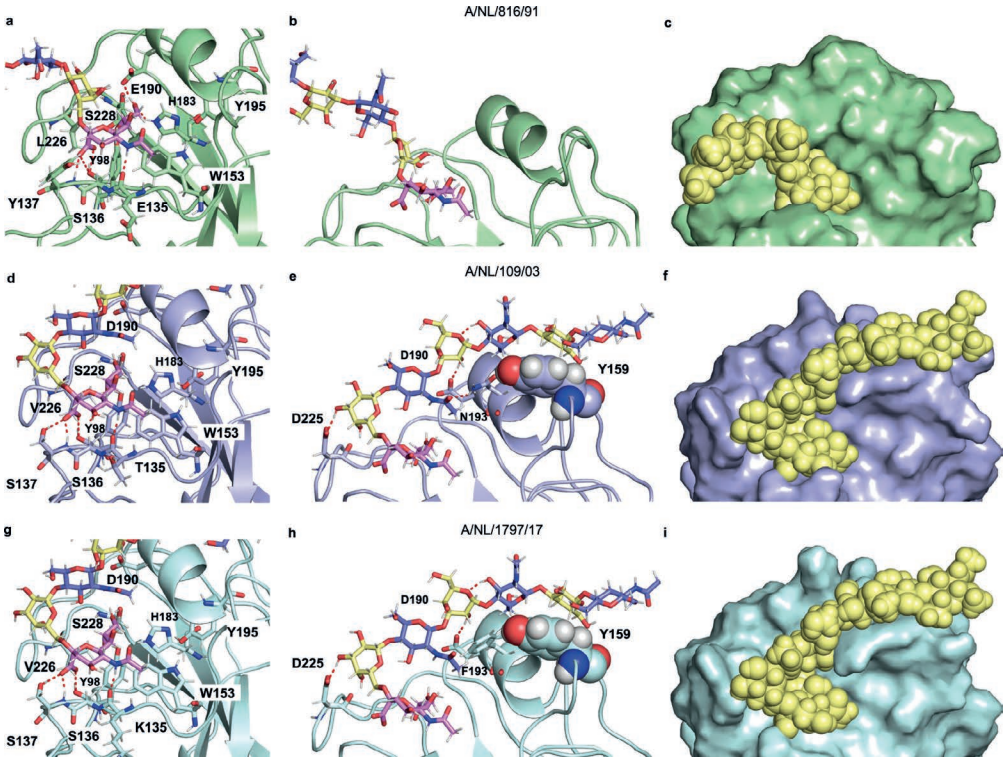

Figure 3. Structural comparison of HAs from evolutionary different strains in complex with extended glycan receptor. Details of the sialic acid binding sites are shown for A/NL/816/91 (**a**), A/NL/109/03 (**d**) and A/NL/1797/17 (**g**). The interactions of the poly-LN chain with the protein are shown for A/NL/816/91 (**b**), A/NL/109/03 (**e**) and A/NL/1797/17 (**h**). The surface and spheres representations of HA/glycans complexes are shown for A/NL/816/91 (**c**), A/NL/109/03 (**f**), and A/NL/1797/17 (**i**).

Discussion

Changes in receptor-binding properties of A/H3N2 viruses were first noticed by a lack of agglutination of commonly employed red blood cells and poor recovery of isolated viruses that were propagated in laboratory hosts such as eggs and MDCK cells[29,43]. Conventional binding assays using a limited set of relevant glycans showed these viruses had lost the ability to bind to what was regarded as the canonical human-type receptors, namely α2,6-sialyl-Gal[21,44]. Screening of a glycan microarray populated with symmetrical *N*-glycans (each arm modified by the same epitope) identified receptors for contemporary A/H3N2. In particular, these viruses could bind biantennary *N*-glycans having an extended sialo-LaNAc epitope at each of its arm. Modeling studies indicated that the two sialic acid moieties are sufficiently spaced to bind to a protomer of the same HA trimer. It was proposed that the resulting bidentate binding mode increased the binding avidity[22].

Progress in methods for the chemoenzymatic synthesis of glycans[45] allowed us to construct a glycan microarray populated with biantennary *N*-glycans that more closely resemble structures expressed in human respiratory tissue[25,26], and include asymmetrical glycans having

either one or two sialic acid moieties linked to LacNAc chains of different length. It made it possible, for the first time, to uncover the minimal receptor of contemporary A/H3N2 viruses, which is a biantennary *N*-glycan in which one of the arms is extended by three consecutive LacNAc units that is modified by an α2,6-sialoside. It demonstrated that the previously proposed bidentate binding event does not substantially contribute to binding[22]. Based on our microarray data, sequence alignments, reported crystal structures and MD simulations, we developed alternative binding model for A/H3N2 of the 3C.2 clade. In this model, mutations remote to the receptor-binding domain resulted in the rotation of the side chain of tyrosine at position 159 which gives rise to an extended binding site. Furthermore, a 225G/D mutation reoriented the poly-LacNAc chain allowing it to make interactions with the extended binding site. These interactions compensate for reduced contacts with sialic acid caused by mutations in the receptor-binding site arisen from antigenic pressure[4]. It is, however, possible that factors other than antigenic pressure may have contributed to adaptations of receptor specificity. For example, a binding requirement for sialic acid on poly-LacNAc chain may provide a benefit because such structures are usually not found on *O*-glycans of mucins, and therefore such a receptor specificity may contribute to escaping the mucosal barrier.

The identification of the minimal receptor for contemporary A/H3N2 viruses made it possible to engineer the surface of erythrocytes with functional receptors allowing easy antigenic characterization of recent A/H3N2 isolates using the HI assay. It confirmed that antigenically distinct viruses are circulating in humans and that egg-passaged A/H3N2 vaccine components match poorly to circulating strains. Due to the failure of the classical HI, FRAs have been employed to antigenically characterize A/H3N2. These assays are, however, time-consuming, have low throughput, suffer from low reproducibility, and can lead to adapted mutations thereby providing incorrect results[12]. These limitations are addressed by the glyco-engineered red blood cells described here. The altered receptor requirement of A/H3N2 viruses is also complicating propagation in the laboratory. Recently, an MDCK cell line (hCK) was introduced in which α2,3-sialyl transferases were genetically removed and ST6Gal1, which introduces human-type receptors, was overexpressed[33]. This cell line supports efficient replication of contemporary human A/H3N2 viruses that maintain higher genetic stability[46]. The minimal receptor requirements of contemporary A/H3N2 viruses established in this study support further engineering of such cells to biosynthesize extended α2,6-sialylated LacNAc moieties. Furthermore, it is the expectation that the described glycan engineering approach for erythrocytes can be extended to other cells, such as MDCK cells, to quickly provide laboratory hosts for virus replication. The results presented here may also provide a rationale for why certain sialylated inhibitors do not bind HA when expressed in CHO vs. HEK cells where the nature of the sialylated linkages are different[47]. Finally, an understanding of the evolution of receptor specificities of A/H3N2 viruses and associated antigenic changes will facilitate the development of predictive evolutionary models for the reliable selection of vaccine strains.

Methods

Virus production

Materials

Eagle's minimal essential medium (EMEM), penicillin, streptomycin, L-glutamine, sodium bicarbonate, HEPES, 1x non-essential amino acids and *N*-tosyl-L-phenylalanine chloromethyl ketone (TPCK) treated trypsin were purchased at Lonza Benelux BV, Breda, The Netherlands. Fetal bovine serum was obtained from Greiner.

MDCK, MDCK-Siat and hCK (a humanized MDCK knock-out cell line, deficient of several 2,3-specific sialyltransferase enzymes and overexpressing human-type 2,6-sialylated receptors)[33] cells were cultured in EMEM supplemented with 10% fetal bovine serum (FBS), 100 U mL^{-1} penicillin (P), 100 U mL^{-1} streptomycin (S), 2 mM L-glutamine (L-glu), 1.5 mg mL^{-1} sodium bicarbonate ($NaHCO_3$), 10 mM HEPES, and 1x non-essential amino acids (NEAA)[33]. In addition, hCK cells were supplemented with 2 µg mL^{-1} puromycin and 10 µg mL^{-1} blasticidin and MDCK-Siat cells were supplemented with 1 mg mL^{-1} Geneticine. To produce virus stocks, cells were washed twice with PBS 1 h after inoculation with the virus of interest and cultured in infection media, consisting of EMEM supplemented with 100 U mL^{-1} penicillin, 100 µg mL^{-1} streptomycin, 2 mM glutamine, 1.5 mg mL^{-1} sodium bicarbonate, 10 mM HEPES, 1x non-essential amino acids, and 20 µg mL^{-1} TPCK treated trypsin. To produce virus stocks in eggs, 100 µL of virus was inoculated in the allantoic cavities of 11-day-old embryonated hens' eggs. The allantoic fluid was harvested after 2 days.

Microarray studies

Materials

Virus isolates were produced as described above. Oseltamivir was purchased from Sigma-Aldrich [Cat# SML1606]. CR8020 A/H3N2 stem antibody was kindly provided by Dr. Dirk Eggink and expressed following previously published procedures[48]. Goat anti-human Alexa-647 [Cat# A21445] and streptavidin-AlexaFluor 635 [Cat# SA1011] antibodies were obtained from Thermo Fisher. Control lectins *Erythrina cristagalli* agglutinin (ECA) [Cat#B-1145], Sambuca nigra agglutinin (SNA) [Cat# B-1305], Maackia amurensis lectin I (Mal-I) [Cat# B-1315] were purchased from Vector Labs.

Arrayer and printing surfaces

Compounds were printed on amine reactive, NHS-activated glass slides (NEXTERION ® Slide H) from Schott Inc exploiting the free amine of an asparagine moiety at the reducing end of the *N*-glycans. Scienion sciFLEXARRAYER S3 non-contact microarray printer equipped with a Scienion PDC80 nozzle (Scienion Inc) was used for printing. Glycans were dissolved in printing buffer (sodium phosphate, 250 mM, pH 8.5) at a concentration of 100 µM. Each compound was printed in replicates of six with a spot volume of ~400 pL, at 20 °C and 50% humidity. Slides were blocked with 5 mM ethanolamine in tris buffer (pH 9, 50 mM) for 1 h at 50 °C and rinsed with DI water after printing.

Glycan microarray

Quality control was performed using the plant lectins ECA (specific for terminal Gal), SNA (specific for α2,6-linked Neu5Ac) and MAL-I (specific for α2,3-linked Neu5Ac) and is shown in Figure S1. Quality control of the CR8020 A/H3N2 influenza hemagglutinin stem specific antibody specificity was performed by incubation of the antibody to the array as described

below, in the absence of a virus (Supplementary Figure 1). The printed library of compounds comprised the glycans described in the supplementary information (#8, #9, #11, #12, #13, #15, #16, #17) and published previously (#1-#7, #10, #14)[49].

Sample

Virus isolates (25 µL) were diluted with PBS-T (PBS + 0.1% Tween, 25 µL) and applied to the array surface in the presence of oseltamivir (200 nM) in a humidified chamber for 1 h, followed by successive rinsing with PBS-T (PBS + 0.1% Tween), PBS and deionized water (2x) and dried by centrifugation. The virus-bound slide was incubated for 1 h with the CR8020 A/H3N2 influenza hemaglutinin stem specific antibody (100 µL, 5 µg mL^{-1} in PBS-T) and washed according to previous washing procedure. A secondary goat anti-human AlexaFluor-647 antibody (100 µL, 2 µg mL^{-1} in PBS-T) was applied, incubated for 1 h in a humidified chamber and washed again as described above. The control lectins containing a biotin tag were visualized with Streptavidin-AlexaFluor635. Slides were dried by centrifugation after the washing step and scanned immediately.

Detection and data processing

The slides were scanned using an Innopsys Innoscan 710 microarray scanner at the appropriate excitation wavelength. To ensure that all signals were in the linear range of the scanner's detector and to avoid any saturation of the signals various gains and PMT values were employed. Images were analyzed with Mapix software (version 8.1.0 Innopsys) and processed with our home written Excel macro. The average fluorescence intensity and SD were measured for each compound after exclusion of the highest and lowest intensities from the spot replicates (n=4).

Glycomic analysis

Materials

Acetic acid [Cat# 5330010050], MS-grade FA [Cat# 5330020050], 2-aminoanthrallic acid (2-AA) [Cat#10680], dimethyl sulfoxide (DMSO) [Cat# W387520] and sodium cyanoborohydride [Cat# 156159] were obtained from Sigma-Aldrich. Trifluoro acetic acid (TFA) was purchased from Acros Organics [Cat#434161000]. MS-grade acetonitrile (MeCN) was obtained from Biosolve [Cat# 200-835-2]. PNGase F was purchased from Roche Diagnostics (1U defined as the amount of enzyme catalyzing the conversion of 1 µmol (substrate) min^{-1}) [Cat#06538355103]. Denaturation buffer (0.5% SDS, 40 mM dithiothreitol (DTT)), 1% NP-40, and glycobuffer (50 mM sodium phosphate) were obtained from New England Biolabs. Ammonium formate was purchased from Fluka chemicals [Cat# AGG1946-85021], C18 SPE Sep-Pak® Vac (1cc) columns from Waters Corporation [Cat# WAT054955], PGC SPE Hypercarb Hypersep (1cc) columns from Thermo Scientific [Cat# 60106-303] and PD Minitrap Sephadex G-10 size exclusion cartridges from GE Healthcare [Cat# 28-9180-10]. MilliQ water was obtained from a Synergy® water purification system.

N-glycan extraction and release from erythrocytes

Cell-surface *N*-glycans were extracted according to a reported protocol[35]. Briefly, erythrocytes (400 µL, 50%) were concentrated by centrifugation (430 rcf, 10 min) and removal of the supernatant. Erythrocytes were lysed under gentle shaking at room temperature for 1 h using deionized water (3x pellet size). The suspension was centrifuged (4000 rcf, 10 min), the supernatant removed, and the pellet resuspended in deionized water. The process was repeated until the pellet decolorized, indicating an efficient lysis of the erythrocytes. Denaturing of the cell membrane pellet was performed by heating for 10 min to 95 °C in denaturation buffer

(0.5% SDS, 40 mM DTT in H_2O). The *N*-glycans were released during overnight incubation at 37 °C with PNGase F (5 U) in a sodium phosphate buffer (50 mM, pH 7.5) or with Endo F2 in sodium acetate buffer (50 mM, pH 4), both containing NP-40 (1%).

Purification and labeling of *N*-glycans

The released *N*-glycans were applied to a C18 SPE cartridge and glycans were eluted with 5% MeCN in H_2O (0.05% TFA, 1 mL). The eluate was further purified on a PGC SPE cartridge by gradually increasing the hydrophobicity from 100% H_2O (0.05% TFA, 1 mL) to 5% MeCN in H_2O (0.05% TFA, 1 mL), and to 50% MeCN in H_2O (0.05% TFA, 1 mL) which eluted the glycans. After drying in a N_2 flow, the sample was dissolved in H_2O (10 µL) and labeled by addition of a solution (10 µL) of 2-AA (48 mg mL^{-1}) and sodium cyanoborohydride (63 mg mL^{-1}) in DMSO/acetic acid (10:3 *v/v*) for 2 h at 65 °C. The crude mixture was diluted with H_2O (80 µL) and purified on a Minitrap Sephadex G-10 gravity column by washing with of H_2O (700 µL) and eluting with H_2O (600 µL). The eluate was dried under N_2 flow and dissolved in 20 µL of 50% MeCN in H_2O prior to LC-MS analysis.

HILIC-IMS-QTOF analysis of *N*-glycans and data treatment

The *N*-glycan analysis was performed on a 1260 Infinity LC system (Agilent Technologies) coupled to a 6560 IM-QTOF mass spectrometer (Agilent Technologies) and high-performance liquid chromatography (HPLC) separation with a ZIC®-cHILIC column (3 µm, 100 Å, 150 mm x 2.1 mm, Merck) and a similar guard column (20 mm x 2.1 mm, Merck) using a gradient from 30% A to 50% A within 25 min (A: 50 mM $(NH_4)_2CO_3$ in H_2O; B: MeCN; 0.2 mL min^{-1}; 60 °C). MS analysis was performed with a drying gas temperature of 300 °C and a flow of 8 mL min^{-1}. The nebulizer pressure was set to 40 psi, the sheath gas flow to 11 L min^{-1} and the temperature to 350 °C. Measurements were run in negative mode with the capillary established at 3500 V. During the runs the Agilent tuning mix was infused for mass calibration based on reference signals at *m/z* 112.9855 and *m/z* 1033.9881.

The data analysis was performed with the Mass Hunter IM-MS Browser and the find feature function filtering for masses with an ion intensity of ≥ 500. Found masses were processed with the online Glycomod tool to identify glycan related masses[50].

Glyco-engineering of erythrocytes

Materials

AU neuraminidase was purchased at New England Biolabs (1 U defined as the amount of enzyme catalyzing the conversion of 1 µmol(substrate) min^{-1}) [Cat# P0722L]. Mammalian glycosyltransferases were expressed according to literature reports[37]. B3GnT2 and ST6Gal1 were cleaved and purified from GFP tags prior to use. Alkaline phosphatase (FastAP) was purchased at Thermo Scientific [Cat# EF0651]. Nucleotide sugars UDP-Gal, UDP-GlcNAc and CMP-Neu5Ac were obtained from Roche Diagnostics [UDP-Gal: Cat# 07703562103; UDP-GlcNAc: Cat# 06369855103; CMP-NeuAc: Cat# 05974003103].

Erythrocyte preparation

Fresh blood from chicken or turkey was centrifuged (10 min, 430 rcf) followed by removal of the supernatant. Pellets were washed three times in PBS with intermittent centrifugation (430 rcf, 10 min). Erythrocyte solutions were stored in a 50% solution in PBS until further use.

Enzymatic extension

To a suspension of fowl erythrocytes (250 µL, 50%), PBS (900 µL) and AU neuraminidase (12 U) were added. The cells were incubated for 6 h at 37°C while tilting. Next, glycosyltransferases B4GALT1 (37.5 µL, 1 mg mL^{-1}) and B3GnT2 (37,5 µL, 1 mg mL^{-1}), the nucleotide sugars UDP-Gal (4.4 mM) and UDP-GlcNAc (4.4 mM), alkaline phosphatase (6 U), MnCl2 (2 mM) and BSA (6 µL, 2 mg mL^{-1}) were added. This reaction mixture was incubated overnight at 37 °C while tilting. The erythrocytes were washed in PBS (2x, 600 µL) and the pellet was reconstituted in 900 µL PBS. Resialylation of the erythrocytes was performed using ST6Gal1 (37.5 µL, 1 mg mL^{-1}) and CMP-Neu5Ac (4.4 mM) in the presence of alkaline phosphatase (6 U) and BSA (6 µL, 2 mg mL^{-1}) for 4 h at 37 °C while tilting. The erythrocytes were washed in PBS (1x, 600 µL) and diluted to a 1% solution for hemagglutination (inhibition) assays.

Stability assay

Fresh fowl erythrocytes were glyco-engineered as described above or used unmodified. A hemagglutination assay was performed every two days using two viruses, A/NL/761/09 and A/NL/816/91. Hemagglutination assays were performed as described below in full biological triplicates. The means were plotted ± SEM and are shown in Supplementary Figure 6.

Hemagglutination assay

Hemagglutination assays were performed following standard procedures[7]. Briefly, virus stocks were two-fold serial diluted in the presence of oseltamivir (20 nM). Turkey erythrocytes (1%, 25 µL) were mixed with the serial diluted viruses and incubated for 1 h at 4 °C before recording of the results. Titers were expressed as the highest dilution of virus stock that completely agglutinated the turkey erythrocytes.

Hemagglutination inhibition assay

HI assays were performed following standard protocols[7]. Briefly, for the preparation of the antisera, ferrets were inoculated intranasally and blood was obtained 14 d later. Experiments were performed in strict compliance with European guidelines (EU Directive on Animal Testing 86/609/EEC) and Dutch legislation (Experiments on Animals Act, 1997). An independent animal experimentation ethical review committee (Dutch Stichting Dier Experimenten Commissie Consult) approved all animal studies (license AVD101002015340). Antisera were pre-treated with receptor destroying enzyme (RDE) by incubating overnight with an in-house produced filtrate of Vibrio cholera at 37 °C followed by 1 h incubation at 56 °C. The treated antisera were pre-absorbed with extended turkey erythrocytes (10%) in two cycles of 1 h incubation at 4 °C. Pre-absorbed antisera were twofold serial diluted (starting at 1:10) and mixed with virus stock (25 µL) containing 4 hemagglutinating units. Viruses were incubated with the antisera for 1 h at 4 °C in the presence of BSA (0.25%) and oseltamivir (20 nM). Turkey erythrocyte solution (25 µL, 1%) was added and after 1 h incubation at 4 °C inhibition patterns were recorded. Titers were expressed as the value of the highest serum dilution that gave complete inhibition of agglutination.

Focus reduction assay

FRAs were performed following standard protocols[51]. First, infectious titers of the virus stocks were determined in hCK cells as described previously[52]. RDE-treated sera were twofold diluted in a 96-well plate (starting at 1:10) and mixed 1:1 with 100 $TCID_{50}$/50 µL of virus. After 1 h

incubation at 35 °C, 100 µL of the mixtures were transferred to hCK cells and after 90 min incubation at 35 °C, cells were washed and overlaid with 1.6% carboxymethylcellulose. After 48 h at 35 °C, cells were washed and fixed with formalin and permeabilized using 0.5% Triton X-100 for 10 min at room temperature. Subsequently, immunostaining was performed using a mouse monoclonal antibody (HB65; EVL, Woerden, The Netherlands) directed against the viral nucleoprotein (NP), followed by a horseradish peroxidase-labeled goat anti-mouse immunoglobulin preparation (GAM-HRPO, Invitrogen, Foster city, CA), both for 1 h at room temperature. After washing, True-Blue substrate (KPL, Gaitherburg, Maryland) was added followed by a 10 min incubation at room temperature. The plates were washed, dried, and submitted to automated image capture using a Series 6 ImmunoSpot Image Analyzer (CTL ImmunoSpot, Cleveland OH, USA) to quantitate the percentage well area covered by spots of infected cells. Inhibition ≥ 90% was considered positive for neutralization.

Structural studies

Alignment

To investigate the relevance of specific mutations in defining receptor preferences during antigenic drift, primary amino acid sequences were compared of A/H3N2 HAs from 1968 to 2019. Protein sequences and structures were derived from the 3DPlu database (http://3dflu.cent.uw.edu.pl/index.html)[53] and the GISAID webpage (https://www.gisaid.org). It identified specific mutations that may influence receptor-binding preferences. We paid specific attention to mutations in the four structural elements that define the RBS, including the 130-loop, the 150-loop, the 190-helix and the 220-loop. The results from this analysis are summarized in Supplementary Table 2.

MD simulations

A starting pose of the NL91 from 1991 was generated by superimposition of the model derived structure (id code ACU12494) [http://3dflu.cent.uw.edu.pl/index.html] onto the X-ray crystal structure of the A/HK/1/1968 H3N2 influenza virus hemagglutinin in complex with 6'-SLNLN (pdb code 6TZB)[41]. The starting pose of NL03 was generated by using the X-ray crystal structure of the A/Wy/3/03 influenza virus hemagglutinin in complex with 6'-SLN (pdb code 6BKR)[37]. Glycan receptors, NeuAcα2-6(LacNAc)$_2$ and NeuAcα2-6(LacNAc)$_3$, were generated by using the carbohydrate builder GLYCAM-web site [http://glycam.org]. The glycosidic torsion angles of the monosaccharides were maintained as observed by X-ray crystallography, while those not resolved were defined according to the lower energy values predicted by the GLYCAM-web modeling tool. The structural model of the NL17 was obtained by using the mutagenesis tool implemented in PyMOL. The resulting poses were used as starting points for MD simulations. The MD simulations were performed using the Amber16 program4 with the protein.ff14SB, the GLYCAM_06j-1 and the water.tip3p force fields parameters. Next, the starting 3D geometries were placed into a 10 Å octahedral box of explicit TIP3P waters, and counter ions were added to maintain electroneutrality. Two consecutive minimization steps were performed involving (1) only the water molecules and ions and (2) the whole system with a higher number of cycles, using the steepest descent algorithm. The system was subjected to two rapid molecular dynamic simulations (heating and equilibration). The equilibrated structures were the starting points for a final MD simulations at constant temperature (300 K) and pressure (1 atm). In all, 100 ns MD simulations without constraints were recorded, using an NPT ensemble with periodic boundary conditions, a cut-off of 10 Å, and the particle mesh Ewald method. A total of 50,000,000 MD steps were run with a time step of 1 fs per step. Coordinates and energy values were recorded every 50,000 steps (50 ps) for a total of 1,000 MD models. The detailed analysis

of the H-bond and CH-π interactions was performed along the MD trajectory using the cpptraj module included in Amber-Tools 16 package.

Data availability: The data supporting the findings in this paper are available in the manuscript and Supporting Information. A full overview of the identified glycomic structures can be found in Supplementary data 1 and Supplementary data 2.

Code availability: The script for Microsoft Excel Macro for batch processing glycan microarray data is uploaded to https://github.com/enthalpyliu/carbohydrate-microarray-processing. https://doi.org/10.5281/zenodo.5146251

Ethics statement: Animal studies were performed in accordance to relevant guidelines and approved by an independent animal experimentation ethical review committee "stichting DEC consult".

Acknowledgments

This project is supported by the Netherlands Organization for Scientific Research (NWO TOPPUNT 718.015.003) to G.-J.B., R.P.dV is a recipient of ERC starting grant 802780 and a Beijerinck Premium of the Royal Dutch Academy of Sciences. S.H. is supported by NWO VIDI grant 91715372, R.A.F. by NIAID/NIH contract HHSN272201400008C, and K.W.M and G.-J.B by U.S. National Institutes of Health grants (R01GM130915, P41GM103390 and U01GM120408). We thank T. Manders, Dr. H.G.R. Matthijs and Dr. R.M. Dwars (Faculty of Veterinary Sciences, Utrecht University) for providing chicken blood and M. Pronk and R. van Beek (Department of Viroscience, Erasmus MC) for technical assistance. Dr. L. Liu (CCRC) and Dr. M.A. Wolfert (Utrecht University) developed, printed and validated the glycan microarray. We would like to thank Dirk Eggink from the Amsterdam Medical Center for supplying the CR8020 antibody.

Author Contributions

G.-J.B., R.P.dV., F.B., and R.J.vB. designed the project; R.J.vB., F.B., L.U., T.B., and R.P.dV. performed experiments and data analysis; R.A.F., G.-J.B., S.H., and R.P.dV. provided scientific guidance on experimental setup and data interpretation; K.W.M., D.C., and J.Y.Y. provided recombinant enzymes; G.-J.B., R.J.vB., F.B., L.U., S.H., R.A.F., and R.P.dV. wrote the manuscript; and all authors provided comments and suggestions on the manuscript.

Competing Interests

F.B., R.J.vB., R.P.dV., and G.-J.B are inventors for a patent application for the glyco-engineered red blood cells described in this publication for antigenic charterization of influenza viruses. Title: Means and methods for detecting, producing, isolating or characterizing influenza. Application number: EP20179197. Status: provisional application.

References

1. Allen, J. D. & Ross, T. M. H3N2 influenza viruses in humans: Viral mechanisms, evolution, and evaluation. Hum. Vaccin Immunother. 14, 1840-1847 (2018).
2. Paules, C. I., Sullivan, S. G., Subbarao, K. & Fauci, A. S. Chasing seasonal influenza- the need for a universal influenza vaccine. N. Engl. J. Med. 378, 7-9 (2018).
3. Wiley, D. C., Wilson, I. A. & Skehel, J. J. Structural identification of the antibody-binding sites of Hong Kong influenza haemagglutinin and their involvement in antigenic variation. Nature 289, 373-378 (1981).
4. Koel, B. F. et al. Substitutions near the receptor binding site determine major antigenic change during influenza virus evolution. Science 342, 976-979 (2013).
5. Belongia, E. A. & McLean, H. Q. Influenza vaccine effectiveness: defining the H3N2 problem. Clin. Infect. Dis. 69, 1817-1823 (2019).
6. Monto, A. S. Reflections on the global influenza surveillance and response system (GISRS) at 65 years: an expanding framework for influenza detection, prevention and control. Influenza Other Respi. Viruses 12, 10-12 (2018).
7. WHO Global Influenza Surveillance Network. Manual for the laboratory diagnosis and virological surveillance of influenza. (World Health Organization, 2011).
8. Coudeville, L. et al. Relationship between haemagglutination-inhibiting antibody titres and clinical protection against influenza: development and application of a bayesian random-effects model. BMC Med. Res. Methodol. 10, 18 (2010).
9. Noah, D. L., Hill, H., Hines, D., White, E. L. & Wolff, M. C. Qualification of the hemagglutination inhibition assay in support of pandemic influenza vaccine licensure. Clin. Vaccine Immunol. 16, 558-566 (2009).
10. Black, S. et al. Hemagglutination inhibition antibody titers as a correlate of protection for inactivated influenza vaccines in children. Pediatr. Infect. Dis. J. 30, 1081-1085 (2011).
11. Stohr, K., Bucher, D., Colgate, T. & Wood, J. Influenza virus surveillance, vaccine strain selection, and manufacture. Methods Mol. Biol. 865, 147-162 (2012).
12. Truelove, S. et al. A comparison of hemagglutination inhibition and neutralization assays for characterizing immunity to seasonal influenza A. Influenza Other Respi. Viruses 10, 518-524 (2016).
13. Reichert, T. A. et al. Influenza and the winter increase in mortality in the United States, 1959–1999. Am. J. Epidemiol. 160, 492-502 (2004).
14. Jester, B. J., Uyeki, T. M. & Jernigan, D. B. Fifty years of influenza A(H3N2) following the pandemic of 1968. Am. J. Public Health 110, 669-676 (2020).
15. Chambers, B. S., Li, Y., Hodinka, R. L. & Hensley, S. E. Recent H3N2 influenza virus clinical isolates rapidly acquire hemagglutinin or neuraminidase mutations when propagated for antigenic analyses. J. Virol. 88, 10986-10989 (2014).
16. Zost, S. J. et al. Contemporary H3N2 influenza viruses have a glycosylation site that alters binding of antibodies elicited by egg-adapted vaccine strains. Proc. Natl. Acad. Sci. U.S.A. 114, 12578-12583 (2017).
17. Rogers, G. N. & Paulson, J. C. Receptor determinants of human and animal influenza virus isolates: differences in receptor specificity of the H3 hemagglutinin based on species of origin. Virology 127, 361-373 (1983).

18. Moremen, K. W., Tiemeyer, M. & Nairn, A. V. Vertebrate protein glycosylation: diversity, synthesis and function. Nat. Rev. Mol. Cell Biol. 13, 448-462 (2012).

19. Chandrasekaran, A. et al. Glycan topology determines human adaptation of avian H5N1 virus hemagglutinin. Nat. Biotechnol. 26, 107-113 (2008).

20. Gambaryan, A. S. et al. 6-sulfo sialyl Lewis X is the common receptor determinant recognized by H5, H6, H7 and H9 influenza viruses of terrestrial poultry. Virol. J. 5, 85 (2008).

21. Yang, H. et al. Structure and receptor binding preferences of recombinant human A(H3N2) virus hemagglutinins. Virology 477, 18-31 (2015).

22. Peng, W. et al. Recent H3N2 viruses have evolved specificity for extended, branched human-type receptors, conferring potential for increased avidity. Cell Host Microbe 21, 23-34 (2017).

23. Byrd-Leotis, L. et al. Antigenic pressure on H3N2 influenza drift strains imposes constraints on binding to sialylated receptors, but not phosphorylated glycans. J. Virol. 93, JVI.01178-01119 (2019).

24. Blixt, O. et al. Printed covalent glycan array for ligand profiling of diverse glycan binding proteins. Proc. Natl. Acad. Sci. U.S.A. 101, 17033-17038 (2004).

25. Walther, T. et al. Glycomic analysis of human respiratory tract tissues and correlation with influenza virus infection. PLoS Pathog. 9, e1003223 (2013).

26. Jia, N. et al. The human lung glycome reveals novel glycan ligands for influenza A virus. Sci. Rep. 10, 5320 (2020).

27. North, S. J., Hitchen, P. G., Haslam, S. M. & Dell, A. Mass spectrometry in the analysis of N-linked and O-linked glycans. Curr. Opin. Struc. Biol. 19, 498-506 (2009).

28. Ito, T. et al. Receptor specificity of influenza A viruses correlates with the agglutination of erythrocytes from different animal species. Virology 227, 493-499 (1997).

29. Medeiros, R., Escriou, N., Naffakh, N., Manuguerra, J. C. & van der Werf, S. Hemagglutinin residues of recent human A(H3N2) influenza viruses that contribute to the inability to agglutinate chicken erythrocytes. Virology 289, 74-85 (2001).

30. Lin, Y. P. et al. Neuraminidase receptor binding variants of human influenza A(H3N2) viruses resulting from substitution of aspartic acid 151 in the catalytic site: a role in virus attachment? J. Virol. 84, 6769-6781 (2010).

31. Lin, Y. P. et al. Evolution of the receptor binding properties of the influenza A(H3N2) hemagglutinin. Proc. Natl. Acad. Sci. U.S.A. 109, 21474-21479 (2012).

32. Mögling, R. et al. Neuraminidase-mediated haemagglutination of recent human influenza A (H3N2) viruses is determined by arginine 150 flanking the neuraminidase catalytic site. J. Gen. Virol. 98, 1274-1281 (2017).

33. Takada, K. et al. A humanized MDCK cell line for the efficient isolation and propagation of human influenza viruses. Nat. Microbiol. 4, 1268-1273 (2019).

34. Joziasse, D. H. et al. Branch specificity of bovine colostrum CMP-sialic acid: N-acetyllactosaminide alpha 2----6-sialyltransferase. Interaction with biantennary oligosaccharides and glycopeptides of N-glycosylproteins. J. Biol. Chem. 260, 714-719 (1985).

35. Aich, U. et al. Glycomics-based analysis of chicken red blood cells provides insight into the selectivity of the viral agglutination assay. FEBS J. 278, 1699-1712 (2011).

36. Mbua, N. E. et al. Selective exo-enzymatic labeling of N-glycans on the surface of living cells by recombinant ST6Gal I. Angew. Chem. Int. Ed. 52, 13012-13015 (2013).

37. Moremen, K. W. et al. Expression system for structural and functional studies of human glycosylation enzymes. Nat. Chem. Biol. 14, 156-162 (2018).

38. WHO. Recommended composition of influenza virus vaccines for use in the 2019–20 northern hemisphere influenza season. (2019).

39. Jorquera, P. A. et al. Insights into the antigenic advancement of influenza A(H3N2) viruses, 2011-2018. Sci. Rep. 9, 2676 (2019).

40. Wu, N. C. et al. A complex epistatic network limits the mutational reversibility in the influenza hemagglutinin receptor-binding site. Nat. Commun. 9, 1264 (2018).

41. Wu, N. C. et al. Major antigenic site B of human influenza H3N2 viruses has an evolving local fitness landscape. Nat. Commun. 11, 1233 (2020).

42. Asensio, J. L., Ardá, A., Cañada, F. J. & Jiménez-Barbero, J. Carbohydrate–aromatic interactions. Acc. Chem. Res. 46, 946-954 (2013).

43. Lee, H. K. et al. Comparison of mutation patterns in full-genome A/H3N2 influenza sequences obtained directly from clinical samples and the same samples after a single MDCK passage. PLoS One 8, e79252 (2013).

44. Gulati, S. et al. Human H3N2 influenza viruses isolated from 1968 to 2012 show varying preference for receptor substructures with no apparent consequences for disease or spread. PLoS One 8, e66325 (2013).

45. Liu, L. et al. Streamlining the chemoenzymatic synthesis of complex N-glycans by a stop and go strategy. Nat. Chem. 11, 161-169 (2019).

46. Matrosovich, M., Matrosovich, T., Carr, J., Roberts, N. A. & Klenk, H. D. Overexpression of the alpha-2,6-sialyltransferase in MDCK cells increases influenza virus sensitivity to neuraminidase inhibitors. J. Virol. 77, 8418-8425 (2003).

47. Blundell, P. A., Lu, D., Dell, A., Haslam, S. & Pleass, R. J. Choice of host cell line is essential for the functional glycosylation of the Fc region of human IgG1 inhibitors of influenza B viruses. J. Immunol. 204, 1022-1034 (2020).

48. Ekiert, D. C. et al. A highly conserved neutralizing epitope on group 2 influenza A viruses. Science 333, 843 (2011).

49. Broszeit, F. et al. N-Glycolylneuraminic acid as a receptor for influenza A viruses. Cell Rep. 27, 3284-3294.e3286 (2019).

50. Cooper, C. A., Gasteiger, E. & Packer, N. H. GlycoMod–a software tool for determining glycosylation compositions from mass spectrometric data. Proteomics 1, 340-349 (2001).

51. van Baalen, C. A. et al. ViroSpot microneutralization assay for antigenic characterization of human influenza viruses. Vaccine 35, 46-52 (2017).

52. van Baalen, C. A. et al. Detection of nonhemagglutinating influenza A(H3) viruses by enzyme-linked immunosorbent assay in quantitative influenza virus culture. J. Clin. Microbiol. 52, 1672-1677 (2014).

53. Mazzocco, G. et al. 3DFlu: database of sequence and structural variability of the influenza hemagglutinin at population scale. Database 2016, baw130 (2016).

Supplementary information

Materials and Methods

Synthesis of biantennary *N*-glycans

Materials

Enzymes were expressed as previously described (B3GnT2 and B4GalT1[1], PmST1 M144L P34H[2]). The reaction mixtures were purified using a size exclusion Biogel (P2) from BioRad in Econo glass columns (0.7 x 30 cm / 1.5 x 30 cm / 1.5 x 50 cm) coupled to a BioFrac fraction collector (BioRad). Carbohydrate-containing fractions were detected by thin layer chromatography and an appropriate staining reagent (15 mL AcOH and 3.5 mL p-Anisaldehyde in 350 mL EtOH and 50 mL H_2SO_4). Reagents were purchased from Sigma-Aldrich. Uridine 5' diphosphogalactose (UDP-Gal), uridine 5' diphospho-N acetylglucosamine (UDP-GlcNAc) and cytidine-5'-monophospho-*N*-acetylneuraminic acid (CMP-Neu5Ac) were obtained from Roche Diagnostics [UDP-Gal: Cat# 07703562103; UDP-GlcNAc: Cat# 06369855103; CMP-Neu5Ac: Cat# 05974003103]. Final products were purified by HPLC using an XBridge HILIC column (10 mm (Ø) x 250 mm (l), 5 µm particle size) on a semi-preparative LC system from Shimadzu (LC-20AT, SIL-20A, CBM-20A, SPD-20A, FRC-10A). The purification was done using 10 mM NH_4HCOO in 10% H_2O in MeCN (buffer B) and 10 mM NH_4HCOO in 100% H_2O (buffer A). The progress of the reactions was monitored on a LC-MS system from Shimadzu (system controller: SCL10A-VP; HPLC pumps: LC10AD-VP; injector: SIL10AD-VP) using a ZIC HILIC column (ZeQuant, PEEK coated guard HPLC column, 3.5 µm particle size, 20 x 2.1 mm). The LC system was attached to a Bruker Daltonics microTOF-Q mass spectrometer.

Synthesis of N-glycans

Sialylglycopeptide (SGP) was extracted from egg yolk and further enzymatically modified to yield compound **1**, which was used as a starting material for the synthesis[3,4]. The terminal galactose of compound **1** was sialylated with an α2,6-specific sialyltransferase mutant P34H/M144L from *Pasteurella multocida* and CMP-Neu5Ac providing compound **2**[2]. This compound was subsequently extended with *N*-acetyllactosamine (LacNAc) repeats by using mammalian β1,4-galactosyltransferase 1 (B4GalT1) and β1,3-*N*-acetylglucosamine transferase (B3GnT2) with their corresponding nucleotide sugars UDP-Gal and UDP-GlcNAc, respectively. As a result, compound **3**, **4** and **6** with one, two and three consecutive LacNAc repeats on the MGAT1 (Mannose-3) branch and a terminal α2,6-linked *N*-acetylneuraminic acid (Neu5Ac) on the MGAT2 (Mannose-6) branch were obtained. These intermediates were used to synthesize the bisialylated compounds **5** and **7** by sialylating the extended MGAT1 (Mannose-3) branch with the α2,6-specific sialyltransferase mutant from *Pasteurella multocida* and CMP-Neu5Ac. Compounds **9** and **11**, modified with a single terminal Neu5Ac on either branch, were prepared by first quantitatively desialylating the intermediates **4** and **6** in an aqueous solution of acetic acid. Afterward, sialyltransferase ST6Gal1 and CMP-Neu5Ac were used to install a single terminal Neu5Ac moiety providing the products **9** and **11**.

General procedure for the installation of α2,6-Linked Neu5Ac using PmST1 (P34H/M144L)[2]

The acceptor and CMP-Neu5Ac (2.5 eq) were dissolved in a Tris buffer (100 mM, pH 9, 0.1 wt% BSA) to obtain a concentration of 5 mM. PmST1 M144L P34H (42 µg per µmol acceptor) and CIAP (1 u μL^{-1}, 1 u per µmol of added nucleotide) were added to the reaction mixture and it was incubated overnight at 37 °C with gentle shaking. The progress of the reaction was monitored by LC-MS. In case of incomplete conversion after 18 h, additional PmST1 M144L P34H (20 µg per µmol acceptor) was added and the reaction mixture incubated at 37 °C for an additional 24

h. After completion, the reaction mixture was lyophilized and applied to size exclusion chromatography. Carbohydrate-containing fractions were purified by HPLC (**2**: 68%B-66%B in 60 min, 3.3 mL min^{-1}; **5**: 65%B-64%B in 60 min, 3.3 mL min^{-1}; **7**: 65%B-50%B in 100 min, 3.3 mL min^{-1}) providing the product as a white powder (**2**: 16.9 mg, 82%, **5**: 0.48 mg, 17%; **7**: 1.7 mg, 46%).

General procedure for the installation of β1,3-linked glucose using B3GnT2

The acceptor and UDP-GlcNAc (1.5 eq) were dissolved in a HEPES buffer (50 mM, pH 9.6, 0.1 wt% BSA) containing DTT (1 mM) and MnCl2 (20 mM) to obtain a concentration of 5 mM. B3GnT2 (30 µg per µmol acceptor) and CIAP (1 u $µL^{-1}$, 1 u per µmol of added nucleotide) were added to the reaction mixture and it was incubated overnight at 37 °C with gentle shaking. The progress of the reaction was monitored by LC-MS. In case of incomplete conversion after 18 h, additional UDP-GlcNAc (0.5 eq), CIAP (1 u $µL^{-1}$, 1 u per µmol of added nucleotide) and B3GnT2 (15 µg per µmol acceptor) were added and the reaction mixture incubated at 37 °C for an additional 24 h. After completion, the reaction mixture was lyophilized and applied to size exclusion chromatography. Carbohydrate-containing fractions were lyophilized and used without further purification.

General procedure for the installation of β1,4-linked galactose using B4GalT1

The acceptor and UDP-Gal (1.5 eq) were dissolved in a Tris buffer (50 mM, pH 7.3, 0.1wt% BSA) containing MnCl2 (20 mM) to obtain a concentration of 5 mM. B4GalT1 (20 µg per µmol acceptor) and CIAP (1 u $µL^{-1}$, 1 u per µmol of added nucleotide) were added to the reaction mixture and it was incubated overnight at 37 °C with gentle shaking. The progress of the reaction was monitored by LC-MS. In case of incomplete conversion after 18 h, additional UDP-Gal (0.5 eq), CIAP (1 u $µL^{-1}$, 1 u per µmol of added nucleotide) and B4GalT1 (10 µg per µmol acceptor) were added and the reaction mixture incubated at 37 °C for 24 h. After completion, the

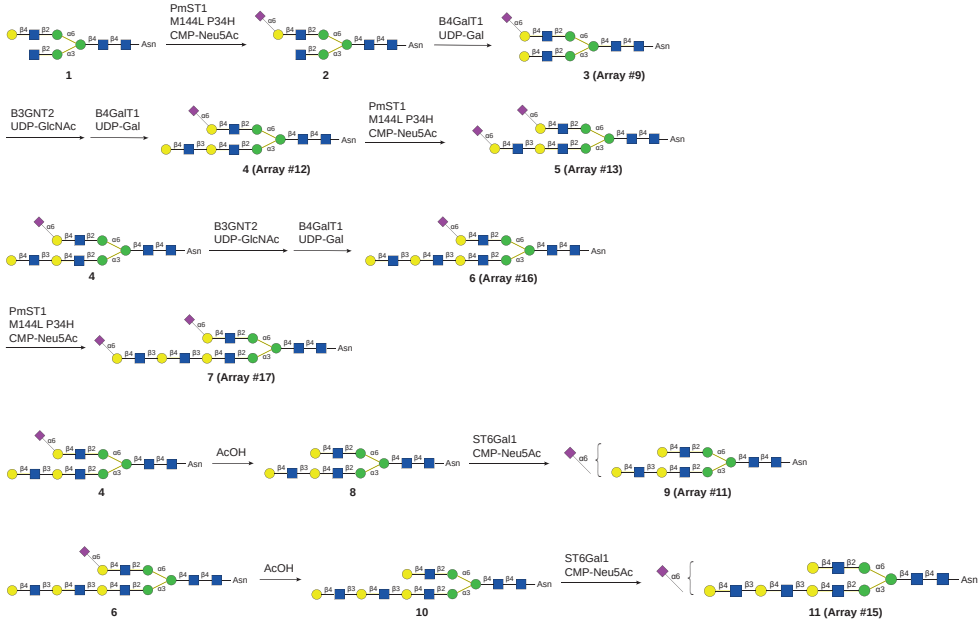

Supplementary scheme 1. Synthesis of asymmetric biantennary N-glycans.

reaction mixture was lyophilized and applied to size exclusion chromatography. Carbohydrate-containing fractions were purified by HPLC (**3**: 68%B-65%B in 60 min, 3.4 mL min^{-1}; **4**: 65%B for 60 min, 3.4 mL min^{-1}; **6**: 65%B for 60 min, 3.3 mL min^{-1};) providing the products as white powders (**3**: 16.4 mg, 88%; **4**: 19.2 mg, 89%; **6**: 11.3 mg, 75%).

General procedure for the removal of terminal Neu5Ac

The substrate was dissolved in an aqueous solution of acetic acid (2 M) and kept at 65 °C for 24 h. The solvent was removed in an N_2 flow and the reaction mixture was applied to size exclusion chromatography. Carbohydrate-containing fractions were lyophilized and used without further purification.

General procedure for the installation of α2,6-linked Neu5Ac using ST6Gal1

The acceptor and CMP-Neu5Ac (1.1 eq) were dissolved in a Tris buffer (50 mM, pH 7.3, 0.1 wt% BSA) to obtain a concentration of 2 mM. ST6Gal1 (42 µg per µmol acceptor) was added to the reaction mixture and it was incubated overnight at 37 °C with gentle shaking. The progress of the reaction was monitored by LC-MS. In case of incomplete conversion after 18 h, additional ST6Gal1 (20 µg per µmol acceptor) was added and the reaction mixture incubated at 37 °C for 24 h. After completion, the reaction mixture was lyophilized and applied to size exclusion chromatography. Carbohydrate-containing fractions were purified by HPLC (**9**: 68%B-64%B in 80 min, 3.4 mL min^{-1}; **11**: 67%B-62%B in 80 min, 3.4 mL min^{-1}) providing the product as a white powder (**9**: 47 µg, 17%, **11**: 50 µg, 10%).

Analytical data

VnmrJ 4 and TopSpin 4 were used to collect NMR data. NMR data was obtained at room temperature on a 600 MHz instrument from Bruker. The chemical shift δ is given in parts per million (ppm) and refers to tetramethylsilane and the residual solvent peak [^{1}H-NMR: δ(D_2O) = 4.79 ppm]. NMR data is given as follows: ^{1}H-NMR: chemical shift (multiplicity, coupling constants, relative integral, functional group); 13C data are extracted from HSQC spectra and given as follows: chemical shift. Multiplicity is defined as follows: s = singlet; d = doublet; t = triplet; m = multiplet. Signals were assigned by numbering the monosaccharide units starting at the reducing end of the oligosaccharide. Monosacharides attached to the mannose 6 branch are indicated by a " ' " (prime) and those attached to the mannose 3 branch without any mark. The assignment was done by using corresponding 2D-NMR spectra (COSY, HSQC). Due to the use of ammonium formate containing buffers during final purification, several spectra show residual FA (8.46 ppm, not shown in the NMR spectra) contamination. The yield/concentration of the final products was determined by NMR spectroscopy, using n-propanol as an internal standard. High resolution masses were measured on an Agilent 6560 Ion Mobility Q-TOF LC-MS system. NMR data can be found in the supplementary information of the online article.

Structural studies

It has been found that during the transition from late 90s to early-2000, HA of A/H3N2 viruses have a reduced affinity for the prototypic human receptor, the 6'-SLN[5]. Analysis of protein sequence alignment shows that the main sequences differences reside at the 130-loop (residues 131, 135 and 137), the 150-loop (residues 155-159), the 220-loop (residues 222, 225 and 226), the E190D mutation at the 190-helix, and the appearance of a new glycosylation site at residue 144 and 158. Other residues which contribute to sialic acid binding are highly conserved among HAs including Y98, H183, Y195 and W153 (Supplementary Table 3).

Although X-ray structural studies[5-8] have provided an understanding of the structural basis of changes in receptor-binding specificity, it has not uncovered interactions with extended glycan receptors. Such structural data is difficult to obtain by X-ray crystallography, and therefore we performed docking experiments of a sialoside having an extended LacNAc moiety with HAs of A/H3N2 viruses representing different evolutionary time points including A/NL/816/91 from 1991 (NL91), A/NL/109/03 from 2003 (NL03) and A/NL/1797/17 from 2017 (NL17).

Modeling of A/NL/816/91 (NL91)

NL91 recognized most of the human-type receptors, including compounds that have an α2,6-sialoside on a mono-LacNAc residue (glycans **7-9**, Figure 1A). A somewhat higher responsiveness was observed for receptors having an α2,6-sialoside onto di-LacNAc residue (glycans **10-13**, Figure 1A), while tri-LacNAc containing receptors did not further improve HA binding (glycans **14-17**). Collectively, the results showed that the optimal receptor for NL91 is an *N*-glycan having two repeating LacNAc moieties modified by a 2,6-linked sialoside (glycan **10** and **13**). Thus, we performed all atoms MD simulations of the complex between the NL91 and the receptor $(LacNAc)_2$α2-6Neu5Ac. The MD simulation showed that the glycan receptor binds the HA protein almost exclusively through the terminal sialic acid. In fact, the analysis of the MD derived trajectory revealed a stable binding pose for the α2,6-sialoside, while the underlying di-LacNAc chain explores multiple orientations along the simulation, where only transient intermolecular interactions exist. Comparing X-ray data and the molecular modeling derived structures indicated that the interaction network is preserved in HK68 and NL91. This is consistent with the high structural homology of the sialic binding site of HK68 and NL91 for which only two mutations exist, G135E and N137Y. Actually, these two residues contribute to receptor binding through their backbone atoms (Figure 3A). Specifically, all the hydrophobic interactions, such as those with Y98, H183, Y195 and W153, and H-bond interactions with residues 135-137 and S228 are preserved. In line with the X-ray studies[7], we found that in NL91 the Glu190 engages the Sia-1 O9 through H-bond interaction with an average distance of ~2.9 Å, while L226 makes hydrophobic interactions with the C-6 of the galactose-2 (Figure 3A). For the underlying di-LacNAc chain, the MD simulation showed that only the Gal-2 contributes to binding by either engaging E190 or G225 in an H-bond interaction. However, these interactions populate only 10% of the whole MD simulation, which results in a badley defined binding pose for the di-LacNAc chain. The results demonstrate that the HA protein of NL91 recognizes the human receptor through the terminal α2,6-sialoside while the underlying glycan does not significantly contribute to binding.

Modeling of A/NL/109/03 (NL03)

NL03 recognized far fewer glycans and did not bind to structures having their α2,6-sialosides at a mono-LacNAc moiety (glycans **7-9**, **12** and **16**, Figure 1A). It recognized structures having the sialoside on at least one di-LacNAc moiety (glycans **10** and **13**), although it shows a significant improvement in responsiveness when interrogated against structures which contain tri-LacNAc residues (glycans **14**, **15** and **17**). Thus, we performed all atoms MD simulations of the complex between the NL03 and the receptor $(LacNAc)_3$α2-6NeuAc. The MD simulation showed that the extended LacNAc chain contributes to HA binding. The analysis of the MD derived trajectory revealed a stable binding pose for both the α2,6-sialoside and the underlying tri-LacNAc chain. In agreement with previously reported X-ray studies[7], the analysis of the MD simulations showed that in NL03, the D190 does not participate in sialic acid binding. Instead, the D225 engages the Gal-2 O_3 through a H-bond interaction which results in a change in a dihedral angle of the sialic acid-galactose glycosidic bond. The rotation of the Gal-2 residue places all subsequent moieties toward the 190-helix[8]. The MD simulations showed that the Asp190

engages the Gal-4 O2 through H-bond interaction, while the Asn193 provides a H-bond interaction with the acetamide moiety of GlcNAc-3 with an average distance of ~2.5 Å (Figure 3E). Inspection of X-ray crystal structures[7,8] of post 2003 HAs shows that distal mutations to the RBD (A131T, H155T and E156H) reoriented the side chain of Y159, which resulted in an extended receptor-binding site (Supplementary Figure 9). The molecular modeling study showed that Gal-6 makes a CH-π interaction with the aromatic ring of Y159 (Figure 3E). The contribution of Y159 in further stabilizing receptor binding was analyzed by monitoring the distance of Gal-6 H3, H4 and H5 against the aromatic ring along the MD simulation (Supplementary Figure 10), which showed a stable interaction. These additional interactions support the hypothesis that post-2000 strains have undergone mutations that compensated for the reduced affinity for the terminal sialoside. Interestingly, the extensive epistatic network which correlates mutations at the RBS with those occurring at distal antigenic site, such as the 150-loop and 190-helix, has been demonstrated by large-scale mutagenesis experiments[7].

Modeling of A/NL/1797/17 (NL17)

NL17 and NL19 (3C.2a) showed strong responsiveness only to glycans **14**, **15** and **17** (Figure 1A). These glycans have in common that at least one of the arms is extended by three consecutive LacNAc units that is further modified by an α2,6-sialoside. Thus, a glycan having four LacNAc units arranged in an asymmetrical manner (**15**) represents the minimal receptor for these viruses. Mono-sialylated derivative **15** gave a similar responsiveness compared to the bis-sialosides **14** and **17** indicating that a bidentate binding event does not substantially contribute to recognition as previously suggested[9]. We docked the structure of the NL17 HA protein in complex with the receptor $(LacNAc)_3$α2-6NeuAc based on the results from MD simulation of NL03 in which we replaced the mutated residues by using the mutagenesis tool implemented in PyMOL. The resulting structure was minimized by using the steepest descent algorithm implemented in the Amber MD program. The orientation of the glycan receptor is very similar in NL03 and NL17. Specifically, NL17 does not present additional amino acid mutations at the sialic acid binding site, leading to the same binding interactions as for NL03 at this site. The Gal-2 is also bound in a similar manner, thus orienting the GlcNAc-3 against the 190-helix. However, in NL17 residue 193 is substituted by Phe for which H-bond interaction is not possible, suggesting that F193 does not contribute to receptor binding (Figure 3G, H and I). The missing interaction with the GlcNAc-3 may be the reason for the lack of binding of di-LacNAc containing glycans observed for NL17 with respect to the reduced binding of NL03 (Figure 1A). Instead, the Y159 is preserved and allows for CH-π interaction with the Gal-6 of the internal LacNAc moiety. The importance of Y159 in extended *N*-glycan binding is confirmed by the receptor specificity of 3C.3a clade which present the Y159S and F193S mutations. It is expected that these viruses lost the ability to engage the Gal-6 through CH-π interactions while compensate by H-bond interaction between the GlcNAc-3 and the S193, which reflect the regained ability of binding sialilated di-LacNAc glycans (glycans **10** and **13**). The molecular modeling study herein presented support a notion that A/H3N2 viruses have undergone mutations to create an extended binding site.

References

1 Moremen, K. W., Ramiah, A., Stuart, M. et al. Expression system for structural and functional studies of human glycosylation enzymes. Nat. Chem. Biol. 14, 156-162 (2017).

2 McArthur, J. B., Yu, H., Zeng, J. & Chen, X. Converting pasteurella multocida α2–3-sialyltransferase 1 (pmst1) to a regioselective α2–6-sialyltransferase by saturation mutagenesis and regioselective screening. Org. Biomol. Chem. 15, 1700-1709 (2017).

3 Seko, A., Koketsu, M., Nishizono, M., Enoki, Y., Ibrahim, H. R., Juneja, L. R., Kim, M. & Yamamoto, T. Occurrence of a sialylglycopeptide and free sialylglycans in hen's egg yolk. Biochim. Biophys. Acta 1335, 23-32 (1997).

4 Liu, L., Prudden, A. R., Capicciotti, C. J., Bosman, G. P., Yang, J.-Y., Chapla, D. G., Moremen, K. W. & Boons, G.-J. Streamlining the chemoenzymatic synthesis of complex n-glycans by a stop and go strategy. Nat. Chem. 11, 161-169 (2018).

5 Lin, Y. P., Xiong, X., Wharton, S. A., Martin, S. R., Coombs, P. J., Vachieri, S. G., Christodoulou, E., Walker, P. A., Liu, J., Skehel, J. J., Gamblin, S. J., Hay, A. J., Daniels, R. S. & McCauley, J. W. Evolution of the receptor binding properties of the influenza a(h3n2) hemagglutinin. Proc. Nat. Acad. Sci. USA 109, 21474 (2012).

6 Wu, N. C., Zost, S. J., Thompson, A. J., Oyen, D., Nycholat, C. M., McBride, R., Paulson, J. C., Hensley, S. E. & Wilson, I. A. A structural explanation for the low effectiveness of the seasonal influenza h3n2 vaccine. PLOS Pathogens 13, e1006682 (2017).

7 Wu, N. C., Thompson, A. J., Xie, J., Lin, C.-W., Nycholat, C. M., Zhu, X., Lerner, R. A., Paulson, J. C. & Wilson, I. A. A complex epistatic network limits the mutational reversibility in the influenza hemagglutinin receptor-binding site. Nat. Commun. 9, 1264 (2018).

8 Wu, N. C., Otwinowski, J., Thompson, A. J., Nycholat, C. M., Nourmohammad, A. & Wilson, I. A. Major antigenic site b of human influenza h3n2 viruses has an evolving local fitness landscape. Nat. Commun. 11, 1233 (2020).

9 Peng, W., de Vries, R. P., Grant, O. C., Thompson, A. J., McBride, R., Tsogtbaatar, B., Lee, P. S., Razi, N., Wilson, I. A., Woods, R. J. & Paulson, J. C. Recent h3n2 viruses have evolved specificity for extended, branched human-type receptors, conferring potential for increased avidity. Cell Host Microbe 21, 23-34 (2017).

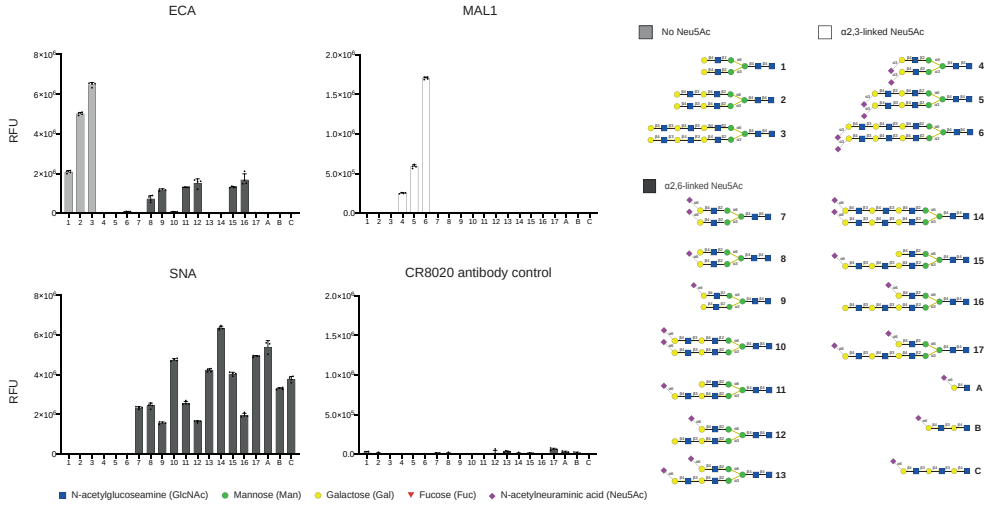

Supplementary Figure 1. Binding specificity of control lectins ECA, MAL1 and SNA and CR8020 A/H3N2 stem antibody. Glycans were printed on NHS glass slides and receptor specificity of the biotinylated lectins and the CR8020 antibody was visualized using Streptavidin-AlexaFluor-635 and a goat anti-human AlexaFluor-647 antibody. Bars represent the background-subtracted average relative fluorescence units (RFU) of four replicates ± SD. Values for all individual datapoints are represented in the Supplementary Source Data file. Glycans **1-3**: non-sialylated; **4-6**: α2,3-linked Neu5Ac; **7-17**: α2,6-linked Neu5Ac; **A-C**: linear α2,6-linked Neu5Ac.

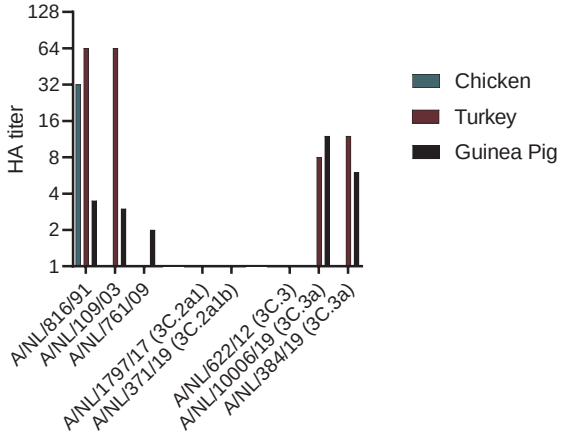

Supplementary Figure 2. Evolution of A/H3N2 hemagglutination ability of fowl and guinea pig erythrocytes. Hemagglutination (HA) titers are shown for a representative set of A/H3N2 viruses over the course of evolution in the last two decades. All HA assays were performed in the presence of 20 nM oseltamivir.

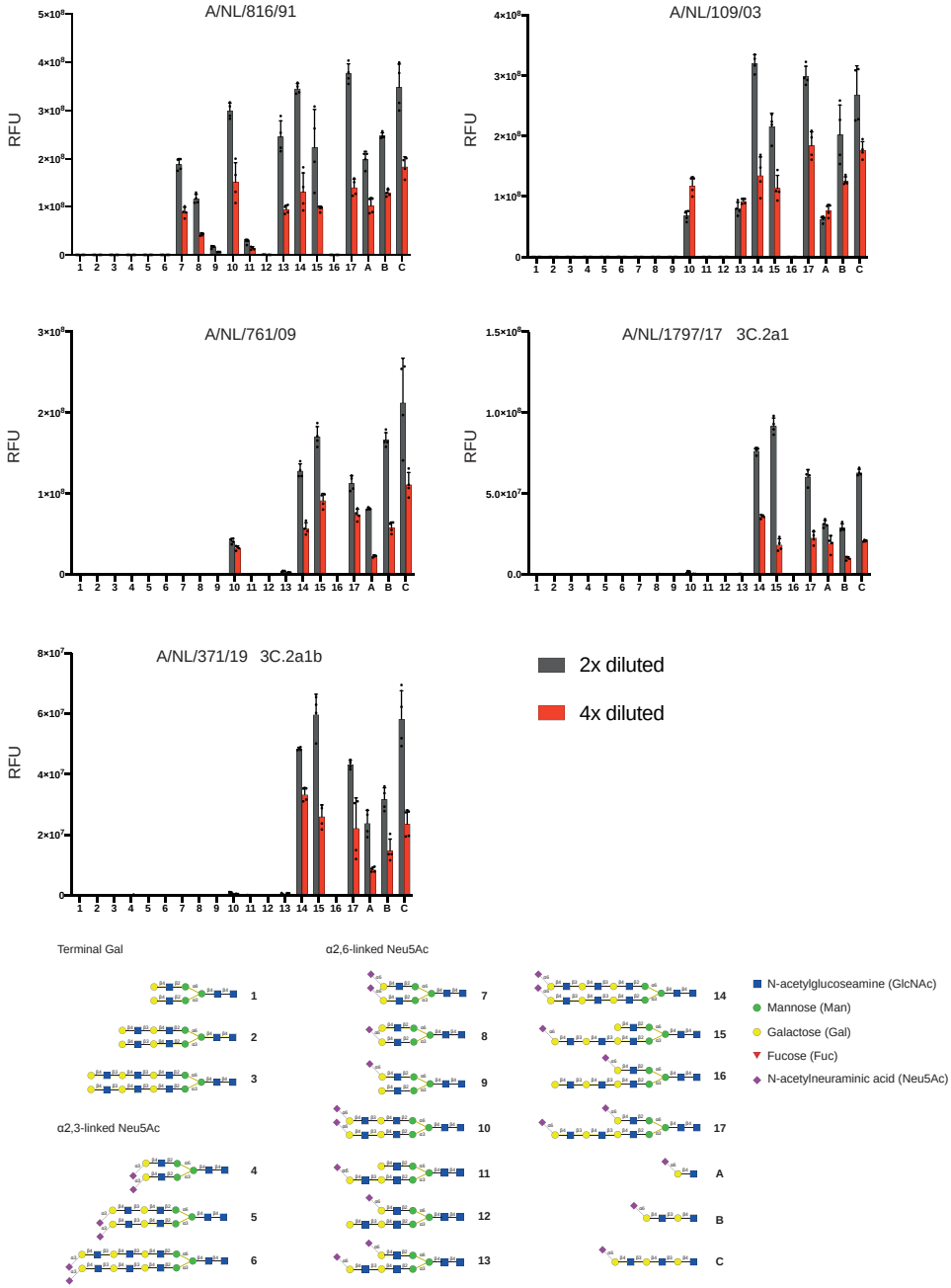

Supplementary Figure 3. Concentration-dependent response of representative A/H3N2 viruses in glycan microarray analysis. Glycans were printed on NHS glass slides and receptor specificity was visualized using the human CR8020 antibody followed with a goat anti-human AlexaFluor-555 antibody. Viruses were applied to the assay 2x and 4x diluted from the original isolate. Bars represent the background- subtracted average relative fluorescence units (RFU) of four replicates ± SD. Values for all individual datapoints are represented in the Supplementary Source Data file. Glycans **1-3**: non-sialylated; **4-6**: α2,3-linked Neu5Ac; **7-17** and **A-C**: α2,6-linked Neu5Ac.

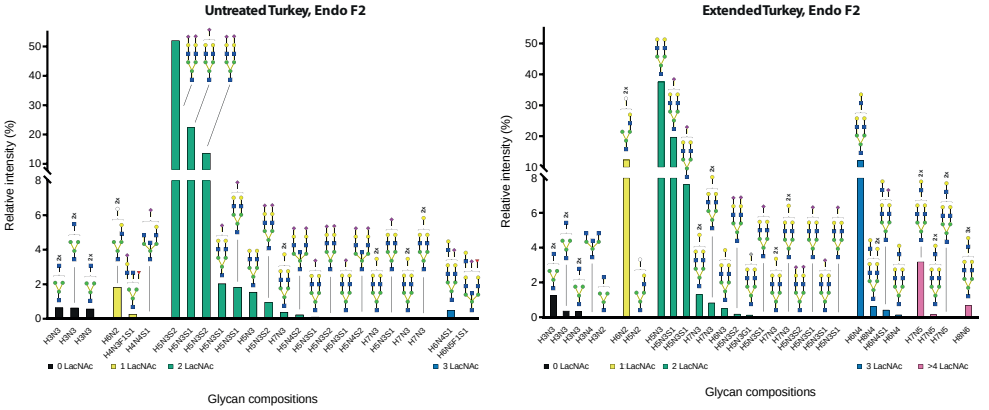

Supplementary Figure 4. Glycomic analysis of N-glycosylation of turkey erythrocytes released by Endo F2. The data is sorted by abundance and number of LacNAc units. Proposed structures are assigned to detected glycan compositions.

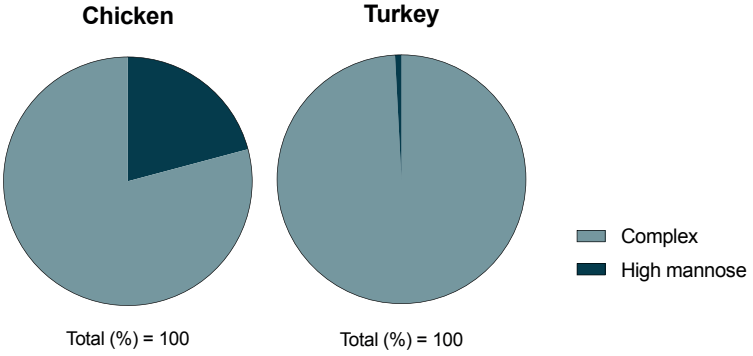

Supplementary Figure 5. Relative cell surface occupation of complex and high mannose glycans on chicken and turkey erythrocytes. The percentual distribution of complex and high mannose glycans was calculated based on the data from the glycomic analysis of untreated erythrocytes. The full overview of the glycomic data can be found in Data S1-S2.

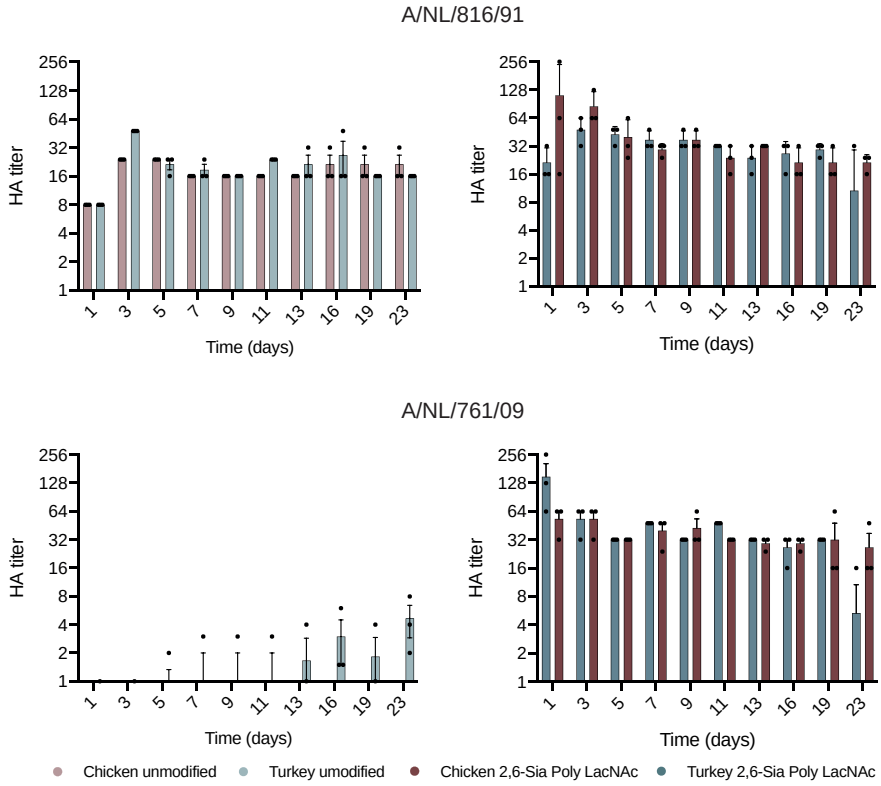

Supplementary Figure 6. Stability assay of glyco-engineered erythrocytes. Shown are the HA titers of A/H3N2 A/NL/761/09 and A/H3N2 A/NL/816/91 using unmodified (left) or glyco-engineered (right) erythrocytes from chicken (red) and turkey (blue). Glyco-engineering and HA assays were performed in full biological triplicates and means are plotted ± SEM.

Supplementary table 1. Focus reduction assay of recent A/H3N2 virus isolates.

			Post-infection ferret sera raised against						
Virus	Passage	Clade	NIB-104 3C.2a1a	A/NL/314/19 3C.2a1b	NIB-112 3C.2a2	A/NL/3466/17 3C.2a2	A/NL/1802/18 3C.2a2	X-327 3C.3a	A/NL/384/19 3C.3a
NIB-104 (A/Singapore/INFH-16-0019/16)	E7Mdck_Siat2hCK	3C.2a1a	240	80	240	*n.t.*	160	30	<20
A/Netherlands/1797/18	Mdck1Siat2hCK	3C.2a1	<20	160	<20	20	40	<20	<20
A/Netherlands/314/19	MdckSiat2hCK	3C.2a1b	<20	160	<20	30	60	<20	<20
A/Netherlands/10009/19	mixhCK2	3C.2a1b	<20	60	<20	*n.t.*	80	<20	<20
A/Netherlands/371/19	MdckSiatmixhCK	3C.2a1b	<20	240	<20	30	60	<20	<20
NIB-112 (A/Switzerland/8060/17)	E7E1hCK	3C.2a2	480	5120	5120	3840	240	<20	<20
A/Netherlands/3466/17	Siat1hCK1	3C.2a2	30	80	480	960	80	<20	<20
A/Netherlands/1802/18	Siat1hCK1	3C.2a2	<20	80	<20	30	640	<20	<20
A/Netherlands/10616/19	MdckSiatmixhCK	3C.2a2	<20	120	120	640	80	<20	<20
X327 (A/Kansas/014/17)	E17E1Siat1hCK	3C.3a	<20	<20	<20	<20	<20	960	30
A/Netherlands/384/19	Siat2hCK	3C.3a	<20	<20	30	<20	30	40	80
A/Netherlands/10006/19	MdckSiatmixhCK2	3C.3a	<20	<20	<20	<20	<20	20	60

n.t. = not tested

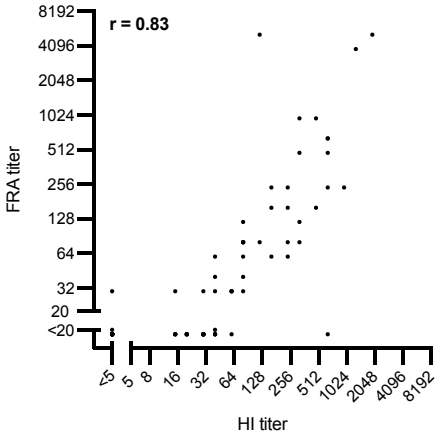

Supplementary Figure 7. Correlation of hemagglutination inhibition and focus reduction titers by recent A/H3N2 viruses. Shown is the correlation between every HI titer and FRA titer for all viruses and sera as depicted in Table 1 and Supplementary Table 1. The titers of the focus reduction assay duplicates were averaged for the graph. Spearman's rank correlation coefficient was measured using Prism 8.3.1 (graphpad).

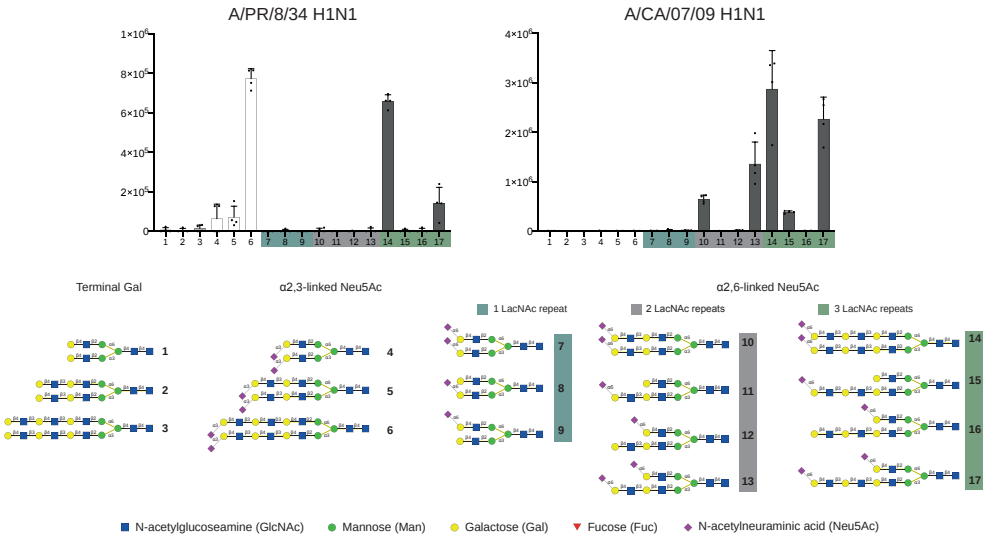

Supplementary Figure 8. Receptor binding specificities of representative H1N1 viruses using glycan microarray analysis. Binding was visualized using a human anti-H1 stalk antibody (CR6261). Bars represent the background-subtracted average relative fluorescence units (RFU) of four replicates ± SD. Values for all individual datapoints are represented in the Supplementary Source Data file.

Supplementary Table 2. Sequence analysis. Alignment of A/H3N2 HA sequence spanning from 1968 to 2019. Amino acid mutation refers to the A/HK/1/68 sequence. Amino acid Substitutions are labelled in color code according to the changes in polarity: mutations that led to amino acids of similar polarity are labelled in gray, mutations that led to less polar aa are in pink, mutations to more polar uncharged residue are labeled in light blue, mutations to amino acids with negatively charged side chain are labeled in red, mutations to amino acids with positive charged side chain are labeled in dark blue. New occurring glycosylation sites are labeled in green.

			aa sequence																														
Subtype	Year	Id	98	131	133	134	135	136	137	143	144	145	146	153	155	156	157	158	159	160	182	183	188	189	190	193	194	195	196	221	222	223	224	225	226	227	228
H3N2	1968	A/Hong Kong/1/68	Y	T	N	G	G	S	N	P	G	S	G	W	T	K	S	G	S	T	V	H	N	O	E	S	L	Y	V	P	W	V	R	G	N	S	S
H3N2	1991	A/Netherlands/816/91	Y	A	S	G	E	S	Y	S	V	K	S	W	H	E	S	E	Y	T	V	H	D	R	E	S	L	Y	V	P	W	V	R	G	L	S	S
H3N2	1991	A/Siena/3/91	Y	A	S	G	E	S	Y	S	V	K	S	W	H	E	S	D	Y	K	V	H	D	R	E	S	L	Y	V	P	W	V	R	G	L	S	S
H3N2	2003	A/Netherlands/109/03	Y	T	N	G	T	S	S	S	N	K	S	W	T	H	L	K	Y	K	V	H	D	S	D	S	L	Y	A	P	R	V	R	D	I	S	S
H3N2	2003	A/New York/18/03	Y	T	N	G	T	S	S	S	N	K	S	W	T	H	L	K	Y	R	V	H	D	S	D	N	L	Y	A	P	R	V	R	D	V	S	S
H3N2	2005	A/Wisconsin/67/05	Y	T	N	G	T	S	S	S	N	N	S	W	T	H	L	K	F	K	V	H	D	N	D	F	L	Y	A	P	R	I	R	N	I	P	S
H3N2	2007	A/Brisbane/10/07	Y	T	N	G	T	S	S	S	N	N	S	W	T	H	L	K	F	K	V	H	D	N	D	F	L	Y	A	P	R	V	R	N	I	P	S
H3N2	2009	A/Perth/16/09	Y	T	N	G	T	S	S	S	K	N	S	W	T	H	L	N	F	K	V	H	D	K	D	F	L	Y	A	P	R	V	R	N	I	P	S
H3N2	2009	A/Netherlands/761/09	Y	T	N	G	T	S	S	S	N	N	S	W	T	H	L	R	F	K	V	H	D	N	D	F	L	Y	A	P	R	V	R	N	I	P	S
H3N2	2011	A/Victoria/361/11	Y	T	N	G	T	S	S	S	N	N	S	W	T	Q	L	N	F	K	V	H	D	K	D	F	L	Y	A	P	R	I	R	N	I	S	S
H3N2	2012	A/Texas/53/12	Y	T	N	G	T	S	S	S	N	N	S	W	T	H	L	N	F	K	V	H	D	K	D	F	L	Y	A	P	R	I	R	N	I	P	S
H3N2	2014	A/Hong Kong/4801/14	Y	T	N	G	T	S	S	S	S	S	S	W	T	H	L	N	Y	T	V	H	D	K	D	F	L	Y	A	P	R	I	R	D	I	P	S
H3N2	2016	A/Singapore/INFH-16-0019/16	Y	T	N	G	T	S	S	S	S	S	S	W	T	H	L	N	Y	T	V	H	D	K	D	F	L	Y	A	P	R	I	R	D	I	P	S
H3N2	2017	A/Netherlands/1797/17	Y	T	N	G	K	S	S	S	S	S	S	W	T	H	L	N	Y	T	X	H	D	K	D	F	L	Y	A	P	R	I	R	D	I	P	S
H3N2	2019	A/Netherlands/371/19	Y	T	N	G	K	S	S	S	S	S	S	W	T	H	L	N	Y	T	X	H	D	K	D	F	L	Y	A	P	R	I	R	D	I	P	S
H3N2	2013	A/Swiss/971529/13	Y	T	N	G	T	S	S	S	N	S	S	W	T	H	L	N	S	K	V	H	D	K	D	F	L	Y	A	P	R	I	R	D	I	P	S
H3N2	2012	A/Netherlands/622/12	Y	T	N	G	T	S	S	S	N	S	S	W	T	H	L	N	F	K	V	H	D	K	D	F	L	Y	A	P	R	I	R	N	I	P	S
H3N2	2016	A/Netherlands/153/16	Y	T	N	G	T	S	S	S	N	S	S	W	T	H	L	N	S	K	V	H	D	K	D	F	L	Y	A	P	R	I	R	D	I	P	S
H3N2	2017	A/Kansas/14/17	Y	T	N	G	T	S	S	S	K	S	S	W	T	H	L	N	S	K	V	H	D	K	D	S	L	Y	A	P	R	I	R	D	I	P	S
H3N2	2019	A/Netherlands/10002/19	Y	T	N	G	T	S	S	S	K	S	S	W	T	H	L	N	S	K	V	H	D	K	D	S	L	Y	A	P	R	I	R	D	I	P	S
		consensus sequence	Y	T	N	G	T	S	S	S	.	S	S	W	T	H	L	N	.	K	V	H	D	K	D	F	L	Y	A	P	R	I	R	.	I	P	S

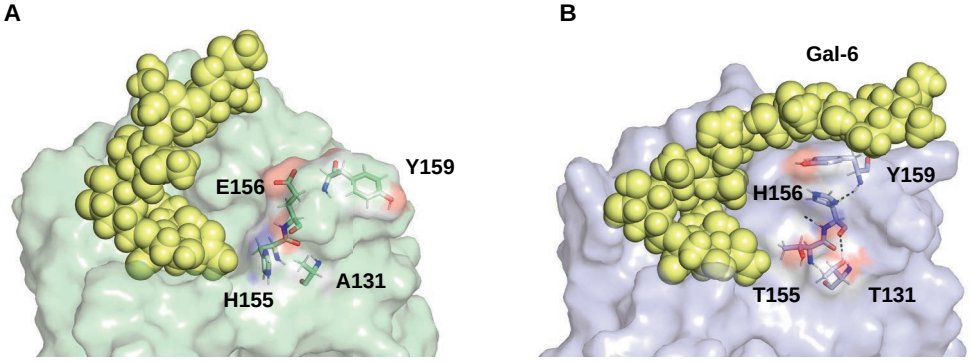

Supplementary Figure 9. Comparison of the last frames from MD simulation of (a) NL91 and (b) NL03 highlighting the amino acid substitutions which shaped the orientation of the side chain of Y159. The CH-π interaction with the proximal Gal-6 is possible only for NL/03 due to the favorable interaction between the H156 and Y159 rings. On the other hand, the unfavorable contacts between the negatively charged Glu156 and the aromatic ring displaces the Y159 side chain away from the Gal-6 residue, hampering the CH-π interaction. The H-bond network which shape the orientation of Y159 is defined by the dashed black line.

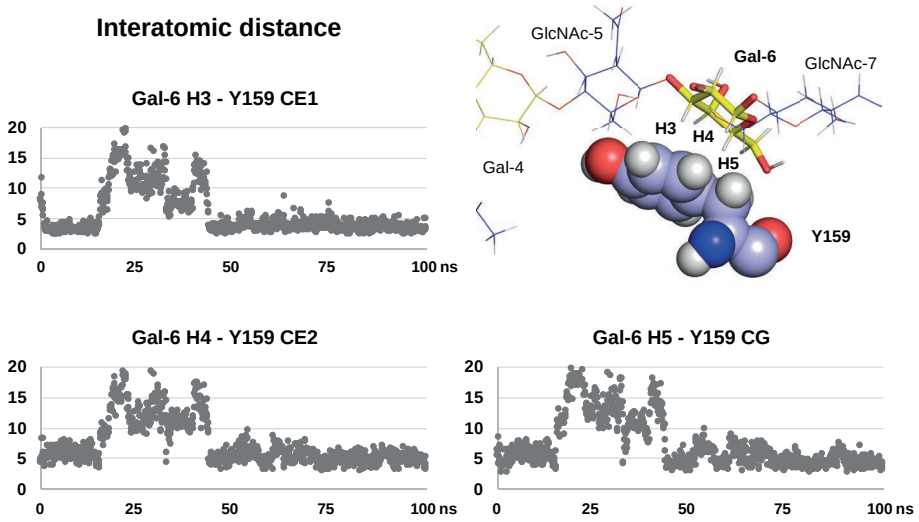

Supplementary Figure 10. Details of the CH-π interactions for Gal-6 residue as determined by measuring the distance among the Gal-6 H3, H4 and H5 and the Y159 aromatic ring along the MD simulation.

Supplementary Data 1 & 2. Full glycomic data of *N*-glycans on 2,6-Sia Poly-LN fowl erythrocytes. Provided as a separate pdf file.

Supplementary Data 3. Microarray Source data.

Chapter 4

Glutaraldehyde Fixation of Glycan-Remodeled Erythrocytes

Rosanne J. van Beek[1], Frederik Broszeit[1], Mark Pronk[2], Pascal Lexmond[2] & Geert-Jan Boons[1]

[1]Department of Chemical Biology & Drug Discovery, Utrecht Institute for Pharmaceutical Sciences, Utrecht University, 3584 CG Utrecht, The Netherlands;

[2]Department of Viroscience, Erasmus MC, P.O. Box 2040, 3000 CA, Rotterdam, The Netherlands;

4

Abstract

Glycan engineered erythrocytes offer a solution for the increased challenges with the antigenic characterization of influenza A/H3N2 viruses by HI assay, and thereby aid the surveillance of circulating viruses for vaccine updates. However, their relatively short shelf life after engineering limits their use and increases their costs. Therefore, in this study we aimed to increase the shelf life of our engineered erythrocytes by preservation of the cells with glutaraldehyde. Glutaraldehyde is a fixative that preserves erythrocytes by crosslinking proteins by a reaction between the bifunctional aldehyde groups and amino acids, and provides excellant ultrastructural preservation. We showed that glutaraldehyde fixated erythrocytes stayed stable for at least 20 weeks for the use in hemagglutination assays. Also, when performing an HI assay we observed a strong positive correlation between the inhibition titers obtained using fresh or fixated erythrocytes, indicating that the glutaraldehyde fixation does not interfere with the binding of antigens and antisera in the HI assay. One difficulty of working with the glutaraldehyde fixated erythrocytes that we observed was the altered sedimentation of the erythrocytes, which decreases the sensitivity of the assay.

Introduction

Influenza viruses circulate the globe and compromise public health during seasonal outbreaks[1]. Their ability to rapidly evolve and evade our immunity requires regular vaccine updates for good protection. To timely monitor if antigenic changes in circulating viruses require a vaccine update, the Global Influenza Surveillance and Response System (GISRS) from the WHO closely monitors the antigenic evolution of influenza viruses[2,3]. This surveillance primarily relies on the Hemagglutination inhibition (HI) assay. The HI assay measures the ability of serum antibodies to block receptor binding by the virus HA protein through the inhibition of virus-mediated agglutination of erythrocytes[4]. This inhibition can be quantified and gives a direct correlate of protection. Therefore, the HI assay is a useful measure to select representative virus strains for vaccine production and has been the golden standard for the last 50 years. HI assays are preferably performed with fowl erythrocytes, which are nucleated, heavy and thereby show a sedimentation that facilitates the interpretation of the assay.

In the recent decades, antigenic characterization of A/H3N2 viruses by the HI assay has become increasingly challenging[5,6]. Evolution of influenza A/H3N2 viruses has shifted its receptor specificity towards α2,6-linked sialic acids presented on extended glycans containing multiple LacNAc repeats due to a loss of binding towards shorter glycans, starting between 1999 and 2003[7–9]. The absence of this minimal receptor on the cell surface of fowl erythrocytes has led to a loss in agglutinating ability of these viruses, making the HI assay inapplicable for a growing number of A/H3N2 viruses[10]. Applying the knowledge of this evolved receptor specificity, an exo-enzymatic cell-surface glycan remodeling strategy was developed to install the minimal receptors on the surface of fowl erythrocytes. This remodeling strategy resulted in an efficient agglutination of the remodeled cells by contemporary A/H3N2 viruses[11]. The compatibility of the recent A/H3N2 viruses with the standard HI assay using the engineered erythrocyts could offer a solution to the current problem with the antigenic characterization of these viruses.

To make glycan remodeled erythrocytes available for the antigenic characterization of circulating viruses, increasing the stability of the erythrocytes is desirable. Erythrocytes are officially stated to have a shelf life of 21 days when used for blood transfusions[12]. However, when stored in PBS erythrocytes will show hemolysis within a few days after isolation from blood and most laboratories render them inapplicable for HI assays after 1 week of storage in PBS. This limitation is overcome in most virology laboratories by inhouse animal facilities to provide fresh blood on a weekly basis. However, the glycan remodeling takes several days, decreasing the window to perform HI assays using the glycan remodeled cells. Prolonging the shelf-life of the engineered erythrocytes will aid both production and distribution of the cells by allowing more efficient use of the received batches and facilitating the production of larger batches of engineered erythrocytes.

One way that has been used to preserve erythrocytes is fixation of the cells with glutaraldehyde[13–15]. Glutaraldehyde is a fixative that crosslinks proteins by a reaction between the bifunctional aldehyde groups and amino acids[16,17]. The extensive crosslinking of this fixative provides excellent ultrastructural preservation of the cells. Fixation by glutaraldehyde can stabilize red blood cells up to 18 months[18], and was found to be compatible with hemagglutination and hemagglutination inhibition assays for human influenza viruses when using turkey erythrocyts[19]. Therefore, we here tested the applicability of glutaraldehyde fixation to increase the shelf life of our engineered cells.

Results

Stability time-course of glutaraldehyde fixated RBCs

To assess the effect of glutaraldehyde fixation on the binding properties and stability of the engineered erythrocytes we modified fresh turkey erythrocytes using our previously published glycan remodeling procedure[11] in biological triplicates. After modification, the cells in each sample were split and 50% of the erythrocytes were fixated in a 0.3 % glutaraldehyde PBS solution. 0.3 % Glutaraldehyde has proven in previous literature to efficiently fixate red blood cells without any effects on the protein conformation and antigenicity of the cell surface[20,15]. Both fixated and fresh glycan remodeled erythrocytes were stored in a 10% PBS solution and their stability was tested weekly in a hemagglutination assay using the influenza virus A/Netherlands/371/2019 (Figure 1). This A/H3N2 virus from the clade 3C.2a1b has lost its binding ability to unmodified turkey erythrocytes[11]. On day zero and week 1 both fixated and fresh modified erythrocytes showed stable titers, and the fixation did not significantly influence the agglutination of the erythrocytes (Figure 1). From week 2, the fresh erythrocytes showed hemolysis, causing instable titers and from week 3 no titers could be obtained from the fresh cells. The fixated cells however showed very stable titers until week 4. The dramatic drop in titer and increased SEM of the fixated cells in week 5 and 6 appeared to be due to increased sedimentation of the erythrocytes during the hemagglutination assay. We adjusted the method of resuspension of the cells by rotating them at 4 °C for one hour before performing the hemagglutination assay (method 2), after which stable titers were obtained until week 20.

Antigenic characterization of A/H3N2 viruses by HI assay

After confirming the increased stability of the fixated erythrocytes in the stability time course, we continued by performing an HI assay with the fixated erythrocytes using a subset of representative recent A/H3N2 viruses. In the hemagglutination assay, performed to set the virus concentrations for the HI assay, we observed the same sedimentation pattern of the fixated cells as we observed in the stability time course in week five and six. This caused the hemag-

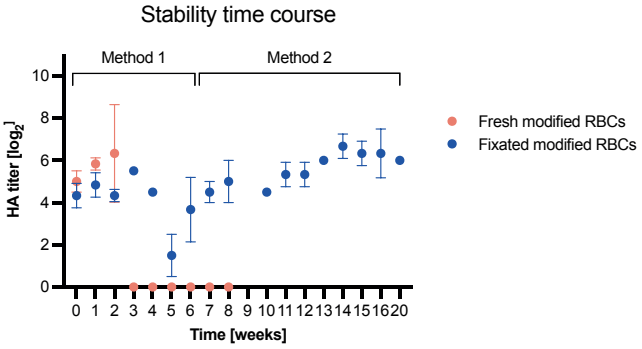

Figure 1. Stability time course. Hemagglutination assays were performed using the influenza A/H3N2 virus A/NL/371/2019 (clade 3C.2a1b), using fresh or fixated glycan remodeled erythrocytes. After week 6 erythrocytes were resuspended by rotating for 1 hour (method 2) before performing the assay. The mean titers (+/-SEM) of the triplicates obtained in the hemagglutination assays were plotted, starting at day 0.

glutinating titers of the virus stocks to be on average seven times lower when using the fixated erythrocytes compared to fresh engineered erythrocytes (Table S1). For this reason, separate virus dilutions were made for the fixated and fresh modified erythrocytes for the HI assay. Both fixated and fresh cells were employed to antigenically characterize a set of representative recent A/H3N2 viruses of various clades using post-infection ferret sera (Table 1 & 2). Sera 17A3466 and 19A384 used in the HI assay showed increased serum control titers when using the fixated erythrocytes, which decreased the sensitivity of the HI data compared to fresh erythrocytes. For both the fixated and the fresh cells all antisera showed robust inhibition of their homologous viruses and sera 19A314 and 17A3466 showed a clear clade specificity in their inhibition pattern. Egg derived vaccine strain NIB-104 showed greater inhibition by most antisera than the cell grown viruses. Also, post infection ferret serum obtained from NIB-104 showed no cross reactivity with any other than its homologous virus. In some cases, antisera showed aberrant inhibition when using fixated erythrocytes. Most of the aberrant titers in fixated cells showed a lower inhibition compared to the fresh cells. Viruses A/Netherlands/384/2019 and A/Netherlands/10006/2019 did not show inhibition by any of the heterologous antisera when using fixated erythrocytes. The titers from the HI matrices were plotted in an X-Y scatter to determine the correlation between the titers obtained using both conditions (Figure 2). There is a strong positive correlation between the titers obtained using both erythrocyte (r = 0.851). Most deviations from the trend line can be assigned to lower titers obtained when using the fixated cells compared to the fresh erythrocytes.

Antigenic cartography

The antigenic distances between the viruses as measured in the HI assay were visualized in an antigenic map. Using the antigenic cartography R package Racmacs[21], we plotted the HI data in a two-dimensional map, where the antigenic distance (visualized in antigenic units) corresponds to the inverse $\log_2$ of the HI titers. Multidimensional scaling methods are used to place all antigens and antisera on the map in a way that best fits the calculated distances from the HI

Table 1. Hemagglutination inhibition assay of A/H3N2 virus isolates using fresh modified erythrocytes.

			Post-infection ferret sera raised against				
			NIB-104	19A314	17A3466	18A1802	19A384
Virus	Passage	Clade	*3C.2a1a*	*3C.2a1b*	*3C.2a2*	*3C.2a2*	*3C.3a*
NIB-104 (A/Singapore/INFH-16-0019/16)	MdckSiat1_hCK2	3C.2a1a	**320**	320	80	640	80
A/Netherlands/1797/2017	MDCKSiat2_ hCK2	3C.2a1	<20	320	40	80	<20
A/Netherlands/314/2019	MDCKSiat2_ hCK2	3C.2a1b	<20	**640**	80	160	40
A/Netherlands/371/2019	MDCKSiat2_MDCK1_hCK2	3C.2a1b	<20	640	<20	160	60
A/Netherlands/3466/2017	Siat2_hCK2	3C.2a2	<20	80	**960**	80	<20
A/Netherlands/1802/2018	Siat1_hCK2	3C.2a2	<20	40	60	**960**	20
A/Netherlands/10616/2019	Mdck_SiatMix_hCK2	3C.2a2	<20	80	640	80	<20
A/Netherlands/384/2019	Siat2_hCK4	3C.3a	<20	<20	30	40	**320**
A/Netherlands/10006/2019	MDCK_Siatmix_ hCK3	3C.3a	<20	<20	20	30	320
		Serum control	*20*	*20*	*0*	*0*	*20*

Table 2. Hemagglutination inhibition assay of A/H3N2 virus isolates using fixated modified erythrocytes.

			Post-infection ferret sera raised against				
			NIB-104	19A314	17A3466	18A1802	19A384
Virus	Passage	Clade	*3C.2a1a*	*3C.2a1b*	*3C.2a2*	*3C.2a2*	*3C.3a*
NIB-104 (A/Singapore/INFH-16-0019/16)	MdckSiat1_hCK2	3C.2a1a	**320**	320	640	320	80
A/Netherlands/1797/2017	MDCKSiat2_ hCK2	3C.2a1	<20	<20	40	40	<40
A/Netherlands/314/2019	MDCKSiat2_ hCK2	3C.2a1b	<20	**320**	40	60	<40
A/Netherlands/371/2019	MDCKSiat2_MDCK1_hCK2	3C.2a1b	<20	320	40	80	<40
A/Netherlands/3466/2017	Siat2_hCK2	3C.2a2	<20	80	**640**	80	<40
A/Netherlands/1802/2018	Siat1_hCK2	3C.2a2	<20	80	40	**640**	<40
A/Netherlands/10616/2019	Mdck_SiatMix_hCK2	3C.2a2	<20	80	640	40	<40
A/Netherlands/384/2019	Siat2_hCK4	3C.3a	<20	<20	<20	<20	**240**
A/Netherlands/10006/2019	MDCK_Siatmix_ hCK3	3C.3a	<20	<20	<20	<20	240
		Serum control	*20*	*20*	*20*	*0*	*40*

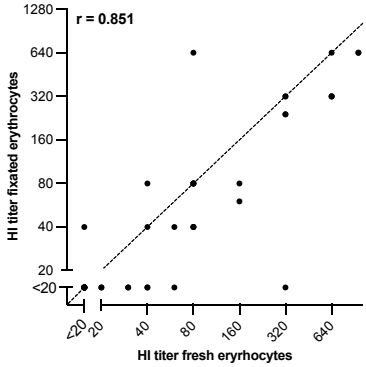

Figure 2. Correlation of hemagglutination inhibition titers obtained from fresh and fixated remodeled erythrocytes. Shown is the correlation between every HI titer for all viruses and antisera as depicted in table 1 and 2. Spearman's rank correlation coefficient was measured using graphpad Prism 9. To aid the readout of the plot, all titers below the detection threshold are depicted as <20 in the graph.

data. The maps were selected out of 500 optimizations and were aligned in their orientation. Figure 3 shows the antigenic maps created using the fresh modified erythrocytes (Figure 3A) and the fixated modified erythrocytes (Figure 3B), presented as blob plots to visualize the uncertainty of each antigen and antiserum. The viruses and sera are color coded based on their antigenic clade. There are multiple factors that influence the placement of antigens and antisera on an antigenic map. Generally, the data obtained from the HI matrix can be split into high reactors and low reactors. Low reactors are those values that are equal to or fall below the detection threshold of the assay, which in this study is 20-40. These low reactors are given the same values but can differ in their binding affinities. Therefore, they are unreliable and will be placed on the map with less certainty, resulting in larger blobs in the map. Additionally, all antigens placed on the map with the use of only one or two datapoints are placed with less certainty. Together these uncertainties influenced the resolution of the antigenic map and resulted in a change in orientation of multiple antigens and antisera between both erythrocyte conditions (Figure S1). We quantified the resolution of the antigenic maps by correlating the theoretical antigenic distances calculated from the HI matrix (the inverse 2log of the titer) with the fitted antigenic distances on the antigenic map. Figure 4 shows correlations of the data obtained with fresh erythrocytes (Figure 4A, r = 0.837) and with fixated erythrocytes (Figure 4B, r = 0.528), underlining the decreased resolution when using fixated erythrocytes.

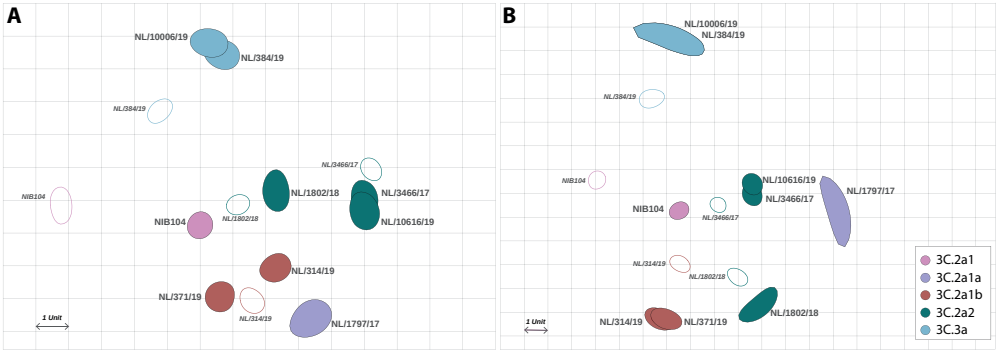

Figure 3. Antigenic cartography. Shown are the antigenic distances of A/H3N2 viruses based on serological data obtained using fresh (**A**) and fixated (**B**) engineered erythrocytes. Antigens and antisera are depicted as blobs, representing areas in which a particular antigen or antisera can be positioned without increasing the total stress of the map above one unit. All are color-coded by their clades as depicted in the legend. 1 unit on the antigenic map corresponds to a 2-fold serial dilution in the HI assay.

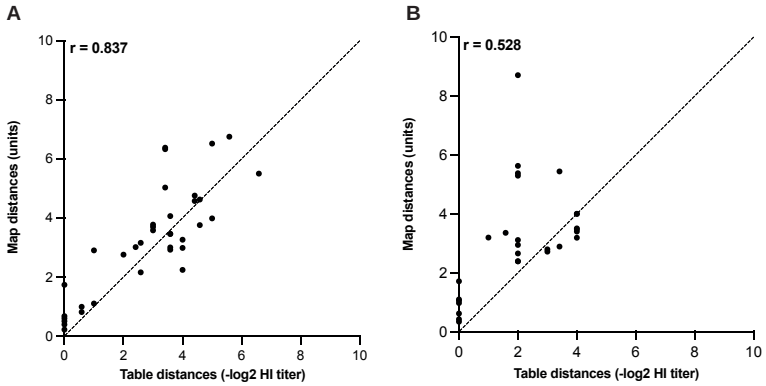

Figure 4. Correlation of HI data and map distances. Shown are the correlations between the -log2 values of the HI titers and the distances in the antigenic maps using fresh (**A**) and fixated (**B**) erythrocytes. Spearman's rank correlation coefficient was measured using graphpad Prism 9.

Discussion

Glycan engineered erythrocytes offer a solution for the increased challenges with the antigenic characterization of influenza A/H3N2 viruses by HI assays. However, their relatively short shelf life after engineering limits their use and increases their costs. Therefore, in this study we investigated the use of glutaraldehyde fixation to increase the stability and shelf life of our engineered erythrocytes for efficient distribution and use of the cells for antigenic characterization.

In a stability time course with the recent A/H3N2 influenza virus A/Netherlands/371/2019 (clade 3C.2a1b) we showed that glutaraldehyde fixated erythrocytes stayed stable for at least 20 weeks. This is in accordance with previous studies that showed a stability of glutaraldehyde fixated cells for up to 18 months[18,22]. Also, when performing an HI assay we observed a strong

positive correlation between the inhibition titers obtained using fresh or fixated erythrocytes, indicating that the glutaraldehyde fixation does not interfere with the binding of antigens and antisera in the HI assay.

However, one difficulty of working with the glutaraldehyde fixated erythrocytes that we observed was the altered sedimentation of the erythrocytes. The fixated cells required an increased resuspension to obtain stable titers, an adjustment that proved to be very delicate in the performance of the HI assay when using larger volumes of blood. Glutaraldehyde fixation decreases the cell volume of erythrocytes by 9%, thereby increasing the density of the cells[17]. This increased density might influence the sedimentation of the erythrocytes. However, this does not explain the fact that this increased sedimentation could be prevented by prolonged resuspension of the cells prior to agglutination.

Even though the set of antigens and antisera used in the current study was too small to draw definitive conclusions, the results indicate that glutaraldehyde fixated erythrocytes can be used to identify antigenically distinct A/H3N2 viruses in an HI assay. However, use of the fixated erythrocytes did result in an increased number of titers below the detection threshold of the assay. This resulted in a lower resolution in the generated antigenic map, meaning that the use of fixated erythrocytes potentially decreases the chance of correctly detecting smaller antigenic changes between circulating viruses. This could make them less suitable for global influenza surveillance than fresh modified erythrocytes. A solution for this might be found in alterations to the fixation protocol. Eventually, future endeavors might create the opportunity to completely replace erythrocytes as the carrier for the glycan receptors in HI assays. Recently, synthrocytes were introduced as a synthetic alternative to the use of RBCs in HI assays[24]. Synthetic beads might be the ultimate solution to create stable beads for the use in HI assays.

References

1. Iuliano, A. D. et al. Estimates of global seasonal influenza-associated respiratory mortality: a modelling study. Lancet 391, 1285–1300 (2018).
2. WHO GISRS. https://www.who.int/initiatives/global-influenza-s
3. Hay, A. J. & McCauley, J. W. The WHO global influenza surveillance and response system (GISRS)—A future perspective. Influenza Other Respi. Viruses 12, 551–557 (2018).
4. Who. Manual for the laboratory diagnosis and virological surveillance of influenza. World Heal. Organ. 2011 153 (2011).
5. Medeiros, R., Escriou, N., Naffakh, N., Manuguerra, J. C. & Van Der Werf, S. Hemagglutinin residues of recent human A(H3N2) influenza viruses that contribute to the inability to agglutinate chicken erythrocytes. Virology 289, 74–85 (2001).
6. Nobusawa, E., Ishihara, H., Morishita, T., Sato, K. & Nakajima, K. Change in receptor-binding specificity of recent human influenza A viruses (H3N2): A single amino acid change in hemagglutinin altered its recognition of sialyloligosaccharides. Virology 278, 587–596 (2000).
7. Gulati, S. et al. Human H3N2 Influenza Viruses Isolated from 1968 To 2012 Show Varying Preference for Receptor Substructures with No Apparent Consequences for Disease or Spread. PLoS One 8, (2013).

8. Hn, A. et al. Structure and receptor binding preferences of recombinant. Virology 477, 18–31 (2015).

9. Peng, W. et al. Recent H3N2 Viruses Have Evolved Specificity for Extended, Branched Human-type Receptors, Conferring Potential for Increased Avidity. Cell Host Microbe 21, 23–34 (2017).

10. Cc, W. H. O. WORLDWIDE INFLUENZA CENTRE THE FRANCIS CRICK INSTITUTE 1 MIDLAND ROAD LONDON NW1 1AT the composition of influenza vaccine for the Northern. 1–95 (2021).

11. Broszeit, F. et al. Glycan remodeled erythrocytes facilitate antigenic characterization of recent A/H3N2 influenza viruses. Nat. Commun. 12, 1–12 (2021).

12. García-roa, M. et al. Red blood cell storage time and transfusion: current practice, concerns and future perspectives. (2017). doi:10.2450/2017.0345-16

13. Morel, F. M. M., Baker, R. F., Wayland, H. & Knust-Graichen, P. V. Quantitation of human red blood cell fixation by glutaraldehyde. J. Cell Biol. 48, 91–100 (1971).

14. S, J. M. I. A. R. D., Brooks, D. E., Itagenberger, B. & Ag, N. B. ON T H E H U M A N EFFECTS OF A L D E H Y D E S ERYTHROCYTE Neuraminidase Assay of Aldehydes Glutaraldehyde Osmomet ~ ? t. 809–818

15. Koganei, A., Tsuchiya, T., Samura, K. & Nishikibe, M. Use of whole sheep red blood cells in ELISA to assess immunosuppression in vivo. J. Immunotoxicol. 4, 77–82 (2007).

16. Kawahara, Ji., Ishikawa, K., Uchimaru, T., Takaya, H. Chemical crosslinking by Glutaraldehyde between amino groups: Its mechanism and effects. in Polymer modification 119–131 (1997).

17. Abay, A. et al. Glutaraldehyde - A subtle tool in the investigation of healthy and pathologic red blood cells. Front. Physiol. 10, 1–14 (2019).

18. Swanepoel, R., Struthers, J. K. & McGillivray, G. M. Reversed passive hemagglutination and inhibiton with Rift Valley fever and Crimean-Congo hemorrhagic fever viruses. Am. J. Trop. Med. Hyg. 32, 610–617 (1983).

19. Kode, S. S., Pawar, S. D., Tare, D. S. & Mullick, J. Application of frozen and stored glutaraldehyde-fixed turkey red blood cells for hemagglutination and hemagglutination inhibition assays for the detection and identification of influenza viruses. J. Virol. Methods 289, 114046 (2021).

20. Branch, M. Methods for binding cells to plastic: application to a solid-phase radioimmunoassay for cell-surface antigens. 33, 87–95 (1980).

21. Github. Racmacs. https://github.com/acorg/Racmacs (2022).

22. Tanya, V. N. & Scott, G. R. Viral haemagglutination erythrocytes of sheep Results Introduction and conclusion. Virol. Commun. 47, 283–284 (1994).

23. Burry, R. W. & Wood, J. G. Contributions of lipids and proteins to the surface charge of membranes. An electron microscopy study with cationized and anionized ferritin. J. Cell Biol. 82, 726–741 (1979).

24. Sánchez-Cano, A. et al. Detection of Viruses and Virus-Neutralizing Antibodies Using Synthetic Erythrocytes: Toward a Tuneable Tool for Virus Surveillance. ACS Sensors 6, 83–90 (2021).

25. Smith, D. J. Mapping the Antigenic and Genetic. Science (80-.). 305, 371–376 (2004).

Material & Methods

Influenza viruses

A total of nine human A/H3N2 influenza viruses were chosen for this study to represent the different circulating clades. A/Singapore/INFH-16-0019/16 (NIB-104) and A/Netherlands/1797/2017 were chosen to represent clade 3C.2a1 and 3C.2a1a. A/Netherlands/371/2019 and A/Netherlands/314/2019 represented clade 3C.2a1b. Clade 3c.2a2 was represented by the viruses A/Netherlands/3466/2017, A/Netherlands/1802/2018 and A/Netherlands/10616/2019. Lastly, the viruses A/Netherlands/384/2019 and A/Netherlands/2019 represented viruses from clade 3C.3a. All viruses were kindly provided by the department of Viroscience at Erasmus Medical Center.

Erythrocyte preparation

Erythrocytes were obtained by centrifuging fresh Turkey blood (10 min, 430 rcf). After centrifugation, the supernatant was removed and the pellet was washed three times in PBS. Erythrocytes were stored in a 50% solution at 4 °C until further use.

Glyco-engineering of red blood cells

Materials

Mammalian glycosyltransferases were expressed according to literature reports. B3GnT2 and ST6Gal1 were cleaved and purified from GFP tags prior to use. Nucleotide sugars UDP-Gal, UDP-GlcNAc and CMP-Neu5Ac were purchased at Roche Diagnostics (UDP-Gal: Cat# 07703562103; UDP-GlcNAc: Cat# 06369855103; CMP-NeuAc: Cat# 05974003103). *Arthrobacter ureafaciens* neuraminidase was obtained from New England Biolabs (1 U defined as the amount of enzyme catalyzing the conversion of 1 µmol(substrate) min^{-1}) (Cat# P0722L). Alkaline phosphatase (FastAP) was obtained from Thermo Scientific (Cat# EF0651).

The enzymatic extenstion of the erythrocytes was perfomed following previously reported protocol[11]. Briefly, PBS (900 µL) and *Arthrobacter Ureafaciens* neurmanidase (12 U) were added to a suspension of 50% fowl erythrocytes (250 µL) and incubated for 6 hours at 37 °C while tilting for the desialylation of the glycans. Next, the desialylated glycans were extended by the addition of the glycosyltransferases B4GALT1 (37.5 µL, 1 mg mL^{-1}) and B3GNT2 (37.5 µL, 1 mg mL^{-1}), the nucleotide sugars UDP-Gal (4.4 mM) and UDP-GlcNAc (4.4 mM), alkaline phosphatase (6 U), MnCl2 (2mM) and BSA (6 µL, 2 mg mL^{-1}). This reaction mixture was incubated overnight at 37 °C while tilting. After overnight incubation the erythrocytes were washed two times and resialylted using ST6Gal1 (37.5 µL, 1 mg mL^{-1}) and CMP-Neu5Ac (4.4mM) in the presence of BSA (6 µL, 2 mg mL^{-1}) and alkaline phosphatase (6U) for 4 hours at 37 °C while tilting. Glycan remodeled erythrocytes were washed in PBS and stored in a 50% solution at 4 °C for further use.

Glutaraldehyde fixation

For the glutaraldehyde fixation of erythrocytes, firstly a stock solution of 0.3 % glutaraldehyde (Sigma Aldrich) in PBS was prepared. A 50% erythrocyte solution was fixated in 0.3% glutaraldehyde PBS in a volume ratio of 1:15 for 1 hour at room temperature while rotating. During fixation the color of the erythrocytes change from bright red to dark brown. After fixation the cells were washed three times in PBS and stored in a 10% solution in PBS at 4 °C until use in hemagglutination (inhibition) assays.

Stability time-course

For the stability assay Turkey erythrocytes were glycan remodeled in full biological triplicates like described above. After modification, 50 % of the glycan engineered erythrocytes was fixated with glutaraldehyde as described above and stored in a 10 % solution. Hemagglutination assays were performed every week using 1% erythrocytes and the influenza virus A/Netherlands/371/2019. Hemagglutination assays were performed following standard protocols[4]. Briefly, virus stocks were two-fold serial diluted in the presence of oseltamivir (20 nM) in a 96-wells plate. The erythrocytes (1%) were mixed with the serial diluted viruses and incubated for 1 hr at 4 °C before titers were determined. Titers were expressed as the highest dilution of virus stock that completely agglutinated the turkey erythrocytes. The means of the titers over the triplicates were plotted +/- SEM.

Hemagglutination inhibition assay

Hemagglutination inhibition assays were performed following standard procedures. Post-infection ferret sera raised against the viruses NIB-104, A/Netherlands/314/2019, A/Netherlands/3466/2017 and A/Netherlands/1802/2018 were kindly provided by the department of Viroscience at Erasmus Medical Center. The treated antisera were pre-absorbed with either fixated or fresh erythrocytes (10%) by incubation for 1,5 hrs at 4 °C, while mixing every 30 minutes. Pre-absorbed antisera were two-fold serial diluted (starting at 1:10) and mixed with virus stock (25 µL) containing 4 hemagglutinating units. Viruses were incubated with the antisera for 1 hr at 4 °C in the presence of oseltamivir (20 nM) and BSA (0.5%). Turkey erythrocyte solution (25 µL, 1%) was added and after a 1 h incubation at 4 °C inhibition patterns were recorded. Titers were expressed as the value of the highest serum dilution that gave complete inhibition of agglutination.

Antigenic cartography

We created a geometric interpretation of the inhibition titers against the tested A/H3N2 viruses using R Antigenic Cartography Macros (Racmacs) software, R package21. Based on the data from the Hemagglutination inhibition assay, antigenic maps were constituted in R using the package Racmacs (https://github.com/acorg/Racmacs). The Racmacs package provides a toolkit for making antigenic maps from assay data such as HI assays as described in literature[25]. Minimal column bases were set to none, and the maps were picked based upon 500 optimizations. The maps are presented on a grid in which each square indicates 1 antigenic unit, corresponding to a two-fold dilution of the antibody in the Hemagglutination inhibition assay. Antigenic distance was measured in any direction on the map, and the directions of both maps were aligned. Spearman's correlation coefficients between the data from the HI matrix and the distances on the antigenic maps were calculated using graphpad Prism 9.

Supplementary Table 1. Hemagglutination assay of A/H3N2 virus isolates using unmodified, 2,6-Sia Poly-LN modified and 2,6-Sia Poly-LN modified and fixated turkey erythrocytes.

Virus	Type	Clade	Hemagglutination titers (HAU per 25 µl)		
			Unmodified	Modified	Modified & Fixated
NIB-104 (A/Singapore/INFH-16-0019/16)	H3N2	3C.2a1a	*n.d.*	64	32
A/Netherlands/1797/2017	H3N2	3C.2a1	*n.d.*	256	48
A/Netherlands/314/2019	H3N2	3C.2a1b	*n.d.*	256	48
A/Netherlands/371/2019	H3N2	3C.2a1b	*n.d.*	48	4
A/Netherlands/3466/2017	H3N2	3C.2a2	*n.d.*	256	32
A/Netherlands/1802/2018	H3N2	3C.2a2	*n.d.*	256	32
A/Netherlands/10616/2019	H3N2	3C.2a2	*n.d.*	256	32
A/Netherlands/384/2019	H3N2	3C.3a	*n.d.*	192	24
A/Netherlands/10006/2019	H3N2	3C.3a	*n.d.*	192	32

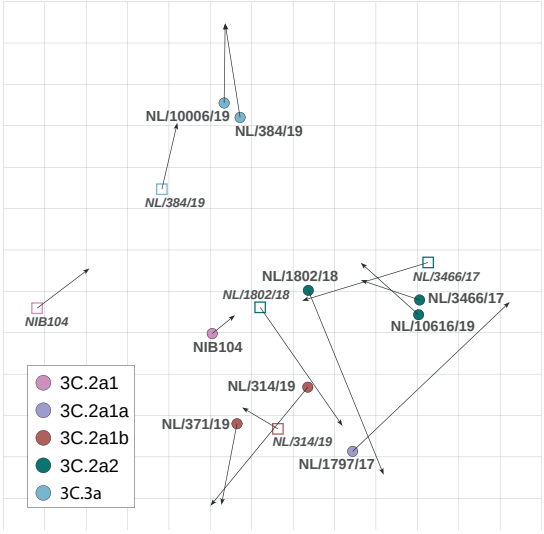

Supplementary Figure 1. Comparison of antigenic maps. Shown is the antigenic map of fixated erythrocytes with arrows indicating the location of antisera and antigens on the antigenic map generated with fresh erythrocytes. Antisera are color-coded based on their antigenic clade. 1 unit represents a 2-fold dilution of antisera in the HI assay.

Chapter 5

Glycomic Analysis Reveals Increased Sialylation, α-Gal and Extended Glycans in hCK Cells Compared to MDCK

Rosanne J. van Beek[1], Igor Sweet[1], Karli R. Reiding[2,3]

[1]Department of Chemical Biology & Drug Discovery, Utrecht Institute for Pharmaceutical Sciences, Utrecht University, 3584 CG Utrecht, The Netherlands.

[2]Biomolecular Mass Spectrometry and Proteomics, Bijvoet Center for Biomolecular Research and Utrecht Institute for Pharmaceutical Sciences, University of Utrecht, 3584 CH Utrecht, The Netherlands.

[3]Netherlands Proteomics Center, The Netherlands.

5

Abstract

For the identification and characterization of circulating influenza viruses, it is essential to isolate and propagate viruses from clinical specimens. MDCK cells are the most widely used cell line for the propagation of influenza viruses because of their high susceptibility to infection by various influenza virus strains and their easy maintenance. However, recent human influenza A/H3N2 viruses show poor propagation in MDCK cells. A humanized MDCK cell line, called hCK, was therefore generated with an increased presentation of prototypic human-type receptors. hCK cells were proven successful for the propagation of recent A/H3N2 viruses. While the sialic acid linkages in hCK cells have been studied, only sparse information can be found on the rest of the glycosylation characteristics which might influence infection. Therefore, to gain a better understanding of which cell-line changes may have led to the enhanced infectivity of recent A/H3N2 viruses, we comprehensively investigated the glycosylation characteristics of hCK cells and compared them to the classical MDCK cells. In doing so, we observed an increase in sialylation and poly-LacNAc abundance, leading to increased size of complex glycans in hCK cells, but we also detected considerably increased α-galactosylation, a non-human glycosylation characteristic. Thus, while the hCK cells may provide valuable information on virus-host interactions, care has to be taken to interpret results since changes in glycosylation happened on levels beyond the sialylation linkages.

Introduction

The GISRS is a worldwide network that monitors the spread of influenza viruses to timely detect antigenic mutations that require vaccine adaptations[1]. Currently, two influenza A subtypes (A/H1N1 and A/H3N2) and two lineages of the influenza B virus (B/Yamagata and B/Victoria) circulate the globe to cause seasonal influenza or epidemics[2]. For the identification and characterization of circulating viruses it is essential to isolate and propagate viruses from clinical specimens. MDCK cells are the most widely used cell line for the propagation of viruses because of their high susceptibility to infection by various influenza virus strains and their easy maintenance[3,4].

The surface of human influenza A and B viruses is covered by two main glycoproteins, hemagglutinin (HA) and neuraminidase (NA). HA acts as the receptor-binding protein and recognizes sialic acids presented on the surface of the host cell for infection. HA is also the major antigen that stimulates protective immunity in the host by the generation of neutralizing antibodies. The prototypic receptor for HA proteins on human influenza viruses is a sialic acid linked to the underlying galactose in an α2,6-linkage (Neu5Ac(α2,6)Gal)[5]. This is also thought to be the main determinant of host tropism between human and avian viruses as HA proteins on avian influenza viruses recognize sialic acids linked in α2,3-linkage to the underlying galactose for infection. MDCK cells present both α2,3-linked and α2,6-linked sialic acids on their surface, making them suitable for isolation of influenza viruses from multiple species.

Despite the widely accepted use of MDCK cells for the propagation of influenza viruses, the human influenza virus A/H3N2 has shown a decrease in propagation efficiency in MDCK cells. The rapid evolution of these viruses has coincided with an altered receptor usage, which resulted in the inability of these viruses to agglutinate red blood cells as well as the inability to propagate these viruses in MDCK cells. To overcome this problem, research has focused on increasing the prototypic human receptor on the surface of MDCK cells[6,7]. A humanized MDCK cell line, called hCK, was generated with overexpressed α2,6-specific sialyltransferase (ST6Gal1) to increase presentation of prototypic human-type receptors. Additionally, to further skew the hCK sialylation pattern toward α2,6-linkages, seven different α2,3-specific sialyltransferases were genetically removed[8]. Together, hCK cells were proven successful for the propagation of recent A/H3N2 viruses[8].

However, in recent years studies have shown that A/H3N2 viruses might not only need the prototypic α2,6-linkage for infection, but also require underlying glycan structures like poly-*N*-acetyllactosamine (Poly-LacNAc, poly-LN) structures for their binding[9-12]. While the sialic acid linkages present in hCK cells have been studied, only sparse information can be found on the rest of the glycosylation characteristics which might influence infection[13]. Therefore, to gain a better understanding of the receptor requirements of recent A/H3N2 viruses for infection, we comprehensively investigated the glycosylation characteristics of hCK cells, and compared them to the classical MDCK cells to uncover the full array of glycomic changes that may have led to the enhanced infectivity.

Results

Recent A/H3N2 viruses are efficiently propagated in hCK cells and not in MDCK cells

To verify the findings that only hCK cells are susceptible for infection by recent A/H3N2 viruses[8], we first investigated the propagation efficiency of two A/H3N2 viruses representing two evolutionary time points. A/NL/816/1991 (NL91) represents A/H3N2 viruses that can be propagated in MDCK cells. Also, this virus can be agglutinated by both chicken and turkey erythrocytes and showed efficient binding to α2,6-linked sialic acids presented on both short and extended LacNAc repeats in microarray studies. A/NL/371/2019 (3C.2a1b, NL19) represents A/H3N2 viruses that cannot be propagated in MDCK cells. Also, this virus cannot be agglutinated by both chicken and turkey erythrocytes and in binding studies showed strong binding exclusively to α2,6-linked sialic acids on *N*-glycan structures presenting at least one arm with three consecutive LacNAc repeats in microarray studies[12].

A ten-fold serial dilution of both viruses was prepared and hCK and MDCK cells were inoculated with five different virus dilutions. Infection efficiency of all five virus dilutions was analyzed at 6 hours post-infection using flow cytometry. Both MDCK and hCK cells showed high infection percentages after inoculation with A/NL91 (Figure 1A). Inoculation with A/NL19 however, only led to high infection percentages in hCK cells and showed very low infection percentages even for the highest virus concentration in MDCK cells (Figure 1A). The difference in infection efficiency was visualized by immunofluorescence imaging after an overnight infection of A/NL19 in both cell lines (Figure 1B). The obtained results confirmed previous literature that recent A/H3N2 viruses could not be propagated in MDCK cells but could be propagated in the recently developed hCK cell line[14].

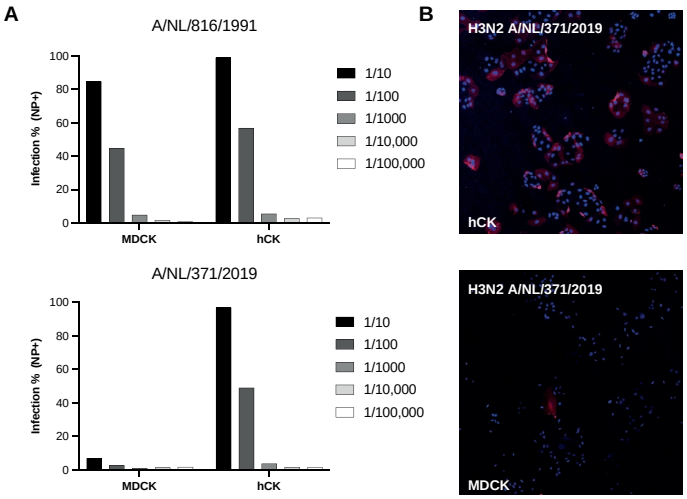

Figure 1. Infection of MDCK and hCK cells by A/H3N2 viruses. (**A**) Inoculation of MDCK and hCK cells with A/NL/816/1991 and A/NL/371/2019 A/H3N2 viruses at five ten-fold serial dilutions. Infection percentages were determined 6 hours post infection by NP staining and flow cytometry. (**B**) Overnight infection of MDCK cells and hCK cells with A/NL/371/2019. Virus particles were visualized with the H3 stem antibody CR8020 and depicted in red.

Glycomic analysis of MDCK and hCK cells

After confirming the infection patterns of recent A/H3N2 viruses in MDCK and hCK cells, we moved on to analyze the *N*-glycosylation patterns presented in these cell lines. Cell lysates were treated with PNGase F to release *N*-glycans from the glycoproteins. The released *N*-glycans were purified by SPE using C18 and porous graphitized carbon (PGC) cartridges. the purified *N*-glycans were labeled with 2-aminobenzoic acid (2-AA) and analyzed using LC-MS, HCD fragmentation for compositional analysis of the detected *N*-glycans[15]. Identification and quantification of the detected *N*-glycans was performed using Skyline (21.2.0.425)[16], where the raw LC-MS traces were analyzed for the presence of 2315 different *N*-glycan compositions. Since little is known about the glycosylation of canine cells, the more uncommon linkage α-galactose and *N*,*N*'-di-*N*-acetyllactosediamine (LacdiNAc) were also included in the search[17].

In total, we detected 63 different glycan compositions in MDCK cells and 93 in hCK cells. Overall, although not significant, we detected more complex-type *N*-glycans and less paucimannose and high-mannose *N*-glycans in hCK cells compared to MDCK cells (Figure 2A). Also, there proved to be a significant difference in the number of sialic acids detected per *N*-glycan between both cell lines (Figure 2B). In MDCK cells, the large majority of the detected *N*-glycans did not contain sialic acids (70%, Figure 2B), where in hCK cells only 30% of the detected *N*-glycans contained no sialic acid (p = 0.009). Additionally, we also observed significant differences between both cell lines in the percentage of *N*-glycan structures containing 2 or more sialic acids. In MDCK cells only 11 % of the detected glycans contained 2 or more sialic acids, whereas in hCK cells 60 % of all detected glycans contained 2 or more sialic acids.

When looking at the glycan compositions, a clear difference could be observed in the detected complex-type *N*-glycans between both cell lines (Figure 3A). In MDCK cells, the largest populations of complex-type *N*-glycans consisted of $HexNAc_5Hex_5$ or $HexNAc_5Hex_6$ compositions. For hCK cells, this distribution was shifted toward $HexNAc_6Hex_7$, $HexNAc_7Hex_8$ and even $HexNAc_8Hex_9$ compositions, indicating that this cell line presents larger complex-type *N*-glycans than the MDCK cell line. Figure 3B shows the chromatographic separation of the detected glycoforms as used for the quantification in Skyline.

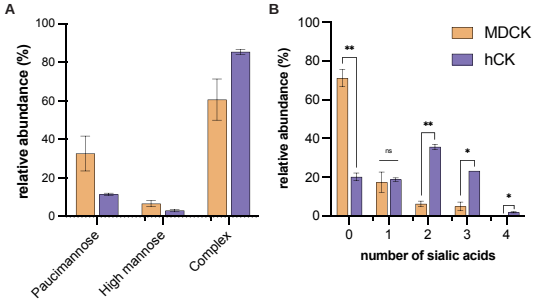

Figure 2. Glycomic statistics. (**A**) Average ± SEM of paucimannose (N = 2, H ≤ 4), high mannose (N = 2, H > 4) and complex *N*-glycans (N ≥3) as detected in MDCK (orange) and hCK (purple) cells. (**B**) Average percentage ± SEM of *N*-glycan compositions detected with 0 (p = 0.009), 1 (p = 0.823), 2 (p = 0.004), 3 (p = 0.014) or 4 (p = 0.019) sialic acids in MDCK (orange) and hCK (purple) cells. Differences between the cell lines were tested with an unpaired t-test with a p-value threshold of 0.05 (* = p <0.05, ** = p <0.01, *** = p <0.001, **** = p <0.0001).

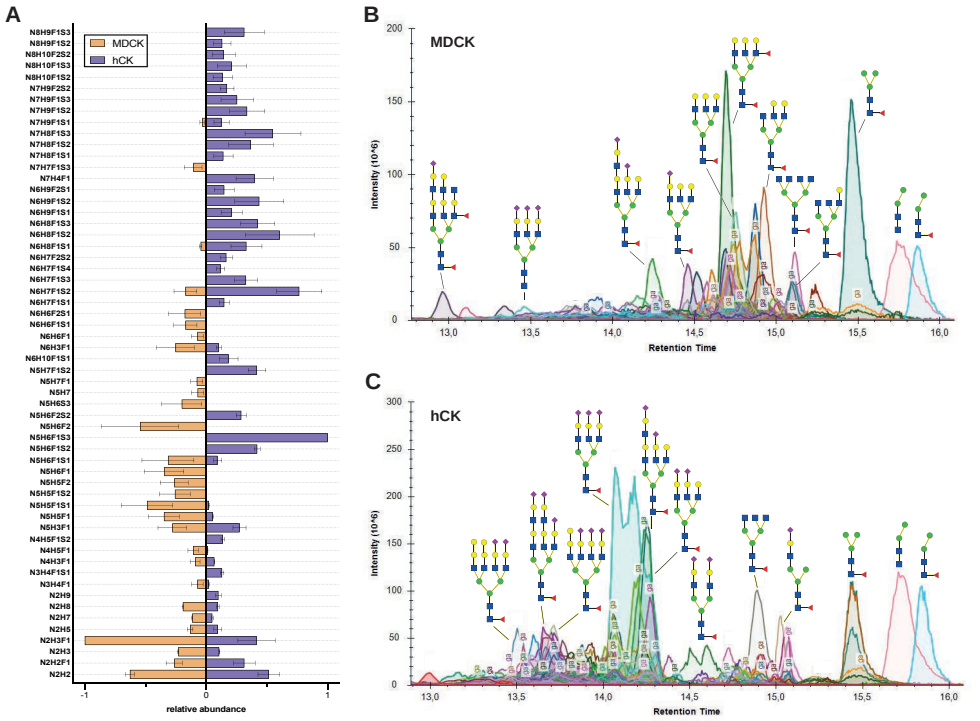

Figure 3. Quantitative overview of glycan detections in MDCK and hCK cells. (**A**) All compositions that showed an abundance of at least 1 % were plotted as the average (+/- SEM) over two replicates and were normalized towards the most abundant glycan species in each sample. Each bar represents one *N*-glycan composition as detected in MDCK (orange) or hCK (purple) cells. (**B**) Chromatographic separation of each of the glycoforms as used for the quantification in Skyline. The depicted antenna composition, fucose location and the location of the sialic acids are based on limited MS^2 fragmentation analysis and the literature on glycan biosynthesis[18].

Detection of poly-LN structures by MS^2 fragmentation

To investigate whether the larger complex-type glycans detected in hCK cells could indicate an increase of poly-LN structures, we manually searched the MS^2 traces for the presence of corresponding oxonium ions (1 LN: *m/z* 366.1395; 2 LN: *m/z* 731.2717; 3 LN: *m/z* 1096.4039; 4 LN: *m/z* 1461.5361). Potential fragmentation of the larger LacNAc fragments into smaller units prevented us from quantifying the poly-LN fragments in an absolute manner, but the overall intensity of single LacNAc fragments in combination with the presence of poly-LN fragments is expected to give an indication of relative numbers of poly-LN structures present. As such, we calculated the sum of the intensity of the detected LacNAc fragments over all scans (Figure 4). To correct for the number of detected glycans in each sample, we also corrected the LacNAc intensities by the intensity of core GlcNAcs in that sample (Figure 4B). The intensity of core GlcNAcs was determined by the sum of intensities of the oxonium ions *m/z* 343.15 (GlcNAc + 2AA) and *m/z* 489.2079 (fucosylated GlcNAc + 2AA) over all spectra in each sample. As shown in Figure 4B, the intensity of detected LacNAc fragments in hCk cells was 2.6-fold higher than in MDCK cells, indicating a potential increase in poly-LN structures in hCK cells compared

to MDCK cells. Additionally, Figure 5 shows the fragmentation spectra of two compositions, N7H8F1S3 and N8H9F1S3, with clearly detectable 3-LN oxonium ions (*m/z* 1096.4039), providing evidence for structural characteristic among the glycan compositions.

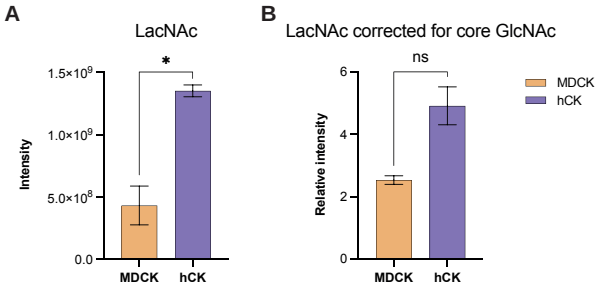

Figure 4. Sum of LacNAc intensity in MDCK and hCK cells. (**A**) The difference in the sum of the intensity of LacNAc fragments detected in MDCK and hCK cells over the full MS trace (p = 0.03). Shown are averages ± SEM for the biological duplicate. Differences between the cell lines were analyzed with an unpaired t-test with a p-value threshold of 0.05. (**B**) The sum of the intensity of LacNAc fragments corrected by the sum of core GlcNAc fragments (*m/z* 343.15 and *m/z* 489.2079) (p = 0.062). Shown are averages ± SEM for the biological duplicate. Differences between the cell lines were analyzed with an unpaired t-test with a p-value threshold of 0.05.

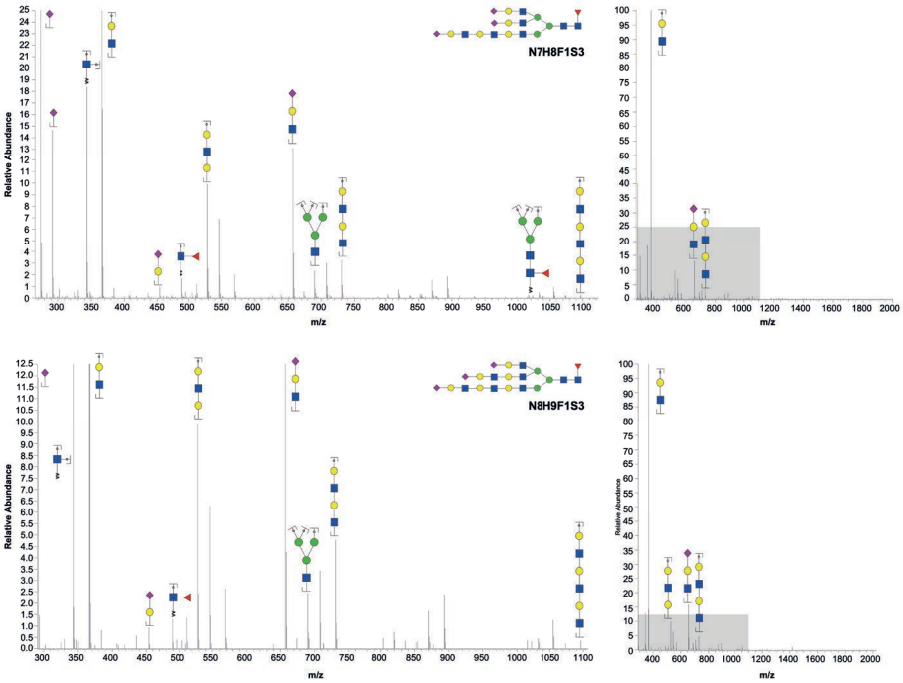

Figure 5. MS/MS fragmentation of poly-LN compositions in hCK cells. HCD product dependent fragmentation of the oxonium ions at *m/z* 1293.8000 (N7H8F1S3, top) and *m/z* 1415.5117 (N8H9F1S3, bottom). Shown are the zoomed spectra showing all oxonium ions on the left and the full spectra on the right.

Galactose-α1,3-galactose compositions

Interestingly, an increase in the number of potential galactose-α1,3-galactose (α-Gal) compositions was also detected in hCK cells compared to MDCK, with HexNAc6Hex8 and HexNAc7Hex9 forming the most abundant compositions (Figure 6). MS^2 traces were manually searched for the presence of oxonium ions at *m/z* 325.1129 (Galα1-3Gal) and *m/z* 528.1923 (Galα1-3Galβ1-4GlcNAc) to confirm the presence of putative α-Gal structures. Figure 7 shows the fragmentation of N7H9F1S1 as detected in MDCK cells and N6H8F1S2 as detected in hCK cells, in which fragments with both masses could be identified. Oxonium ions at *m/z* 528.1923 can also represent Galβ1-4GlcNAcβ1-3Gal fragments of a poly-LN arm instead of a terminal α-Gal structure. However, the changed ratio between the peaks at *m/z* 528.1923 and *m/z* 657.2349 (terminal sialylated LacNAc) in Figure 7 compared to those of N7H8F1S3 and N8H9F1S3 in Figure 5 indicates that the peak can at least partially be assigned to the presence of α-Gal structures.

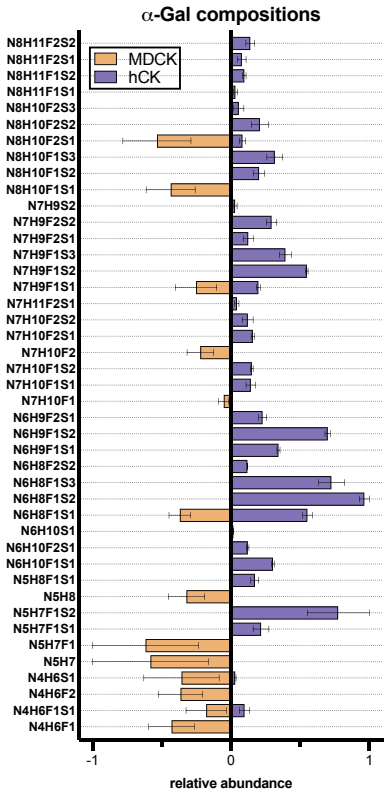

Figure 6. Quantitative overview of detected α-Gal compositions. All potential α-Gal compositions were plotted as the average ± SEM over two replicates and were normalized towards the most abundant glycan species in each sample. Each bar represents one *N*-glycan composition as detected in MDCK (orange) or hCK (purple) cells.

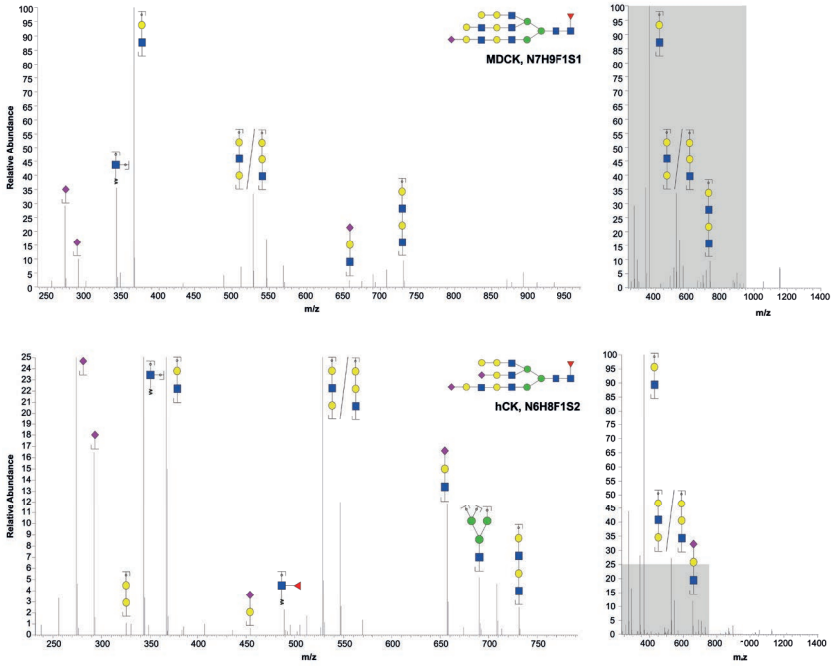

Figure 7. MS/MS fragmentation of α-Gal compositions in MDCK and hCK cells. HCD product dependent fragmentation of the oxonium ions at *m/z* 1153.0894 (MDCK, top panel) and *m/z* 1128.7410 (hCK, bottom panel). Shown are the zoomed spectra showing detected oxonium ions on the left and the full spectra on the right.

Discussion

Even though influenza infection has been highly studied, questions remain about the role of glycan receptors in the process of influenza infection. It was previously indicated that not only sialic acids play a role in the binding affinity of influenza viruses, but that for A/H3N2 viruses the underlying glycan structure also plays a role[9,11,12,19]. In this study, we analyzed the distribution of *N*-glycans presented in MDCK and hCK cells by glycomic analysis to get a better understanding about the glycans presented in these cell lines and thereby the receptor requirements of recent A/H3N2 viruses for infection. In doing so, we identified an increase in sialylation, larger complex *N*-glycan compositions, and an increase in α-galactosylated *N*-glycans in hCK cells compared to MDCK.

hCK cells are genetically engineered to overexpress α2,6-sialoglycans and extremely low levels of α2,3-sialoglycans to mimic the sialylation patterns of the human upper respiratory epithelial cells[20]. To achieve this, seven different α2,3-sialyltransferases were genetically removed. Additionally, the cells were transfected with the human α2,6-sialyltransferase ST6Gal1 to increase the sialylation toward α2,6-linkages. Despite the knock-out of seven different α2,3-sialyltransferase enzymes, we found that hCK cells showed an increase in the number of sialic acids presented per *N*-glycan. This indicates that the transfection of ST6Gal1 is more than able to compensate for the knock-out of the α2,3-sialyltransferases. This increase in sialylation could explain the increased infectivity of hCK cells for recent A/H3N2 viruses.

Next to the increased sialylation in hCK cells, we also observed an increase in the size of the detected complex-type *N*-glycans in this cell line compared to MDCK cells. A search through the MS^2 data proved the presence of poly-LN structures in hCK cells, while we did not find proof of this in MDCK cells. It is known that in the biosynthesis of ***N***-glycans sialic acids act as capping structures, marking the end of a glycan arm and thereby preventing further elongation of that arm[21]. Alterations in the pool of sialyltransferases might have changed the sialylation rate in a way that *N*-glycans had the opportunity to elongate further in hCK cells than in MDCK cells. Recently, our group published a paper in which we found that recent A/H3N2 viruses not only need α2,6-sialylation, but only bind to α2,6-linked sialic acids presented on a poly-LN arm[12]. Only a small percentage of these receptors were needed on the surface of red blood cells to facilitate agglutination by recent A/H3N2 viruses. Thus, the increase of the size of *N*-glycans in hCK cells might also play a role in the infectivity.

Interestingly, next to the altered sialylation pattern and size of the ***N***-glycans, we also found an increase in the presence of likely α-Gal structures in hCK cells. Canine cells have previously been found to present α-Gal structures and we identified α-Gal structures in MDCK cells, even though in considerably lower numbers[17]. α1,3-galactosyltransferases and sialyltransferases both use the terminal LacNAc on glycans as a substrate for galactose or sialic acid transfer. Apparently, the change in the pool of sialyltransferases also induces a competition between the capping enzymes, resulting in an increase of α-Gal structures in hCK cells. Since α-Gal structures do not naturally occur in humans, the increase of these structures on the cell surface of hCK cells generates a less human-like phenotype. This might pose an eventual challange if we want to translate findings from the cell line to the human situation.

Overall, we observed an increase in both the sialylation and the size of complex glycans in hCK cells, indicating an increase in prototypic human receptors present in this cell line. We also found evidence that the increased glycan sizes are partly due to the presence of poly-LN structures in hCK cells. Considering the findings that recent A/H3N2 viruses are evolving toward a binding selectivity to extended glycan structures[9,10,16,19], these changes might play an additional role in the increased susceptibility for infection. A glycomics study of MDCK-SIAT1 cells might give more insight in the contribution of the different glycosylation changes we found in hCK cells, especially about the role of sialylation. Also, a sialic acids linkage-specific derivatization study will help to quantify the presence of both α2,3-linked and α2,6-linked sialic acids. Together, with our results we hope to have contributed valuable information to the study of virus-host interactions.

Acknowledgments

K.R.R. acknowledges support from NWO project number VI.Veni.192.058. We thank Prof. Dr. Kawaoka for kindly making the hCK cells available for us to use for this study and we thank T. Bestebroer and A. de Bruin (Department of Viroscience, Erasmus MC) for the technical assistance in the infection assays.

Author Contributions

R.J.vB. and K.R.R. designed the project; R.J.vB. and I.S. performed experiments; R.J.vB. performed data analysis; K.R.R. provided scientific guidance on experimental setup and data interpretation; R.J.vB. and K.R.R. wrote the manuscript.

References

1. Hay, A. J. & McCauley, J. W. The WHO global influenza surveillance and response system (GISRS)—A future perspective. Influenza Other Respi. Viruses 12, 551–557 (2018).
2. InstituteO, W. I. C. the F. C. Report prepared for the WHO annual consulation on the composition of influenza vaccine for the northern hemisphere 2022-2023. (2022).
3. Gaush, C. R. & Smith, T. F. Replication and plaque assay of influenza virus in an established line of canine kidney cells. Appl. Microbiol. 16, 588–594 (1968).
4. Govorkova, E. A. et al. Selection of receptor-binding variants of human influenza A and B viruses in baby hamster kidney cells. Virology 262, 31–38 (1999).
5. Rogers, G. N. & Paulson, J. C. Receptor determinants of human and animal influenza virus isolates: Differences in receptor specificity of the H3 hemagglutinin based on species of origin. Virology 127, 361–373 (1983).
6. Matrosovich, M., Matrosovich, T., Carr, J., Roberts, N. A. & Klenk, H.-D. Overexpression of the α-2,6-Sialyltransferase in MDCK Cells Increases Influenza Virus Sensitivity to Neuraminidase Inhibitors. J. Virol. 77, 8418–8425 (2003).
7. Ding, Y. O., Barr, I. G., Mosse, J. A. & Laurie, K. L. MDCK-SIAT1 cells show improved isolation rates for recent human influenza viruses compared to conventional MDCK cells. J. Clin. Microbiol. 46, 2189–2194 (2008).
8. Takada, K. et al. A humanized MDCK cell line for the efficient isolation and propagation of human influenza viruses. Nat. Microbiol. 4 (2019).
9. Gulati, S. et al. Human H3N2 Influenza Viruses Isolated from 1968 To 2012 Show Varying Preference for Receptor Substructures with No Apparent Consequences for Disease or Spread. PLOS One 8 (2013).
10. Yang, H. et al. Structure and receptor binding preferences of recombinant human A(H3N2) virus hemagglutinins. Virology 477, 18–31 (2015).
11. Peng, W. et al. Recent H3N2 Viruses Have Evolved Specificity for Extended, Branched Human-type Receptors, Conferring Potential for Increased Avidity. Cell Host Microbe 21, 23–34 (2017).
12. Broszeit, F. et al. Glycan remodeled erythrocytes facilitate antigenic characterization of recent A/H3N2 influenza viruses. Nat. Commun. 12, 1–12 (2021).
13. Byrd-Leotis, L. et al. Sialylated and sulfated N-Glycans in MDCK and engineered MDCK cells for

influenza virus studies. Sci. Rep. 12, 1–12 (2022).

14. Takada, K. et al. A humanized MDCK cell line for the efficient isolation and propagation of human influenza viruses. Nat. Microbiol. 4, 1268–1273 (2019).

15. Reiding, K. R., Bondt, A., Franc, V. & Heck, A. J. R. The benefits of hybrid fragmentation methods for glycoproteomics. TrAC- Trends Anal. Chem. 108, 260–268 (2018).

16. MacLean, B. et al. Skyline: An open source document editor for creating and analyzing targeted proteomics experiments. Bioinformatics 26, 966–968 (2010).

17. Behrens, A. J. et al. Glycosylation profiling of dog serum reveals differences compared to human serum. Glycobiology 28, 825–831 (2018).

18. Pamela Stanley, Naoyuki Taniguchi, M. A. Chapter 9- N-glycans. in Essentials of Glycobiology, 3rd edition (2017). doi:10.1101/glycobiology.3e.009

19. Yang, H. et al. Structure and receptor binding preferences of recombinant human A(H3N2) virus hemagglutinins. Virology 477, 18–31 (2015).

20. Walther, T. et al. Glycomic Analysis of Human Respiratory Tract Tissues and Correlation with Influenza Virus Infection. 9 (2013).

21. Varki, A. Sialic acids in human health and disease. Trends Mol. Med. 14, 351–360 (2008).

22. Al., Damian C. Eckiert, Robert H.E. Friesen, G. B. et al. A highly conserved neutralizing epitope on group 2 influenza A viruses. Aust. Fam. Physician 38, 473–473 (2011).

Material and Methods

Materials

Puromycin (ref. P8833), blasticidin (ref. 15205), trypsin, and Dulbecco's modified eagle medium (DMEM), 2-aminobenzoic acid (2-AA), sodium cyanoborohydride, and dimethyl sulfoxide (DMSO) were obtained from Sigma-Aldrich. The CR8020 A/H3N2 stem antibody was kindly provided by Dr. Dirk Eggink and expressed following previously published procedures[22]. Alexa fluor-555 Goat anti-human (ref. A21433) and DAPI were purchased at Invitrogen. Cytofix/Cytoperm was obtained from BD Biosciences. Influenza nucleoprotein (NP) antibody (H16-L10-4R5, ref. MRO-1168CQ) was purchased from Creative Biolabs. Alexa Fluor 488 Goat anti-mouse (ref. A-21131) was obtained from Thermo Fisher Scientific. MS-grade acetonitrile (ACN) was obtained from Biosolve. Trifluoroacetic acid (TFA) was purchased from Argos Organics. PNGase F was obtained from Roche Diagnostics. Denaturation buffer (0.5 % SDS, 40 mM dithiothreitol (DTT)), 1% NP-40, and glycobuffer (50 mM sodium phosphate) were obtained from New England Biolabs. C18 SPE Sep-Pak Vac (1 cc) cartridges were purchased from Waters Corporation. PGC SPE Hypercarb Hypersep (1 cc) columns were obtained by the Synergy water purification system. EDTA-free protease inhibitor cocktail tablets were purchased from Thermo Fisher.

Viral infection studies

Cell culture

MDCK cells and hCK cells were cultured in Dulbecco's modified eagle medium (DMEM) supplemented with 10% FBS. In addition, hCK cells were supplemented with 2 µg mL^{-1} puromycin and 10 µg mL^{-1} blasticidin. Cells were maintained at a humid 5% CO_2 atmosphere at 37 °C and passaged at 80% confluency using trypsin (1x).

Immmunofluorescent imaging of viral hemagglutinins

Infectivity of the IAV NL/371/2019 was determined by inoculating MDCK and hCK cells for an overnight infection. For the infection, supernatants of the cells were removed, and the cells were incubated with virus input overnight in DMEM medium supplemented with 5% FBS. The next day the cells were washed 3x in PBS and fixated in 4% PFA for 20 min at room temperature. For the immunofluorescent staining the fixated cells were permeabilized in PBS containing 0.1% triton for 5 min. Subsequently, cells were incubated with the primary antibody CR8020 and the secondary antibody Alexa fluor 555 Goat anti-human, both for 1 h with PBS washes in between. DAPI was used as a nuclear staining and cells were mounted on glass slides using Fluorsave. Cells were imaged on a Leica DMi8 confocal microscope equipped with a 10x PL Apo CS2 objective (0.40 DRY). Excitation was achieved with a pulsed white laser (80MHz) at 549 nm for the Alexa fluor 555, and emissions were obtained in the range of 594–666 nm. Laser powers were 10–20% with a gain of a maximum of 200. FIJI was used for the processing of the images.

Detection of nucleoprotein by flow cytometry

MDCK and hCK cells were inoculated with A/H3N2 A/NL/371/2019 in five 10-fold serial dilutions (10^{-1}-10^{-5}) in corresponding culture medium without FBS. Cells were incubated at 37 °C in 5% CO_2. 6 h Post inoculation, cells were washed and trypsinized. After trypsin treatment, the cells were fixated and permeabilized using BD cytofix/Cytoperm according to manufacturer's instructions and subsequently stained or 20 min at 4 °C with the primary antibody influenza NP in BD perm/wash buffer. Subsequently, cells were washed and incubated with Alexa Fluor 488 Goat anti-mouse. The stained cells were measured with flow cytometry and the percentage of NP-positive cells was analyzed using FlowJo v.10.7.2 software. Graphs were created using graphpad Prism 9.

MS analysis of *N*-glycans

N-glycan release from MDCK and hCK cells

Before *N*-glycans were released from MDCK and hCK cells, the cells were first lysed in RIPA lysis buffer for 30 min on ice. To isolate the proteins the cell pellets were centrifuged at 14,000 rpm for 10 min after lysis. Proteins were treated with denaturing buffer (40 mM DTT, 0.5% SDS) at 95 °C for 8 min and cooled on ice. *N*-Glycans were then released from the denatured proteins by overnight incubation with PNGase F (5 U) in a deglycosylation buffer (50 mM sodium phosphate; pH 7.5, 1% NP40) at 37 °C.

Purification and labeling of the *N*-glycans

Released *N*-glycans were purified using a C-18 SPE cartridge, eluting the glycans directly with 5% ACN, 0.05% TFA in H_2O (1 mL). The samples were subjected to a nitrogen flow to remove the TFA and ACN, after which the *N*-glycans were further purified using a PGC SPE cartridge. First two washing steps were applied using 0.05% TFA in H_2O (1 mL) and 5% ACN, 0.05% TFA in H_2O subsequently, after which the glycans were eluted with 50% ACN/H_2O and 0.1% TFA

(1 mL). The purified sample was dried using a speedvac, after which the *N*-glycans were 2-AA labeled. Dried samples were dissolved in 10 µl H_2O and 10 µl labeling mixture, containing 48 mg mL^{-1} of 2-AA and 63 mg mL^{-1} of sodium cyanoborohydride in 10:3 (*v/v*) DMSO/acetic acid. The labeling reactions was carried out for 2 h at 65 °C. Finally, the labeled *N*-glycans were purified from unreacted labeling reagents using a Minitrap Sephadex G-10 gravity column. Samples were diluted in H_2O to reach a total volume of 100 µl and loaded on the column. After a washing step with 700 µl H_2O the glycans were eluted with 600 µL H_2O. Collected samples were dried in a speedvac and stored at-20 °C until use.

LC-MS analysis of *N*-glycans

For LC-MS analysis of the labeled *N*-glycans the dried samples were reconstituted in 80 µL 2% FA and 2 µL sample was analyzed on an Orbitrap Exploris 480 (Thermo Scientific). The samples were reversed-phase separated on an Ultimate 3000 UHPLC using PepMap C18 Trap Cartridges (5 mm, 300 µm i.d.) and a C18 analytical column (50 cm, 50 µm i.d.) (Thermo Scientific). Supplementary Tabel 1 gives an overview of the buffers, flow rates, and gradient program. The mass range for the MS^1 measurements was set from *m/z* 375-1600 with a resolution of 60,000 with a normalized AGC target of 250%. For MS^2 fragmentation a TopN data-dependent acquisition (DDA) method with HCD fragmentation (30% normalized collision energy) was used in a resolution of 15,000 with a standard AGC target and an auto maximum injection time.

Skyline analysis

Raw data was quantified using Skyline (version 21.2.0.425). For this, we used the mass of the 2-AA label as a peptide backbone consisting of an alanine with a static modification called "AA-fixer" (modification formula: $+C_2\text{-}H_1N_1O_1$) and a glycine to hold the glycan modifications. By this, glycopeptide quantification in Skyline could be performed on the 2-AA labeled released glycans as if they were glycopeptides. 2315 glycan compositions, covering 0-13 hexoses, 1-18 N-acetylhexosamines, 0-3 fucoses, 0-4 *N*-acetylneuraminic acids and 0-2 phosphates, were integrated from each MS run. Integrations obtained from the included glycan compositions were curated by the following criteria: 5 ppm error to the theoretical mass, having and idotp of 0.5 or higher with the theoretical isotopic pattern, 3) detection in both replicate samples, 4) elution with maximum two-min difference between the two samples of the same condition, 5) having no apparent overlapping isotopic patterns. The sum of the intensity of oxonium ions over the full MS trace were calculated using an in-house developed software called PeakSuite. The resulting quantification of glycan detections was plotted using graphpad Prism 9.

Supplementary table 1. LC-MS gradient program.

Buffer A	0.1% formic acid
Buffer B	0.1% formic acid 80% acetonitrile

Gradient program

Time (min)	Flow rate (µl/min)	A (%)	B (%)
1.0	0.3	91	9
11.0	0.3	60	40
14.0	0.3	1	99
19.0	0.3	1	99
20.0	0.3	91	9
25.0	0.3	91	9
30.0	0.3	91	9

Chapter 6

Summary and Future Outlook

6

Summary

Glycosylation is a prevalent, yet heterogeneous post translational modification of proteins with a broad range of implications in molecular biology. The heterogeneity and non-template driven nature of glycans and glycoconjugates makes them challenging to study. However, the advent of techniques like glycomics, glycoproteomics and glycoengineering have revolutionized the field of glycobiology as a fast-growing and promising research area. Emerging biochemical glycoengineering and enrichment tools, developments in MS fragmentation methods and detection software continuously open new possibilities to study glycans and glycoconjugates and make glycan research more available for the broader research community.

In this final chapter we summarize how we combined existing and newly developed glycomics, glycoproteomics and glycoengineering techniques to study and engineer cell-surface *N*-glycosylation in the context of genetic glycosylation defects and the evolution of receptor recognition in influenza A/H3N2 viruses.

In **Chapter 2**, we analyzed the changes in membrane protein *N*-glycosylation resulting from dolichol deficiency. Dolichol deficiency can be caused by a genetic defect in the polyprenol reductase enzyme that converts polyprenol to dolichol, leading to the congenital disorder of *N*-glycosylation SRD5A3-CDG. Dolichol is the most important lipid scaffold for oligosaccharides in the biosynthesis of protein *N*-glycosylation, and thus a deficiency is argued to lead to protein hypoglycosylation. Underrepresentation of membrane proteins in dolichol-deficient CDG patient cells and Lec9 cells was previously reported[1]. Lec9 cells are a CHO glycosylation mutant cell line that mimics the dolichol deficiency found in CDG patients. We developed a SEEL derivative with an acid-cleavable linker to enrich membrane glycoproteins and performed a glycoproteomics analysis using hybrid MS fragmentation methods containing HCD, stepping-HCD and EThCD. A significant and site-specific hypoglycosylation in Lec9 cells was found compared to CHO-K1 cells. Interestingly, no direct correlation between the hypoglycosylation and membrane abundance of the proteins was identified, suggesting that proteins are differently affected by hypoglycosylation and dolichol deficiency.

In **Chapter 3**, we shifted focused on the evolution in receptor specificity of human influenza A/H3N2 viruses. Human influenza A viruses have a remarkable ability to evolve and evade neutralization by antibodies elicited by prior infections or vaccinations. During circulation in humans and natural selection to escape antibody recognition for decades, A/H3N2 influenza viruses emerged with altered receptor specificities. These viruses lost their ability to agglutinate fowl erythrocytes, thereby hampering the antigenic characterization of these viruses by the usual HI assays. The HI assay measures the ability of serum antibodies to block receptor binding by the virus HA protein through the inhibition of virus-mediated agglutination of erythrocytes. Glycan microarray analysis revealed that recent A/H3N2 viruses evolved in their receptor recognition from the prototypic human α2,6-LacNAc receptor toward α2,6 sialosides presented on extended LacNAc moieties. Glycomic analysis of fowl erythrocytes confirmed an absence of the minimal required receptor, explaining the lack of agglutinating ability of these viruses. To overcome the agglutination problem, we developed an enzymatic glycan remodeling strategy to install functional receptors on erythrocytes. The glycan-remodeled erythrocytes could be agglutinated by all tested contemporary A/H3N2 viruses, thereby allowing antigenic characterization of these viruses by the HI assay. In collaboration with the department of Viroscience at Erasmus MC we performed antigenic characterization of recent A/H3N2 viruses by HI assay and could confirm the antigenic distances of currently circulating clades and the antigenic distance between egg-derived vaccine strains and cell grown viruses, providing a rationale for poor vaccine efficiency. Our results show that the glycan-remodeled erythrocytes can be used for antigenic characterization of recent A/H3N2 viruses by HI assays and can thereby aid in the selection of protective vaccines.

The glycan remodeling strategy presented in Chapter 3 proved to be compatible for use in an HI assay to antigenically characterize recent A/H3N2 viruses and could therefore offer a solution for the current challenges in the antigenic characterization of these viruses. However, before the remodeled erythrocytes can be made available for the research community, several challenges need to be overcome. Erythrocytes are typically used for HI assays within one week after isolation from the blood. The time of use is limited because the cells start to show hemolysis shortly after isolation, which affects the agglutination. The glycan remodeling strategy further reduces the timeframe in which the erythrocytes can be used for HI assays, which potentially complicates distribution of the erythrocytes. To overcome this issue, in **Chapter 4** we aimed to expand the shelf life of the glycan-remodeled erythrocytes by fixation with glutaraldehyde. In a hemagglutination assay time course we showed that glutaraldehyde fixation prolonged the shelf life of glycan-remodeled turkey erythrocytes and gave stable agglutination titers for a period of at least 20 weeks. We tested the use of glutaraldehyde fixated red blood cells in an HI assay in collaboration with the department of Viroscience at the Erasmus MC. Using a subset of contemporary A/H3N2 viruses with known antigenic characteristics, we tested the ability to identify the antigenic characteristics of circulating A/H3N2 viruses using the fixated glycan-remodeled erythrocytes. In doing this, we found a positive correlation between the HI titers obtained using fresh and fixated engineered erythrocytes, indicating that fixated erythrocytes can be used to identify antigenic differences between viruses. However, we also detected an increase in HI titers below the detection threshold when using fixated erythrocytes, which decreases the sensitivity of the assay and might result in a loss of information about smaller antigenic changes between viruses. It can therefore be interesting to explore alternative methods to increase the shelf life of engineered erythrocytes for HI assays.

Finally, in **Chapter 5** we analyzed the cellular glycosylation of MDCK and hCK cells. MDCK cells are the most widely used cell line to propagate human influenza viruses. The evolution of A/H3N2 viruses however, not only led to the previously discussed agglutination problems, but also hampered propagation of these viruses in MDCK cells. A humanized MDCK cell line, called hCK, was recently developed in which the sialylation pattern was skewed almost exclusively toward α2,6-linked sialic acids, the prototypic human-type receptor. hCK cells were proven successful for the propagation of recent A/H3N2 viruses, and therefore sparked our interest for a glycomic analysis to uncover potential changes in glycosylation of these cells outside of the sialic acid linkages that might contribute to the improved infection. A glycomic analysis of MDCK and hCK cells revealed a higher overall sialylation in hCK cells, but also an increase in the size of detected complex-type glycans with potential poly-LacNAc repeats, as well as an increase in alpha-galactose linkages on the glycan termini.

Future outlook

Glycoproteomics platform for CDG research

There are still many unanswered questions about the way in which CDG defects cause pathology. Analytical methods like the glycoproteomics platform presented in **Chapter 2** may help to gain a better understanding of sensitive pathways and affected glycoproteins in different CDG defects; knowledge that can lead to new therapeutic strategies or biomarkers that can aid diagnosis or assessment of therapy responses.

Chapter 2 exclusively focused on the characterization of *N*-glycosylation of membrane proteins. However, CDGs can be caused by genetic defects in genes involved in all types of glycosylation and in some defects there might even be an interplay between different glycan classes that are affected. As an example, the dolichol deficiency as discussed in Chapter 2 is one of the CDGs that originates from deficiencies in the biosynthesis of the lipid precursors. Although the lipid scaffolds are primarily linked to the biosynthesis of *N*-glycans, the lipid-linked monosaccharides Dol-P-GlcNAc and Dol-P-Man are both essential for different *O*-glycosylation pathways and Dol-P-Man is involved in the biosynthesis of GPI [REFs]. The versatility that SEEL provides in using a range of different glycosyltransferase enzymes to target certain glycan classes offers an opportunity to expand the developed glycoproteomics platform to study the effect of CDG defects on multiple glycan classes and uncover potential interplay between glycan classes in the pathology. The core-1 *O*-glycan-specific sialyltransferase ST3Gal1 for example, is proven to be compatible with SEEL and could offer an expansion of the technique toward the study to *O*-glycans[2,3]. *O*-Glycoproteomic analysis offers unique challenges due to the usually densely packed areas of mucin-type *O*-glycans in serine/threonine-rich protein regions. This makes the areas very resistant against trypsin cleavage and in general leaves peptide sizes that are undetectable in MS-based glycopeptide searches. The use of the recently characterized mucinase, StcE, has proven to be efficient in the cleavage of peptide bonds in *O*-glycan rich serine-threonine sequences and thereby facilitates the generation of smaller *O*-glycopeptides[4]. MS fragmentation using ETD and EThCD was found to be indispensable for the site-specific analysis of *O*-glycopeptides[5], and recently multiple *O*-glycoproteomic analysis pipelines such as O-Pair search for MetaMorpheus and MSFragger-Glyco were developed that aid in the detection of *O*-glycopeptides[6,7]. The use of the unique increment mass added by the cleavable linker as described in **Chapter 2** will further improve the detections of *O*-glycoproteins by glycoproteomic analysis.

SEEL as a diagnostic tool for CDGs

The large heterogeneity of CDGs forms a big challenge in the diagnostic process. The majority of CDGs are diagnosed based on serum transferrin isoelectric focusing[8]. The large heterogeneity of the CDGs however, only results in successful diagnoses in approximately 60% of the cases based on this analysis[9]. Therefore, there is a continuous search to improve diagnostic tools. If interesting target proteins are identified that show a unique glycan pattern in certain CDG types, SEEL might be a useful tool to quickly scan the glycan profiles of these proteins from for example a serum sample. By making use of the versatility that two-step SEEL offers, a 5K PEG molecule can be added to shift the molecular weight of the protein dependent on the amount of glycan receptors present on the protein, creating a shift in the electrophoretic mobility of a glycan in gel electrophoresis. This shift can be used to quantify the glycan loss in specific proteins. The use of different glycosyltransferase enzymes allows the visualization and quantification of several different glycan classes on one protein, and after a single labeling on a cell population all the desired proteins present in the lysate can be analyzed by the use of protein-specific antibodies in a Western blot analysis (Figure 1). A proof of principle for this technique was performed using Jurkat cells by labeling with the sialyltransferases ST6Gal1, ST3Gal1 and ST6GalNac1 to quantify the *N*-glycosylation, core-1 *O*-glycosylation and truncated core-1 *O*-glycosylation respectively (Figure 2). By using protein-specific antibodies we visualized the glycosylation profile of two glycoproteins: CD55 is known to be a heavily *O*-glycosylated protein and LRP1 is known to be a heavily *N*-glycosylated protein.

Antigenic characterization of influenza viruses using synthetic engineered erythrocytes

The continuous evolution of influenza viruses requires constant adaptation in the composition of vaccines, but also in the techniques used for characterization of influenza viruses. A lack of the right receptors on the surface of erythrocytes for a large group of influenza A/H3N2 viruses has resulted in the inapplicability of the HI assay for antigenic characterization of these viruses. The research field has therefore moved more toward the use of viral neutralization assays for the characterization of circulating A/H3N2 viruses. This assay however, has its downsides. The viral neutralization assays takes significantly longer than the HI assay to perform and requires more expertise and specialized equipment. As a result, it is significantly more expensive than the standard HI assay. The engineered erythrocytes as presented in **Chapter 3** offer a solution for the hemagglutination issue but are still relatively expensive compared to regular red blood cells. A fixation strategy to expend the shelf-live and thereby increase the cost-efficiency of the cells as presented in **Chapter 4** gave reliable results but decreased the sensitivity of the assay and might therefore not present an ideal solution for the issue. There are several difficulties involved in the use of biological products like erythrocytes for the HI assay. Genetic variation in the animals used for the extraction of the cells can cause a variation in the agglutination patterns of certain viruses. Additionally, an animal facility is needed for a laboratory to have a steady access to an erythrocyte supply. Hemolysis of the red blood cells after isolation from the blood causes a limited shelf life of approximately one week for the use of HI assays. A solution to these issues may lie in the replacement of erythrocytes by a synthetic carrier for the required glycan receptors. A recent study by Sanchez-Cano et al. presented a synthetic alternative of erythrocytes that are applicable for HI assays[10]. The so-called synthrocytes are 10 µm Sicaster-blue particles cross-linked to the highly sialylated glycoprotein glycophorin A. The sedimentation of the beads is comparable to red blood cells, meaning that the assay can be performed regularly without many adjustments. The synthrocytes were proven to be

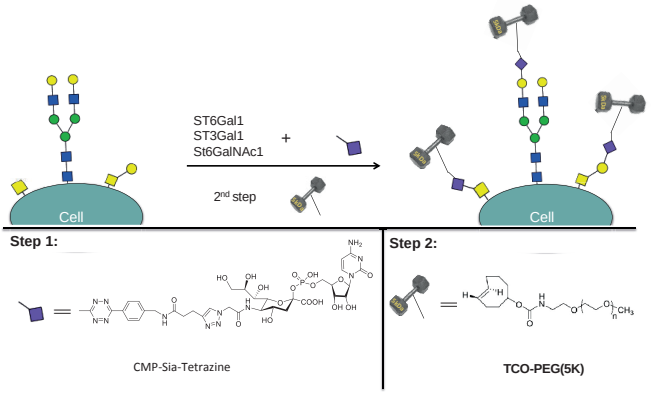

Figure 1. Two-step TCO-tetrazine labeling of cell lysates using 5K-PEG mass tags.

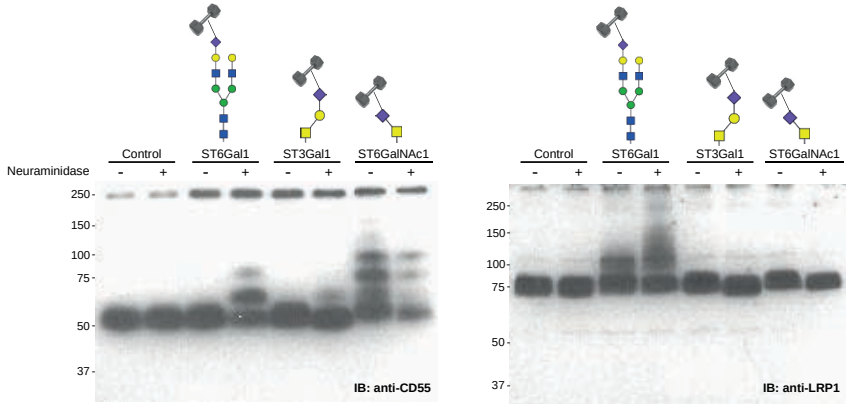

Figure 2. Glycosylation profiles of CD55 and LRP1 in Jurkat cells by two-step SEEL.

suitable for classical HA and HI assays using influenza A/H1N1 and influenza B viruses, but not for influenza A/H3N2 viruses. Glycoengineering glycophorin A using our developed remodeling strategy could make the synthrocytes available for A/H3N2 viruses and thereby generate a stable agglutination reagent that can be up mass-produced and made suitable for global distribution. An extra advantage of using engineered glycoproteins in the future might be the use of genetically engineered cells like the hCK cells to produce recombinant proteins that already present the desired glycan receptors, thereby abolishing the need for an engineering procedure after crosslinking of the proteins to the synthetic erythrocytes.

References

1. He, P., Ng, B. G., Losfeld, M. E., Zhu, W. & Freeze, H. H. Identification of intercellular cell adhesion molecule 1 (ICAM-1) as a hypoglycosylation marker in congenital disorders of glycosylation cells. J. Biol. Chem. 287, 18210–18217 (2012).
2. Yu, S. H. et al. Defective mucin-type glycosylation on α-dystroglycan in COG-deficient cells increases its susceptibility to bacterial proteases. J. Biol. Chem. 293, 14534–14544 (2018).
3. Yu, S. H. et al. Selective exo-enzymatic labeling detects increased cell surface sialoglycoprotein expression upon megakaryocytic differentiation. J. Biol. Chem. 291, 3982–3989 (2016).
4. Malaker, S. A. et al. The mucin-selective protease StcE enables molecular and functional analysis of human cancer-associated mucins. Proc. Natl. Acad. Sci. U. S. A. 116, 7278–7287 (2019).
5. Riley, N. M., Malaker, S. A., Driessen, M. D. & Bertozzi, C. R. Optimal Dissociation Methods Differ for N- A nd O-Glycopeptides. J. Proteome Res. 19, 3286–3301 (2020).
6. Lu, L., Riley, N. M., Shortreed, M. R., Bertozzi, C. R. & Smith, L. M. O-Pair Search with MetaMorpheus for O-glycopeptide characterization. Nat. Methods 17, 1133–1138 (2020).
7. Polasky, D. A., Yu, F., Teo, G. C. & Nesvizhskii, A. I. Fast and comprehensive N- and O-glycoproteomics analysis with MSFragger-Glyco. Nat. Methods 17, 1125–1132 (2020).
8. Bruneel, A., Cholet, S., Tran, N. T., Mai, T. D. & Fenaille, F. CDG biochemical screening: Where do we stand? Biochim. Biophys. Acta- Gen. Subj. 1864 (2020).
9. Francisco, R. et al. The challenge of CDG diagnosis. Mol. Genet. Metab. 126, 1–5 (2019).
10. Sánchez-Cano, A. et al. Detection of Viruses and Virus-Neutralizing Antibodies Using Synthetic Erythrocytes: Toward a Tuneable Tool for Virus Surveillance. ACS Sensors 6, 83–90 (2021).

Apendix

Nederlandse Samenvatting

Curriculum Vitae

Acknowledgments

Nederlandse Samenvatting

Glycosylering is een veelvoorkomende, maar heterogene posttranslationele modificatie van eiwitten met vele implicaties in de moleculaire biologie. De enzym-gedreven biosynthese en de grote heterogeniteit tussen de glycanen en glycoconjugaten maken de studie naar deze moleculen uitdagend. De opkomst van onderzoeksmethoden als glycomics, glycoproteomics en glycoengineering hebben gezorgd voor een revolutie in glycaan onderzoek en hebben de glycobiologie gevormd tot een snel groeiend en veelbelovend onderzoeksveld. Opkomende biochemische technieken voor het modificeren en isoleren van glycanen, de ontwikkeling van fragmentatie methodes in de massa spectrometrie (MS) en software voor de data interpretatie van MS analyses hebben vele nieuwe mogelijkheden geopend en maken glycaan onderzoek bereikbaar voor een bredere onderzoeksgemeenschap.

Dit laatste hoofdstuk vat samen hoe in dit proefschrift gebruik is gemaakt van bestaande en nieuw ontwikkelde glycomics, glycoproteomics en glycoengineering technieken om *N*-glycanen op de celmembraan te modificeren en analyseren.

Hoofdstuk 2 beschrijft de veranderingen in de *N*-glycosylering van membraaneiwitten als gevolg van een dolichol deficiëntie. Een dolichol deficiëntie kan worden veroorzaakt door een defect in het polyprenol reductase enzym dat polyprenol omzet in dolichol, wat leidt tot het congenitale defect in glycosylering genaamd SRD5A3-CDG. Dolichol is het belangrijkste voetstuk voor de opbouw van oligosacchariden in de biosynthese van *N*-glycanen. Er wordt daarom gedacht dat een tekort leidt tot een verminderde glycosylering van eiwitten. Eerder aangetoond is dat in dolichol-deficiënte CDG patiënten en Lec9 cellen bepaalde membraan eiwitten zijn ondervertegenwoordigd. Lec9 is een mutante cellijn afkomstig van chinese hamster ovary (CHO) cellen die dezelfde dolichol deficiëntie laat zien als CDG patiënten. We hebben een biotine-gelabeld siaalzuur ontwikkeld met een splitsbaar label om *N*-geglycosyleerde membraaneiwitten te isoleren en hebben gebruik gemaakt van hybriede MS-fragmentatie methodes (HCD, stepping-HCD en EThCD) om de glyco-eiwitten te analyseren. Een significante en plaats-specifieke onderglycosylering is gevonden in Lec9 cellen in verhouding met CHO-K1 cellen. We hebben geen directe correlatie kunnen identificeren tussen de onderglycosylering en aanwezigheid op de celmembraan, wat suggereert dat eiwitten op verschillende manieren worden beïnvloed door de veranderde glycosylering en dolichol deficiëntie.

In **Hoofdstuk 3** hebben we ons gericht op de evolutie in receptorspecificiteit van humane influenza A/H3N2-virussen. Menselijke influenza A-virussen hebben het opmerkelijke vermogen om te evolueren en neutralisatie te omzeilen door antilichamen die zijn opgewekt bij eerdere infecties of vaccinaties. Door de circulatie in mensen en de decennialange natuurlijke selectie om aan antilichaamherkenning te ontsnappen zijn A/H3N2-influenzavirussen dominant geworden met veranderde receptor specificiteiten. Deze virussen hebben hun vermogen verloren om kippenerytrocyten te agglutineren, waardoor de antigene karakterisering van deze virussen door de gebruikelijke hemagglutinatie inhibitie (HI) test sterk is bemoeilijkt. De HI test meet het vermogen van serumantilichamen om de receptorbinding door het HA-eiwit van het virus te blokkeren. Deze blokkade wordt gevisualiseerd door de remming van virus-gemedieerde agglutinatie van erytrocyten. Een microarray analyse onthulde dat de receptorherkenning van recente A/H3N2-virussen is veranderd van de prototypische menselijke α2,6-LacNAc-receptor naar α2,6-siaalzuren gepresenteerd op verlengde LacNAc-armen. Een MS-analyse

naar de *N*-glycanen op kippenerytrocyten bevestigde de afwezigheid van deze nieuwe vereiste receptor, wat het gebrek aan agglutinerend vermogen van deze virussen verklaart. Om het agglutinatieprobleem aan te pakken hebben we een enzymatische glycaan-modificatiestrategie ontwikkeld om functionele receptoren op erytrocyten te installeren. De gemodificeerde erytrocyten konden worden geagglutineerd door alle geteste recente A/H3N2-virussen, waardoor antigene karakterisering van deze virussen door de hemagglutinatieremming (HI) test weer mogelijk werd. In samenwerking met de afdeling Viroscience van het Erasmus MC hebben we een antigene karakterisering uitgevoerd van recente A/H3N2-virussen door middel van een HI test en konden we succesvol de antigene verschillen tussen de momenteel circulerende A/H3N2 virussen aantonen. Dit antigene verschil tussen circulerende virussen verklaart de lage vaccin-efficiëntie tegen A/H3N2 virussen in recente influenza vaccins. Onze resultaten laten zien dat de gemodificeerde erytrocyten kunnen worden gebruikt voor antigene karakterisering van recente A/H3N2-virussen door middel van HI tests en daardoor kunnen helpen bij de selectie van beschermende vaccins.

De glycaan-modificatiestrategie die in Hoofdstuk 3 wordt gepresenteerd, bleek bruikbaar te zijn in HI tests om recente A/H3N2-virussen antigeen te karakteriseren en zou daarom een oplossing kunnen bieden voor de huidige uitdagingen in de antigene karakterisering van deze virussen. Om de gemodificeerde erythrocyten beschikbaar te kunnen maken voor de bredere onderzoeksgemeenschap moeten een aantal uitdagingen worden overwonnen. Erytrocyten worden normaal gesproken tot een week na isolatie uit het bloed voor HI tests gebruikt. De gebruiksduur is beperkt omdat de cellen kort na isolatie hemolyse beginnen te vertonen, wat de agglutinatie beïnvloedt. De glycaan-modificatiestrategie verkort deze gebruiksduur voor HI tests nog verder, wat de distributie van de erytrocyten bemoeilijkt. Om dit probleem op te lossen, hebben we in **Hoofdstuk 4** geprobeerd de houdbaarheid van de door gemodificeerde erytrocyten te verlengen door fixatie met glutaaraldehyde. In een reeks hemagglutinatie testen over 20 weken toonden we aan dat glutaaraldehyde fixatie de houdbaarheid van de gemodificeerde kalkoenerytrocyten verlengde en stabiele agglutinatie titers gaf gedurende een periode van ten minste 20 weken. We hebben het gebruik van glutaaraldehyde gefixeerde rode bloedcellen in HI tests onderzocht in samenwerking met de afdeling Viroscience van het Erasmus MC. Met behulp van een subset van hedendaagse A/H3N2-virussen met bekende antigene kenmerken hebben we getest of de glutaaraldehydefixatie de resultaten van de HI test beïnvloedt. Daarbij vonden we een positieve correlatie tussen de HI titers verkregen met verse en gefixeerde gemodificeerde erytrocyten, wat aangeeft dat gefixeerde erytrocyten kunnen worden gebruikt om antigene verschillen tussen virussen te identificeren. We ontdekten echter ook een toename in HI titers onder de detectiedrempel bij gebruik van gefixeerde erytrocyten, wat de gevoeligheid van de test vermindert en zou kunnen resulteren in een verlies van informatie over kleinere antigene verschillen tussen virussen. Het kan daarom interessant zijn om alternatieve methoden te onderzoeken om de houdbaarheid van gemanipuleerde erytrocyten voor HI tests te verlengen.

Tot slot hebben we in **Hoofdstuk 5** de cellulaire glycosylering van MDCK- en hCK-cellen geanalyseerd. MDCK-cellen zijn de meest gebruikte cellijn om menselijke influenzavirussen te vermeerderen. De evolutie van A/H3N2-virussen leidde echter niet alleen tot de eerder besproken agglutinatieproblemen, maar belemmerde ook de vermeerdering van deze virussen in MDCK-cellen. Een gehumaniseerde MDCK-cellijn, hCK genaamd, werd onlangs ontwikkeld waarin het sialyleringspatroon is aangepast om bijna uitsluitend α2,6-gekoppelde siaalzuren te presenteren, de prototypische humane receptor. hCK cellen bleken succesvol te zijn voor de vermeerdering van recente A/H3N2-virussen en wekten daarom onze interesse voor een

glycaan-analyse om mogelijke veranderingen in glycosylering in deze cellen te identificeren buiten de siaalzuurbindingen om die zouden kunnen bijdragen aan de verbeterde infectie. Een MS-analyse van de *N*-glycanen in MDCK- en hCK-cellen onthulde een hogere algehele sialylering in hCK cellen, maar ook een toename in de grootte van gedetecteerde complexe *N*-glycanen met potentiële poly-LacNAc-armen, evenals een toename van α-galactose verbindingen.

Curriculum vitae

Personal information

Name: Rosa Joanna van Beek
Date of Birth 15-03-1992
Nationality: Dutch
Telephone: +31 643757338
E-mail (private): rosanne.vanbeek@gmail.com

Work experience

2017-2022 **PhD candidate**, Department of Chemical biology and Drug Discovery, Utrecht University.

Jan-Jul 2021 **NWO take-off 1 Feasibility study**, Utrecht University
Feasibility study to evaluate the commercial potential of modified erythrocytes as a diagnpstic reagent for influenza A analysis.

2020 **Best pitch award**, Utrecht Institute of Pharmacuticle Sciences

Jun-Sept 2017 **Visiting researcher**, Complex Carbohydrate Research Centre, University of Georgia, Georgia, USA.

Education

2014-2016 **Research master Biomolecular Sciences**, VU, Amsterdam
(Completed, degree: Master of Science)

Second year internship: Separation of carbohydrate standards using capillary electrohporesis. Department of Chemical Biology and Drug Discovery, Utrecht University.
First year Internship: Role of SPPL2b on Alzheimers disease pathogenesis. department of clinical chemistry, VUMC.

2010-2014 **Bachelor Psychobiology**, University of Amsterdam,
(Completed, degree: Bachelor of Science)

Internship: The effect of Tau overexpression on the dentritic complexity of primary hippocampal cultures. Swammerdam Institure of Life Science, University of Amsterdam.

List of publications

* Authors contributed equally

Broszeit, F.*, **van Beek, R.J**.*, Unione, L., Bestebroer, T.M., Chapla, D., Yang, J.-Y., Moremen, K.W., Herfst, S., Fouchier, R.A.M., de Vries, R.P., Boons, G.-J.. Glycan remodeled erythrocyte facilitate antigenic characterization of recent A/H3N2 influenza viruses. Nature Communications 12, article number: 5449 (2021)

van Beek, R.J., Moure, M.J., Damen, M.J.A., Bosman, G.P., Heck, A.J.R., Reiding, K.R., Boons, G.-J. SEEL-enriched membrane glycoproteomic reveals hypoglycosylation to be site-specific in dolichol-deficient cells.
To be published

Other

Patent application: Means and methods for detecting, producing, isolating or characterizing influenza. Inventors: Broszeit, F., **van Beek, R.J.**, Boons, G.-J., de Vries, R.P.. Application number: EP20179197.

Acknowledgments - Dankwoord

I would like to make use of this opportunity to thank the many people without whom the work in this dissertation wouldn't have been what it is, but also without whom I wouldn't have been where I am right now.

Roland, I would like to start by thanking you sincerely for giving me the chance to finish my PhD under your guidance. **Karli**, I'm so grateful that we started a collaboration four years ago. I can't thank you enough for all your help in the last four years. I have a great respect for you as a scientist and thanks to you I found an unexpected joy in doing data analysis. I will miss our fruitful discussions about research and of course the many other topics we discussed when our meetings drifted off while enjoying a cup of coffee. **Rob**, thank you for your guidance during our collaborative project, I've enjoyed that journey a lot. **Geert-Jan**, without you I wouldn't have started this PhD.

Maria, during my three months in the Boons lab at the UGA we quickly hit it off. We built the tradition of having Friday night dinners in town, city trips in the weekends, and we watched the total eclipse of the sun together. Even though we barely have pictures of our times together thanks to your phobia for photos, I will always remember that time with a smile on my face. You became a dear friend over the years. I'm very happy that you found your happiness in Bilbao, and I hope that we will stay in touch!

Gerlof, I am very happy that we started our PhDs roughly at the same time. You were always willing to think along or help with anything in the lab. Next to help in the lab, I could always count on you for a good laugh and some healthy criticism on all my Apple gear. I have a great respect for your work ethics, and I truly hope that you end up where you want. I will miss our lunch dates and good conversations!

Dear **Fred**, our collaboration is the best thing that happened during my PhD. What started off as side project for me quickly grew to the biggest project of my PhD and resulted in many great adventures. Working long days in Rotterdam, following the course for science-based startups at UtrechtInc, a patent application and the take-off Grant. I think we both grew a lot during these adventures, and I am very grateful we got to do it together. Your calm and rational approach to research have always inspired me, you are a very good listener, and you care for the people around you. This not only made you a very nice colleague to work with, but also a great friend. Thank you so much for all the support you have given me the last years, I will never forget it.

Igor, even though it was only for a short time I really enjoyed collaborating with you. Thank you for your help with optimizing the sample prep, waiting for all those columns to finish was a lot more pleasant in your company. I wish you all the best with the remaining of your PhD and your future as a teacher at the university!

I would like to thank **Theo**, **Mark**, **Pascal**, **Sander** and **Ron** for a very fruitful collaboration. I loved your working spirit; you were always willing to help with experiments and you taught me a lot. I felt very welcome in your lab, and I found it an inspiring atmosphere to work in.

Soenita and **Mirjam**, thanks a lot for your help with all the sample preparations. You have been great teachers and I really enjoyed working with you both.

Thijs, **Mieke** and **Marius**, thanks a lot that you were always so flexible in helping me. I always enjoyed coming by and learning more about your field of research. I never envisioned that my PhD would entail learning how to hold a chicken, but who knows when it will be useful in the future.

Dear **Ingrid**, already during my internship we hit it off quite well together with Cami. Thank you for the fun you brought to work, fooling around with your light saber or telling an animated story during lunch. I also cherish the many good talks over which we bonded more as colleagues and friends; I got a lot of support out of it.

Dear **Margherita**, I'm so happy that I got to know you and that you want to be my Paranymph. You are compassionate, creative and you inspire me with your approach to life. I keep being amazed by how often we discover new hobbies we have in common, and I hope we can discover many more hobbies together in the future! Thank you for being a great friend.

Dear **Helena**, I'm very happy that you joined our group, you have been such a great support for me during tough times. You are strong, funny, sometimes a little bit crazy, and I'm very happy that I can call you my friend! I appreciate how you can give me perspective on my problems, and I am very happy you want to be my paranymph.

Dear **Tom**, thank you for always being available for advice whenever I needed it, you helped me a lot and I'm very thankful for that.

I would like to thank all my biolab colleagues over the years, **Linda**, **Gerlof**, **Rob**, **Roosmarijn**, **Cindy**, **Ilhan**, **Kim**, **Cyril** and **Suhela**. Thanks for the fun, for your help, for passing my cells when I was sick or on holiday, and for making every day in the biolab an interesting day.

I would also like to thank **Yvette**, **Hanna**, **Enrico**, **Charlotte**, **Emma**, **Jack**, **Nino**, **Vito**, **Gael**, **Francesco**, **Luca**, **Apoorva**, **Tim**, **Seino**, **John**, **Dirk**, **Javier**, **Justyna**, **Arwin**, and all the other **CBDD members** I didn't mention by name for all the fun times, all your help, and the good vibes within the group. I wish you all the best!

Mike, bedankt voor al het lachen tijdens onze master! Ik ken weinig mensen die zo behulpzaam zijn als jij en ik vind het leuk dat wij elkaar af en toe nog spreken. Ik hoop dat we dat contact vast kunnen houden!

Lieve **Go**, **Eef**, **Tes**, **Dynph**, **Merel** en **Soof**, al sinds 2010 zijn jullie mijn familie in Amsterdam (en inmiddels verre omstreken). We hebben eindeloos veel meegemaakt samen, inclusief escalaties op alle mogelijke niveaus. Inmiddels kennen jullie mij soms beter dan ik mezelf ken, waardoor jullie adviezen voor mij van onschatbare waarde zijn. Ik ben zo ontzettend blij met jullie in mijn leven en ik hoop dat we avonturen blijven beleven tot het bejaardentehuis!

Lieve **Marleen**, **Juup**, **Han** en **Esther**, ik ben zo blij dat wij vrienden zijn geworden tijdens onze bachelor. Door jullie humor en relativeringsvermogen ben ik niet (echt) gek geworden de afgelopen jaren. Jullie waren en zijn de beste uitlaatklep die ik mij kan wensen. Bedankt voor alle koffies bij Sjeel, gore afbak lasagnes in de kantine in tentamenweken, pubquizzen in cafe lust, Lowlands weekenden, bardiensten bij de tafeltennis, puzzelavonden en escalerende kerstdiners. Als jullie nou even stoppen met naar het buitenland verhuizen dan kunnen we hopelijk nog vele jaren doorgaan met herinneringen maken.

Lieve **Marin**, ik kan gesprekken met jou voeren die ik met niemand anders kan voeren en ik ben dankbaar dat je altijd bereid bent om te luisteren en te helpen. Je inspireert mij in de manier waarop jij je eigen pad durft te kiezen in het leven. Lieve **Danielle**, ik ben heel blij dat jij erbij bent gekomen in onze familie! Heel erg bedankt voor je hulp met het opschonen van mijn proefschrift.

Lieve **pap** en **mam**, ik weet niet waar ik moet beginnen met jullie bedanken voor alles. Jullie geven mij een ontzettende kracht en rust in het leven omdat ik weet dat jullie mij altijd steunen, ook al zijn jullie het misschien niet altijd eens met mijn keuzes. Ik hou van jullie.

Lieve **Jorin**, wat een achtbaan is het geweest de afgelopen jaren, maar ik ben zo blij dat we er sterker uit zijn gekomen samen. Bedankt dat jij altijd in mij hebt geloofd, ook die talloze keren dat ik het geloof in mijzelf kwijt was. Je geeft mij telkens dat zetje dat ik nodig heb om dingen te blijven doen die ik eigenlijk niet durf. Ik heb ontzettend veel zin in ons leven samen en alle avonturen die we nog gaan beleven! Ik hou van je.